Computational Studies of the Structure of Vanadium Oxide Clusters and their Reactions with Halocarbons

Yin Wei

A Thesis

In

The Department

of

Chemistry and Biochemistry

Presented in Partial Fulfillment of the Requirements
for the Degree of Master of Science (Chemistry) at
Concordia University
Montréal, Québec, Canada

February 2005

Your file Votre référence
ISBN: 0-494-04346-6
Our file Notre référence
ISBN: 0-494-04346-6

Abstract

Computational Studies of Vanadium Oxide Clusters and

their Reactions with Halocarbons

Yin Wei

Vanadium oxides are key industrial catalysts in the oxidation and functionalization of various chemical compounds, and studies of gas-phase vanadium oxide clusters provide an avenue to explore the reactive sites implicated in surface catalysis. An extensive amount of experimental data has been reported on the gas-phase fragmentation of vanadium oxide cluster ions and their reactions with environmentally-relevant halocarbons. Our computational studies aim at further understanding the structure and properties of vanadium oxide clusters, as well as their reactivity towards fluorocarbons. Accordingly, we report a systematic density-functional theory (DFT) study of the structural and electronic properties of $V_xO_y^+$ and V_xO_y clusters, and investigate their reactions with CH_2F_2 and CH_3CF_3 by DFT calculations. Our results suggest that both B3LYP/TZVP and PLAP4/DZVP+aux. are appropriate model chemistries to investigate vanadium oxide clusters, but the latter is less computationally intensive, and thus more suitable for large clusters. Stable ground-state and low-lying excited-state structures and their electronic properties are obtained for both $V_xO_y^+$ and V_xO_y (x=1-4, y=1-10) clusters with the PLAP4/DZVP+aux. model chemistry. The molecular structures and electronic properties of large polyvanadium oxide clusters are systematically investigated and reported for the first time. The reaction of $V_2O_4^+$ with fluorocarbons was investigated with the B3LYP/TZVP model chemistry. Oxygen transfer and stepwise HF abstraction from the fluorocarbon are observed in the reactions of $V_2O_4^+$ with CH_2F_2 and CH_3CF_3, respectively. These reaction mechanisms help explain why larger clusters such as $V_4O_8^+$ were observed to be chemically inert towards CH_2F_2, while the reactivity of $V_xO_y^+$ cluster ions towards CH_3CF_3 was not found to depend on cluster size experimentally.

Acknowledgements

I would like to appreciate my supervisor Dr. Gilles H. Peslherbe for his help, support and guidance in the course of scientific research presented here. He led me into the wonderful world of computational chemistry and trained me to become a researcher in scientific field.

I wish to thank Dr. Philippe G. Merle and Dr. Christine E. DeWolf for being on my research committee and for their helpful suggestions.

I am grateful to all past and current members of Dr. Peslherbe's research group during my study at Concordia University.

I am especially indebted to Dr. Dongqing Wei.

Finally, I am grateful to my family, especially my husband Xiaoyin Yang for their love, encouragement and understanding, as well as all of my friends for their friendship and support.

Table of Contents

List of Tables

List of Figures

Chapter 1.

General Introduction

Catalysis already occupies a pivotal position in many sciences such as chemistry, biology, physics, and it also plays an important role in the chemical industry in particular. In the 20th century, industrial catalysts have proven their worth in industrial processes. However, there are still many practical challenges in the field of catalysis in the 21st century. Conceptually, the future challenges for catalysis can be divided into broad categories such as environmental, technological and fundamental.[1] The public is becoming more concerned with environmental issues, and many catalysts are being designed specifically to degrade toxic materials. How to design highly active, selective catalysts and improve their lifetime is a focus of catalysis technology. Solutions to practical problems will demand a deeper understanding of the fundamentals of catalysis. Obviously, these challenges have intimate relations though they are divided into several categories. Catalysts currently cannot be designed from first principles, rather they must be developed via a sequence of steps involving preparation, characterization and analysis. An important aim of research in catalysis is to accelerate this process by providing critically needed knowledge and techniques. Theoretical studies are becoming an important technique for the study of catalysis. The National Research Council Panel on New Directions in Catalytic Science and Technology listed the following as an important priority of federal research in their report:[2] "*Development and application of theoretical methods for predicting the structure and stability of catalysts, as well as the energetics and dynamics of elementary processes occurring during catalysis, and the use of this*

information for the design of novel catalytic cycles and catalytic materials and structures". It shows that theoretical chemistry has been recognized as an important tool for the study of catalysis.[3] Meanwhile, it illustrates the basic strategy behind our studies.

Transition metal oxides are widely used as catalysts and catalytic supports in industrial processes in heterogeneous catalysis due to their high catalytic activity. Designing catalysts at the molecular level requires knowledge of catalytic mechanisms and structure-reactivity relationships. However, the precise catalytic mechanisms and the structure-reactivity relationships are not understood very well in many catalytic processes. Although modern experimental surface techniques provide some information on the structure of catalysts and the composition of surfaces, it is difficult to probe the relationships between their structure and reactivity directly. In-situ experimental techniques can detect reactive sites directly, but they are rather expensive and have a number of limitations.[1] A valuable alternative to investigate this problem is to employ theoretical calculations to investigate the relevant cluster models of transition metal oxide catalysts. The advantages of this approach lie in the direct insight into the mechanisms at the active site on the transition metal oxide catalysts and a low cost, compared to experimental approaches. This thesis contributes to this issue as it focuses on computational studies of the structure of vanadium oxide clusters and their reactions with halocarbons. We expect our findings to further help people better understand the reactions of vanadium oxide clusters and to contribute to future catalyst design at the molecular level.

1.1. Experimental Studies of Vanadium Oxide Clusters

Recently, an extensive amount of experimental work on vanadium oxide clusters and their reactions have been reported.[4-22] Experimental studies have been performed to understand the formation process and structure of vanadium oxide clusters, and their collision-induced dissociation (CID).[4-8] Further, their reactivity towards various organic compounds was also investigated.[8-11]

1.1.1. Experimental Studies of the Formation, Structure and Dissociation of Vanadium Oxide Clusters

An extensive amount of gas-phase studies have been performed to understand the formation and the structure of vanadium oxide cluster ions. Riley and co-workers were one of the first to study the gas-phase formation of many transition metal oxide clusters including vanadium oxide clusters.[21] Neutral vanadium clusters were formed through laser vaporization of the pure metal in a buffer gas that cools the resulting vaporized metal, promoting cluster growth. The pure V_n clusters were then reacted with O_2 downstream from the point of ablation to form the vanadium oxide clusters. The neutral clusters were ionized by a second excimer laser to form the cationic clusters. The resulting cluster mass distributions showed an oxygen-to-metal ratio of 1.4 to 1.5, which corresponds to species found in the high-temperature vanadium oxygen phase diagram. Bernstein and co-workers[22] found similar mass distributions through the laser vaporization of V_2O_5 or pure vanadium reacted with low concentrations of O_2 (<2%) seeded in a helium carrier gas at the point of ablation. The cluster growth dynamics of the vanadium oxide neutrals were then studied by covariance mapping time-of-flight mass spectrometry.

Castleman and co-workers[8] have performed a series of experiments to investigate the formation and structure of vanadium oxide cluster ions. In these experiments, vanadium oxide cluster ions were formed in a procedure similar to Bernstein's.[22] The investigation of the formation of vanadium oxide cluster ions and their CID were performed by using a triple quadrupole mass spectrometer coupled with a laser vaporization source. A laser was used to ablate the surface of a pure vanadium rod, and then pulses of a mixture of 10% O_2 and helium carrier gas were injected over the ablated metal surface to form vanadium oxide clusters, during which time plasma reactions took place. The structure of mass-selected cluster cations was probed by both collision-induced dissociation and photofragmentation of cationic species. Experimental observations indicate the dominant peaks in the mass distributions corresponding to cluster cations with stoichiometries of the form $(VO_2)_n(V_2O_5)_m(O_2)_q^+$. CID studies of vanadium oxide cluster cations indicated that VO_2, VO_3, and V_2O_5 units were the main building blocks of these clusters. Castleman and co-workers also examined vanadium oxide cluster anions using a guided ion beam mass spectrometer coupled with a laser vaporization source.[12] They found that clusters have stoichiometries of the form $(VO_2)_n(VO_3)_m(O_2)_q^-$, and VO_2, VO_3, and V_2O_5 units are also the main building blocks of these clusters. There are many similarities between the anion mass distributions and these of cations through analysis of mass spectra, but a shift to higher oxygen content by one additional oxygen atom was observed for the $V_xO_y^-$ anions, as compared to cations with the same number of vanadium atoms. They also reported for the first time the V-O bond dissociation energies for small vanadium oxide cations and anions.

Medium-sized vanadium oxide cluster cations $V_xO_y^+$ ($4 \leq x \leq 14$) have been studied by Fielicke and Rademann.[20] The gas-phase medium-sized vanadium oxide clusters were produced via laser vaporization of vanadium metal rod in a continuous flow of He/O_2 carrier gas. Cluster distributions were subsequently characterized in terms of their scattering behaviors with low-density gas targets (10^{-4} -2×10^{-3} mbar). The composition of the dominant oxide clusters revealed the predominance of vanadium atoms in the formal oxidation states +4 and +5. The vanadium oxide clusters with an average O/V ratio of 2.5 were found to be stable towards CID up to collision energies corresponding to a velocity of 900 $m \cdot s^{-1}$.

Experimental information about the formation, structure and CID of vanadium oxide cluster ions provides reference data for our computational studies of vanadium oxide clusters. These experimental data can be used to benchmark the results of our calculations and help us choose a suitable theoretical model to investigate vanadium oxide clusters. Conversely, our calculations can further help understand and explain these experimental data.

1.1.2. Reactions of Vanadium Oxide Clusters

Vanadium oxides have been used extensively as catalysts or catalytic supports in a variety of industrial processes, which include the selective oxidation and ammoxidation of hydrocarbons,[23,24] the reduction of environmental pollutant NO with NH_3,[6,23] and the production of sulfuric acid.[5,25] As mentioned above, catalytic mechanisms and the relationship between the catalyst structure and its reactivity are not very clear and remain challenges in field of catalysis. Gas-phase transition metal oxide clusters can be regarded as the simplest model for the interaction of the active sites on the surface of catalyst with

organic molecules, and comparison of gas-phase cluster reactions with condensed-phase reactions leads to a better understanding of the interaction of organic molecules with catalytically active sites on surfaces.[26]

Vanadium oxide clusters are involved in many reactions, and particularly a considerable amount of experimental work has been reported by Castleman and co-workers[9-11,26] to investigate the properties of vanadium oxide clusters and their reactivity towards industrially-important compounds and environmentally-relevant compounds. Hydrocarbons are one of the industrially-important compounds due to their extensive applications in the petroleum industry. For instance, hydrocarbons are often used as starting materials which are broken into smaller molecules through cleavage of C-C bonds by heterogeneous catalysts. However, the nature of the catalytically active sites and the precise mechanism of this process are still in question. They have done extensive research on reactions of group V transition metal oxide ions, which include vanadium with C_2 and C_4 hydrocarbons to provide a scientific basis for ultimately tailoring the design of transition metal oxide catalysts.[26] The main pathways observed during reactions of $V_xO_y^+$ with ethane and ethylene are association of the C_2 hydrocarbon, $V_xO_y{\cdot}C_2H_z^+$, and atomic oxygen loss to produce $V_xO_{y-1}^+$. In the reactions of vanadium oxide clusters with C_4 hydrocarbons, the observed pathways include association of hydrocarbons ($V_xO_yC_4H_z^+$), C-C activation to form $V_xO_y\ C_2H_4^+$, dehydration to form $V_xO_{y-1}C_4H_{z-2}^+$, and atomic oxygen loss to form $V_xO_{y-1}^+$. The dominant reaction is atomic oxygen loss, however vanadium oxide clusters do not lose a single oxygen atom during collisions in an inert gas, and thus these findings indicate that atom oxygen loss is due to a reaction with

hydrocarbons and not due to a collision process. Therefore, an oxygen transfer pathway is assumed for this reaction.

Castleman and co-workers also reported a large amount of experimental data[9-11] on the reactions of vanadium oxide clusters with halocarbons, which are also environmentally and industrially relevant compounds. The reactions of vanadium oxide cluster cations with hexafluoroethane (C_2F_6), 1,1,1-trifluoroethane (CH_3CF_3), difluoromethane (CH_2F_2) and carbon tetrachloride (CCl_4) were studied to provide further insight into their reaction mechanisms. Experimental results demonstrate that vanadium oxide cluster cations are chemically inert toward C_2F_6 and exhibit a minor association channel between $V_2O_y^+$ and C_2F_6. Several reaction pathways were observed for the reaction of vanadium oxide cluster cations with CH_3CF_3. Most reactions resulted in a HF elimination product, $V_xO_y{\cdot}HF^+$. Only $V_2O_5^+$ was shown to cleave C-C bond to yield $V_2O_5{\cdot}CF_3^+$. Association reactions to form $V_xO_y{\cdot}CH_2F_2^+$ were observed, with a dominant reaction pathway involving the transfer of a single oxygen atom to the neutral reactant, along with the abstraction of two fluorine atoms to form $V_xO_{y-1}F_2^+$. Reactions of vanadium oxide cluster cations with carbon tetrachloride were also examined. The dominant reaction pathway is the transfer of the chloride ion to the small $V_xO_y^+$ cluster cations that contain three or fewer vanadium atoms, while the abstraction of two chlorine atoms with the transfer of oxygen to the neutral reactant molecule was observed for the larger clusters.

Many factors, such as charge distribution, transition metal oxidation state and cluster ionization potential, may influence the reactivity of vanadium oxide clusters towards hydrocarbons and halocarbons. Theoretical studies of vanadium oxide clusters can be

employed to explain how these factors affect the reactivity of vanadium oxide clusters, and this is one major goal of the present study.

1.2. Computational Studies of Vanadium Oxide Clusters

Density-functional theory (DFT), which was developed in recent years, is considered as a reliable theoretical tool to study the structural and electronic properties of transition metal oxide clusters and their relevant reactivity. The origin and basic theory of DFT will be briefly described in Chapter 2, here, follows an overview of the previous applications of DFT to investigate the structural and electronic properties of vanadium oxide clusters and their reactivity.

1.2.1. DFT Studies of the Structure of Vanadium Oxide Clusters

Vyboishchikov and Sauer[27] reported a DFT study of the structural and electronic properties of mononuclear and binuclear vanadium oxide anions, VO_y^- (y=1-4) and $V_2O_y^-$ (y= 4, 6, and 7), as well as the polynuclear $V_3O_8^-$, $V_4O_{10}^-$, and $V_4O_{11}^-$ anions. A triple-ζ valence plus polarization basis set was adopted along with the B3LYP and BP86 functionals to investigate these vanadium oxide cluster anions. The two functionals were found to yield very similar structures for all systems studied. Electron detachment energies of the anions display two important trends. First, they increase strongly with increasing the metal oxidation state. Second, the electron detachment energies increase with a higher delocalization of the unpaired electron. They also investigated the structural properties of neutral $(V_2O_5)_n$ (n=1-12) clusters with DFT calculations,[28] and stable structures were determined with BP86 functional with a double-ζ(V)/triple-ζ(O) valence basis set augmented by polarization function. The most stable structure for the smallest

cluster is doubly O-bridged i.e. of the form $OV\text{-}O_2\text{-}VO_2$, which is less stable in energy by 184 kJ/mol than the periodic bulk V_2O_5 structure.

DFT studies of $V_xO_y^+$ and V_xO_y (x=2-4, y=2-10) have also been carried out to study their structural, thermodynamic and electronic properties with B3LYP/6-31G* model chemistry.[29] The B3LYP/6-31G* model chemistry was used to explore the ground and excited states and characterize the most stable structures and predict their IR spectra. Geometric parameters and calculated frequencies were reported for cationic and neutral clusters $V_xO_y^+$ and V_xO_y (x=2-4, y=2-10). The calculated geometric parameters for the ground electronic states of neutral species are in agreement with the values reported by Vyboishchikov and Sauer.[27] Three sets of V-O distances were found: short (1.55Å), intermediate (1.70-1.80 Å), and large (2.00 Å). These values can be associated to strong (terminal) and weak interactions involving O (-2) and O (-1) oxidation states, respectively.

A systematic DFT study of vanadium oxide clusters $V_xO_y^+$ and V_xO_y (x=1-4,y=1-10) will be presented in Chapter 3. Various basis sets and functionals were tested to determine an appropriate model chemistry to investigate vanadium oxide clusters. Minimum-energy structures for $V_xO_y^+$ and V_xO_y (x=1-4, y=1-10) clusters as well as their electronic properties will then be discussed.

1.2.2. DFT Studies of the Reactions of Vanadium Oxide Clusters

The catalysis of methanol oxidation by V_2O_5 to produce formaldehyde has been studied by DFT calculations by Chermette and co-workers.[30] The proposed mechanism involves adsorption of methanol on V_2O_5 and its mild oxidation to formaldehyde. It was shown that the adsorption of methanol is energetically favorable if the cluster is partially

reduced. The oxidation mechanism occurs in two steps, the first being the dissociation of methanol to form a methoxy group on the surface, the second involving the desorption of formaldehyde. Calculations show that filling of the vanadyl oxygen vacancy created by formaldehyde desorption is crucial to make the reaction pathway energetically feasible.

DFT calculations were also carried out on a vanadium oxide cluster model containing four vanadium atoms to probe the mechanism of the selective catalytic reduction (SCR) of NO with ammonia.[31] They found that the adsorption of ammonia on the O-H sites of the $V_4O_{16}H_{12}$ cluster would lead to the formation of NH_4 species bonded to two vanadyl (V=O) groups, with a bonding energy of 110 kJ/mol. This adsorbed NH_4 species reacts with NO in a series of steps to form an adsorbed NH_2NO species, which subsequently undergoes decomposition to form N_2, H_2O and a reduced vanadium oxide cluster.

DFT calculations were also employed to investigate the reactions of $V_xO_y^+$ with ethylene to elucidate the structure-reactivity relationships by Justes *et al.*[32] Combined theoretical and experimental results provide evidence for the selectivity of $V_xO_y^+$ clusters in reactions toward ethylene, due to different charges and oxidation states of vanadium for different cluster sizes. An oxygen transfer reaction via a radical-cation mechanism was determined to be the most energetically favorable pathway available to $V_2O_5^+$ and $V_4O_{10}^+$. The oxidation of small size alkanes by VO_2^+ in the gas-phase have been studied by Gracia *et al.*[33] and Engeser *et al.*[34] through DFT calculations. The molecular mechanisms of the reactions of VO_2^+ with C_2H_6 and C_3H_8 were investigated respectively and allowed people to understand the mechanism of other analogous reactions. Gracia *et al.* studied the reaction of VO_2^+ with C_2H_6 on different potential energy surface (PES) because many reactions of transition metal oxides involve low lying excited electron

state. The most favorable reaction pathway does not remain on a single PES and the electron states are changed during the course of reaction.

Chapter 4 will focus on the relationship between the structure of vanadium oxide cluster cations $V_xO_y^+$ and their reactions with environmentally-relevant fluorocarbons CH_2F_2 and CH_3CF_3, and the possible oxygen transfer and the HF stepwise abstraction from fluorocarbons pathways will be explored and discussed.

1.3. Conclusions

In recent years, vanadium oxide clusters have been the subject of many theoretical and experimental studies. DFT plays an important role in theoretical studies of vanadium oxide clusters. The main goal of this thesis is to investigate the structural and electronic properties of vanadium oxide clusters with DFT calculations, and to explore their reactivity towards halocarbons and elucidate reaction mechanism. We expect our findings to provide invaluable information, which could in turn be used to better understand the precise molecular-level function of transition metal oxide catalysts.

Chapter 2.

Theoretical Methodology

2.1. Fundamentals of Density-Functional Theory (DFT)

Density-functional theory is rooted in quantum mechanics and has become an active player in the computational chemistry arena. Quantum mechanics provides a set of laws to describe the behavior of small particles such as the electrons and nuclei of atoms and molecules. Many applications of quantum mechanics to chemistry require to solve the time-independent Schoedinger equation (1):

$$\hat{H}\Psi = E\Psi \tag{1}$$

where E is the energy of the system, Ψ is the wavefunction and $\hat{H}$ is the Hamiltonian operator. The Hamiltonian operator for a general N-particle system contains kinetic ($\hat{T}$) and potential ($\hat{V}$) energy terms for all particles.

$$\begin{aligned} \hat{H} &= \hat{T} + \hat{V} \\ \hat{T} &= -\sum_{i=1}^{N} \frac{\hbar}{2m_i} \nabla_i^2 = -\sum_{i=1}^{N} \frac{\hbar}{2m_i} \left(\frac{\partial^2}{\partial x_i^2} + \frac{\partial^2}{\partial y_i^2} + \frac{\partial^2}{\partial z_i^2} \right) \\ \hat{V} &= \sum_{i=1}^{N} \sum_{i>1}^{N} \frac{q_i q_j}{r_{ij}} \end{aligned} \tag{2}$$

The time-independent Schoedinger equation (1) can only be solved exactly for one-electron systems, and approximations must be made for many-electron systems. The approximation of separating electronic and nuclear motions is called the Born-Oppenheimer approximation and it is the first basic approximation used to simplify the solution of the Schoedinger equation (1). An electronic Schoedinger equation (3) is obtained to describe the electronic motion with respect to a fixed nuclear configuration:

$$\hat{H}_e \phi_e(r,R) = E\phi_e(r,R) \tag{3}$$

where r and R are the electronic and nuclear coordinates, respectively. The many-electron Hamiltonian $\hat{H}_e$ includes the kinetic energy of the electrons and the interaction energy of the electrons with nuclei and with each other.

$$\hat{H}_e = \sum_i \frac{-\nabla_i^2}{2} + \sum_{i,I} \frac{-Z_I}{|r_i - R_I|} + \frac{1}{2}\sum_{i \neq j} \frac{1}{|r_i - r_j|} \tag{4}$$

Here the index I refers to the nuclei with atomic number Z_I, i and j refer to electrons. Traditional Hartree-Fock (HF) approaches to electronic structure focus on approximations to the solution of the electronic Schroedinger equation.[35] The HF approximation is to separate the motion of electrons and to represent the many-electron wavefunction as a sum of products of one-electron or two-electron wavefunctions. The final set of HF equations can be written as

$$\hat{F}_i \phi_i = \varepsilon_i \phi_i \tag{5}$$

$$\hat{F}_i = \hat{h}_i + \sum_j^N \left(\hat{J}_i - \hat{K}_i\right)$$

where the Fock operator $\hat{F}_i$ is an effective one-electron energy operator. The Fock operator $\hat{F}_i$ contains the one-electron operator $\hat{h}_i$, which includes the kinetic energy of the electron and attraction to all nuclei, while the Coulomb ($\hat{J}_i$) and Exchange ($\hat{K}_i$) operators represent the repulsion with other electrons. The Coulomb ($\hat{J}_i$) operator represents the repulsion energy between two charge distributions, and the Exchange ($\hat{K}_i$) operator, which has no simple physical significance, arises from the requirement that the wave function is antisymmetric with respect to electron exchange. This simplifies the

problem of accounting for the motion of several electrons to the much simpler problem of accounting for the motion of each electron in a "field" of the nuclei and the remaining electrons. The major shortcoming of HF methods is that they do not include electron correlation arising from the correlated motion of electrons. The electron correlation energy (E_c) is defined as the difference between the exact energy and the corresponding HF value.

$$E_c = E_{exact} - E_{HF} \quad (6)$$

Electron correlation is important to determine molecular geometries and relative energies, and is crucial to describe bond breaking and forming in chemical reactions properly. So-called electron correlation methods such as Møller-Plesset perturbation theory, Coupled-Cluster and Configuration Interaction methods account for electron correlation, but they are orders of magnitude computationally more intensive than HF methods. Recently, DFT has gained acceptance as an alternative to more computationally intensive ab initio correlated methods.

The history of DFT dates back to the work of Thomas,[36] Fermi[37] and Dirac,[38] who devised approximate expressions for the kinetic energy and exchange energy of many-electron systems in terms of simple functionals of the local electron density. The main problem in the Thomas-Fermi-Dirac model is that the kinetic energy cannot be represented accurately.[39] In the 1950s, Slater's X_α method[40] contributed to the development of DFT and its application to molecules in the gas and solid states. The basic idea in Slater's X_α method is to make a simple, one-parameter approximate exchange-correlation functional written in the form of an exchange-only functional. Modern DFT methods originated from the Hohenberg-Kohn theorem[41] published in

1964, which demonstrated the existence of a unique functional that determines the ground state energy and density of a system exactly. The theorem does not provide the form of the functional, but the Kohn-Sham formalism[42] paved the way to a computational breakthrough and promoted DFT to become a full-fledged theory.

The Kohn-Sham density functional theorems state that the ground-state molecular energy and all other molecular electronic properties are uniquely determined by the ground-state electron density.[43] The electron density can be expressed as a sum over occupied Korn-Sham (KS) orbitals ϕ_i that are solutions of the Korn-Sham equations.[42]

$$\rho(r)=\sum_{i=1}^{N}\left|\phi_i(r)\right|^2 \tag{7}$$

DFT expresses the total energy of a system as a functional of the total electron density. A general DFT energy expression can be written as a sum of four terms,

$$E_{DFT}[\rho]=T_s[\rho]+E_{ne}[\rho]+J[\rho]+E_{xc}[\rho] \tag{8}$$

where $T_s[\rho]$ is the kinetic energy of a system of non-interacting electrons of density ρ, $E_{ne}[\rho]$ describes the potential energy of nuclear-electron attractions, $J[\rho]$ is the electron-electron repulsion term, and E_{xc} contains an exchange energy contribution as well as a correlation contribution to the kinetic and potential energy of the electrons. E_{xc} is customarily divided into two parts, referred to as the exchange and correlation functionals, i.e.

$$E_{xc}[\rho] = E_x[\rho]+ E_c[\rho] \tag{9}$$

In DFT, the exchange energy $E_x[\rho]$ is defined as a function of the exact density $\rho(r)$, expressed in terms of KS orbitals, while the HF exchange energy E_x^{HF} is defined exactly

with respect to the HF orbitals. The DFT definition of the correlation energy $E_c[\rho]$ is simply the difference between $E_{xc}[\rho]$ and $E_x[\rho]$.

The advantage of DFT is that the approach has a computational cost that is similar to traditional HF theory, with the possibility of providing more accurate results. The weakness of DFT lies in the fact that there is no way to generate an accurate functional form and only approximate forms of E_{xc} are currently known and employed.

2.2. Local Density Methods

The local density approximation (LDA) provides a model on which virtually all approximate exchange-correlation functionals are based. The LDA assumes that the local electron density can be treated as a uniform electron gas and that the electron density varies slowly in comparison to the exchange and correlation effects. We can write E_{xc} in the following form

$$E_{xc}^{LDA}[\rho]=\int \varepsilon_{xc}[\rho(r)]dr \quad (10)$$

Here, $\varepsilon_{xc}[\rho(r)]$ is the exchange-correlation energy density of a uniform electron gas of density $\rho(r)$, which can be further split into exchange and correlation contributions. The exchange energy for a uniform electron gas is given by the Dirac formula

$$E_x^{LDA}[\rho]= -C_x\int\rho^{4/3}(r))dr \quad (11)$$

$$\varepsilon_x^{LDA}[\rho]=-C_x\rho^{1/3} \quad (12)$$

In the more general case, the LDA has been replaced by the local spin density approximation (LSDA), where the α and β densities are not necessarily equal. The LSDA can be written as:

$$E_x^{LSDA}[\rho] = -2^{1/3}C_x\int[\rho_\alpha^{4/3} + \rho_\beta^{4/3}]\,dr \quad (13)$$

$$\varepsilon_x^{LSDA}[\rho] = -\,-2^{1/3}C_x[\rho_\alpha^{1/3} + \rho_\beta^{1/3}] \quad (14)$$

Slater's X_α method[40,44] can be considered an LDA method where the exchange is written as

$$\varepsilon_{X\alpha}[\rho] = -3/2\alpha C_x\rho^{1/3} \quad (15)$$

and the name Slater is often a synonym for the L(S)DA exchange energy involving the electron density raised to the 4/3 power (1/3 power for the energy density).

The correlation energy of a uniform electron gas has been determined by Monte Carlo methods for a number of different densities. This correlation functional was constructed by Vosko, Wilk and Nusair (VWN).[45] It interpolates between the unpolarized (ζ=0) and spin polarized (ζ=1) limits by the following functional, where ζ is the relative spin polarization.

$$\varepsilon_c^{VWN}(r_S,\zeta) = \varepsilon_c(r_S,0) + \varepsilon_a(r_S)\left[\frac{f(\zeta)}{f''(\zeta)}\right][1-\zeta^4] + [\varepsilon_c(r_S,1) - \varepsilon_c(r_S,0)]f(\zeta)\zeta^4$$

$$f(\zeta) = \frac{(1+\zeta)^{4/3} + (1-\zeta)^{4/3} - 2}{2(2^{1/3}-1)} \;;\; \zeta = \frac{\rho_\alpha - \rho_\beta}{\rho_\alpha + \rho_\beta} \quad (16)$$

The $\varepsilon_c(r_S,0)$ and $\varepsilon_a(r_S)$ functionals are parameterized as follows:

$$\varepsilon_{c/a}(x) = A\left\{\ln\frac{x^2}{X(x)} + \frac{2b}{Q}\tan^{-1}\left(\frac{Q}{2x+b}\right) - \frac{bx_0}{X(x_0)}\left[\ln\frac{(x-x_0)^2}{X(x)} + \frac{2(b+2x_0)}{Q}\tan^{-1}\left(\frac{Q}{2x+b}\right)\right]\right\} \quad (17)$$

$$x = \sqrt{r_S} \;\;;\;\; X(x) = x^2 + bx + c \;;\; Q = \sqrt{4c - b^2}$$

The parameters A, x_0, b and c are fitting constants, different for $\varepsilon_c(r_S,0)$, $\varepsilon_c(r_S,1)$ and $\varepsilon_a(r_S)$.

The L(S)DA functional is made up of the combination of Slater's result for the exchange of a free electron gas and the Vosko-Wilk-Nusair[45] representation of electron correlation (SVWN). The L(S)DA has been proven particularly successful for the determination of molecular properties such as equilibrium structures, harmonic frequencies or moments of charge distributions. However, many studies indicate that the performance of L(S)DA is rather poor for some properties such as bond energies.[46]

2.3. Gradient-Corrected Methods

In order to improve the performance of functionals, one has to consider a non-uniform electron gas. In this case, the exchange-correlation energy depends on both the electron density and its derivatives. Such methods make use of so-called generalized gradient approximation (GGA), or non-local methods are referred to as gradient-corrected methods.

Perdew and Wang[47] proposed an exchange functional in 1986 that is the modified LSDA exchange expression shown in equation (18),

$$\varepsilon_x^{PW86} = \varepsilon_x^{LDA}(1 + ax^2 + bx^4 + cx^6)^{1/15}$$
$$x = \frac{|\nabla \rho|}{\rho^{4/3}} \tag{18}$$

where x is a dimensionless gradient variable, and a, b and c are suitable constants. Becke[48] proposed a widely used correction to the LDA exchange energy, which leads to the B88 exchange functional.

$$\varepsilon_x^{B88} = \varepsilon_x^{LDA} + \Delta\varepsilon_x^{B88}$$
$$\Delta\varepsilon_x^{B88} = -\beta\rho^{1/3}\frac{x^2}{1+6\beta x \sinh^{-1} x} \tag{19}$$

The β parameter is determined by fitting to known atomic data with x defined in equation (18). Perdew and Wang proposed another exchange functional in 1991 that is similar to B88, and can be used in connection with the PW91 correlation functional discussed below. The PW91 exchange energy density is given by

$$\varepsilon_x^{PW91} = \varepsilon_x^{LDA}\left(\frac{1+xa_1\sinh^{-1}(xa_2)+(a_3+a_4e^{-bx^2})x^2}{1+xa_1\sinh^{-1}(xa_2)+a_5x^2}\right) \tag{20}$$

where $a_{1\text{-}5}$ and b are suitable constants and x is defined in equation (18).

Various gradient-corrected correlation functionals have been proposed. One of the popular correlation functionals was proposed by Lee, Yang and Parr (LYP)[49] and is expressed as:

$$\varepsilon_c^{LYP} = -a\frac{\gamma}{\left(1+d\rho^{-1/3}\right)} - ab\frac{\gamma e^{-c\rho^{-1/3}}}{9\left(1+d\rho^{-1/3}\right)\rho^{8/3}}\times\left[\begin{array}{l}18\left(2^{2/3}\right)C_F\left(\rho_\alpha^{8/3}+\rho_\beta^{8/3}\right)-18\rho t_w \\ +\rho_\alpha\left(2t_w^\alpha+\nabla^2\rho_\alpha\right)+\rho_\beta\left(2t_w^\beta+\nabla^2\rho_\beta\right)\end{array}\right] \tag{21}$$

$$\gamma = 2\left[1-\frac{\rho_\alpha^2+\rho_\beta^2}{\rho^2}\right]$$

$$t_w^\sigma = \frac{1}{8}\left(\frac{|\nabla\rho_\sigma|^2}{\rho_\sigma}-\nabla^2\rho_\sigma\right)$$

where the a, b, c and d parameters are determined by fitting data for the helium atom. The t_w functional is the local Weizsacker kinetic energy density. The γ factor becomes zero when all spins are aligned, i.e. the LYP functional does not predict any parallel spin correlation in such a case. Perdew proposed a gradient correction to the LSDA in 1986, which is known as P86. This functional was modified to the following form by Perdew and Wang in 1991 (PW91 and P91).[50]

$$\varepsilon_c^{PW91} = \varepsilon_c^{LDA} + \Delta\varepsilon_c^{PW91}$$

$$\Delta\varepsilon_c^{PW91} = \rho\left(H_0\left(t, r_S, \zeta\right) + H_1\left(t, r_S, \zeta\right)\right)$$

$$H_0\left(t, r_S, \zeta\right) = b^{-1} f(\zeta)^3 \ln\left[1 + a\frac{t^2 + At^4}{1 + At^2 + A^2 t^4}\right]$$

$$H_1\left(t, r_S, \zeta\right) = \left(\frac{16}{\pi}\right)\left(3\pi^2\right)^{1/3}\left[C(\rho) - c\right] f(\zeta)^3 t^2 e^{-dx^2/f(\zeta)^2} \qquad (22)$$

$$f(\zeta) = \frac{1}{2}\left(\left(1+\zeta\right)^{2/3} + \left(1-\zeta\right)^{2/3}\right)$$

$$t = \left(\frac{192}{\pi^2}\right)^{1/6} \frac{|\nabla\rho|}{2f(\zeta)\rho^{7/6}}$$

$$A = a\left[e^{-b\varepsilon_c(r_S,\zeta)/f(\zeta)^3} - 1\right]^{-1}$$

$$C(\rho) = b_1 + \frac{b_2 + b_3 r_S + b_4 r_S^2}{1 + b_5 r_S + b_6 r_S^2 + b_7 r_S^3}$$

Here x is again defined in equation (18), a, b, c and d are suitable constants, and $b_{1\text{-}7}$ are numerical constants. Salahub and co-workers[51,52] proposed the LAP1 functional, which is a nonlocal generalization of the correlation functional PVS1[53] that involves the kinetic energy density and the Laplacian of the electron density, $\nabla^2\rho$. The LAP1 correlation functional is expressed as:

$$E_c^{LAP1} = \int dR n(R) \varepsilon_c^{\uparrow\downarrow}(R)$$

$$\varepsilon_c^{\uparrow\downarrow} = \frac{n_\uparrow n_\downarrow}{n} Q^{\uparrow\downarrow}(k) \qquad (23)$$

$$Q^{\uparrow\downarrow}(k) = -\frac{b_1}{1 + b_2 k} + \frac{b_3}{k}\ln\left(\frac{b_4 + k}{k}\right) + \frac{b_5}{k} - \frac{b_6}{k^2}$$

The kinetic energy density-dependent correlation functional LAP1 does not include any parallel spin correlation beyond E_x. They developed the LAP1 functional further to form LAP3,[54] which includes parallel-spin correlation beyond E_x, and LAP4 with the treatment

of parallel spin correlation is refined further to achieve optimal results for weak interactions.

GGA methods usually perform much better than LSDA methods and yield improved results due to added gradient terms. In particular, GGA methods are more reliable for describing weak interactions.[55]

2.4. Hybrid Methods

In practice, self-consistent Kohn-Sham DFT calculations are performed in an iterative manner that is analogous to a self-consistent HF computation. The similarity to the methodology of Hartree-Fock theory was pointed out by Kohn and Sham.[42] The basic concept behind the so-called hybrid models is to mix the exchange energy calculated in an exact HF manner with those obtained from DFT methods. The most popular hybrid functional is B3LYP, which combines Becke's three-parameter exchange functional (B3) and the Lee-Yang-Parr gradient-corrected correlation functional. The B3LYP exchange-correlation functional is expressed as:

$$E_{xc}^{B3LYP} = E_x^{B3} + E_c^{VWN3} + c\left(E_c^{LYP} - E_c^{VWN3}\right) \tag{24}$$

where E_x^{B3} is a weighted sum of exact HF exchange and gradient-corrected local spin-density approximations.

$$E_x^{B3} = aE_x^{exact} + (1-a)E_x^{LDA} + b\Delta E_x^{B88} \tag{25}$$

Different hybrid functionals can be constructed in a similar fashion by varying the functional components. For instance, B3PW91 can be constructed by substituting the PW91 gradient corrected correlation functional for the LYP one and by adjusting the values of the three parameters.

2.5 Conclusions

The fundamentals of DFT theory were reviewed in this chapter along with the currently popular exchange-correlation functionals. In principle, any exchange functional can be combined with any correlation functional to form an exchange-correlation functional. Functionals such as B3LYP, BLYP and B3PW91 are mainstream in contemporary DFT calculations. Functionals involved in our work include SVWN, BLYP, PW91PW91, B3LYP, B3PW91, BLAP1, BLAP3 and PLAP4.

Chapter 3.

Density-Functional Theory Studies of Vanadium Oxide Clusters $V_xO_y^+$ and V_xO_y (x=1-4, y=1-10)

(Y. Wei & G. H. Peslherbe, *Journal of Physical Chemistry* A, to be submitted)

3.1. Introduction

Recently, vanadium oxide species have been the subject of extensive experimental and theoretical studies,[8-34,56-71] as vanadium oxides are becoming increasingly important catalysts in many industrial processes,[72] such as the selective oxidation and functionalization of hydrocarbons. The main interest of gas-phase studies of neutral and ionic vanadium oxide clusters lies in the possibility of better understanding the nature of the reactive sites on catalyst surfaces by investigating small cluster models.[12]

Castleman and co-workers[8-12] have performed an extensive amount of experimental work on vanadium oxide ions and their reactivity towards industrially and environmentally important compounds, by using a triple-quadrupole mass spectrometer coupled with a laser vaporization source. However, it is cumbersome and expensive to characterize the structural and electronic properties of vanadium oxide clusters directly by experimental techniques.[1] On the other hand, quantum chemistry calculations offer an efficient alternative to obtain molecular geometries, electronic properties, binding energies and description of bonding in these systems. Transition metal-containing species remain a challenge for quantum chemistry calculations, as transition metals have partially filled d-orbitals, which leads to complicated wavefunctions and many nearly degenerate electronic states. However, from the recent literature,[27-33,58-61] density-functional theory (DFT) appears to be a powerful tool for investigating transition metal-containing clusters.

The structure of some small neutral vanadium oxide clusters and cluster ions have been reported from DFT calculations. Calatayud and co-workers[29] have reported the structure of the neutral and cationic monovanadium and bivanadium oxide systems, as well as that of $V_3O_{6-7}^+$, V_3O_{6-7} and V_4O_{10}, along with their electronic properties predicted by the

B3LYP/6-31G* model chemistry. Vyboishchikov and Sauer[28] have reported the results of systematic DFT calculations of the structure of monovanadium and bivanadium oxide anions, VO_y^- (y=1-4) and $V_2O_y^-$ (y= 4, 6, and 7), as well as that of the polyvanadium $V_3O_8^-$, $V_4O_{10}^-$, and $V_4O_{11}^-$ anions. As mentioned above, the partially filled d-orbitals of transition metals result in many nearly degenerate electronic states, which make prediction of reliable structures for vanadium oxide species cumbersome. As a result, conflicting assignments of the electronic ground state of $V_2O_5^+$ and different global minimum-energy structures of some small vanadium oxide clusters have been recently reported,[60,71] even though a similar model chemistry was employed for the vanadium oxide clusters.

Our aim is to further explore the structure of neutral and cationic vanadium oxide clusters and their properties, not only paying attention to monovanadium and bivanadium oxide clusters, but also to polyvanadium oxide clusters $V_xO_y^+$ and V_xO_y ($x\geq3$, $y\geq6$). In this contribution, we first begin with an assessment of basis sets and functionals to determine the model chemistry that is the most appropriate to investigate vanadium oxide clusters. We then report the structure and energetics of monovanadium, bivanadium and polyvanadium oxide clusters $V_xO_y^+$ and V_xO_y (x=1-4, y=1-10) predicted by our most appropriate model chemistry, along with their electronic properties in their ground and excited states.

3.2. Computational Methods

DFT calculations were carried out with the Gaussian 98 suite of programs[73] and the deMon-StoBe2003 program package.[74-76] In order to determine an appropriate model chemistry to investigate vanadium oxide clusters, the reliability and computational cost of several basis sets and functionals were first tested. The reliability of a model chemistry was estimated by comparison of the calculated VO_2^+ dissociation energy to available experimental data,[8] while computational efficiency was inferred from the time required to perform a single-point calculation for VO_2^+ and $V_3O_6^+$. The all-electron basis sets 6-31G* developed by Pople *et al.* [77], the DZVP (double-ζ valence plus polarization) and the TZVP (triple-ζ valence plus polarization function) developed by Ahlrichs and co-workers[78] were combined with Becke's hybrid three parameter nonlocal exchange functional (B3) and the Lee-Yang-Parr gradient corrected functional (LYP), to calculate the dissociation energy of VO_2^+. Similarly, a number of exchange-correlation functionals was tested, such as the Slater local exchange functional combined with the Vosko-Wilk-Nusair correlation functional (SVWN), which is usually referred to as the local density approximation (LDA) functional, the generalized gradient-approximation (GGA) exchange functional of Becke (B) combined with the LYP correlation functional (BLYP), the GGA exchange functional of Perdew-Wang 91 (PW91) combined with the GGA correlation functional of Perdew-Wang 91 (PW91), the B3LYP, the B3 functional combined with PW91 correlation functional (B3PW91) and the B3 functional combined with the GGA correlation functional of Perdew-Wang 86 (PW86 or P). These functionals were combined with the TZVP basis set to calculate the dissociation energy of VO_2^+. Likewise, the combination of B functional with the "pure" DFT Laplacian-corrected

GGA (so-called meta-GGA) functional LAP1, LAP3 (modified LAP1 with inclusion of some parallel spin correlation) and the combination of the P functional with the LAP4 functional (similar to LAP3 but with a refined treatment of the parallel spin correlation) were tested with the DZVP basis set and auxiliary basis sets.[79,80] The geometry of minimum-energy structures was optimized using the default Berny algorithm[81] in Gaussian 98 and the Broyden-Fletcher-Goldfarb-Shanno[82-86] algorithm in deMon-StoBe2003. All stationary points were characterized by a vibrational frequency analysis, and all VO_2^+ dissociation energies calculated by the various model chemistries were corrected for zero-point energy (ZPE) based on harmonic vibrational frequencies. The Mulliken population analysis[87] and the natural population analysis[88,89] were employed to evaluate charge distributions.

3.3. Results and Discussion

3.3.1. Assessment of Basis Sets and Functionals

Three commonly used all-electron basis sets, the 6-31G*, DZVP and TZVP were combined with the B3LYP hybrid functional in order to assess their performance by computing the VO_2^+ dissociation energy defined as the energy change of the dissociation reaction

$$VO_2^+(^1A) \longrightarrow VO^+(^3\Sigma) + O(^3P_2).$$

Our results are listed in Table 3.1, where they are compared with experimental data. The calculated VO_2^+ dissociation energy is significantly overestimated by most model chemistries, compared to experimental data. The errors of the VO_2^+ dissociation energies calculated with the 6-31G* and DZVP basis sets lie within 0.49 eV and 0.38 eV of the upper limit of the experimental dissociation energy, respectively. However, the VO_2^+ dissociation energies calculated by the relatively large TZVP basis set lies in the range of

experimental data, and thus the TZVP basis set gives the best overall performance with the B3LYP functional.

A shortcoming of DFT lies in the fact that the exact exchange-correlation functional is not known, and a number of functionals, all with different approximate forms, have been proposed. We now turn our attention to the choice of functional for vanadium oxide cluster calculations, and our results are also listed in Table 3.1. Not surprisingly, our results indicate that the LDA and GGA functionals produce dissociation energies with large errors (more than 1.23 eV), compared to experimental data. Hybrid functionals seem to produce more reliable dissociation energies, especially the B3LYP and B3PW91 hybrid functionals. For polyvanadium oxide cluster systems V_xO_y ($x \geq 3$), a model chemistry that is less computationally intensive and yet yields acceptable results is desirable, since the computational cost increases roughly quadratically with system size. The BLAP1, BLAP3 and PLAP4 functionals were also tested to assess their accuracy. These functionals were combined with the DZVP basis set and auxiliary (aux.) basis sets,[79,80] instead of a TZVP basis set, to calculate the dissociation energy of VO_2^+. "Pure" DFT methods are not so sensitive to basis sets,[46] and thus reducing the basis set size may save computational time without loss of accuracy. Results of our test calculations are again listed in Table 3.1. The PLAP4/DZVP+aux. model chemistry obviously yields the same accuracy as B3LYP/TZVP.

We also evaluated the computational time of a single-point calculation for VO_2^+ and $V_3O_6^+$ with various model chemistries (cf. Table 3.2). The computational time of model chemistries that make use of the LYP correlation functional appears to be smaller than that of other model chemistries except for the "pure" DFT methods. The B3LYP/TZVP

model chemistry appears to be an appropriate model chemistry for investigating vanadium oxide clusters. However, calculations with the PLAP4/DZVP+aux. model chemistry are more than twice as fast as those with the B3LYP/TZVP model chemistry. Hence, the PLAP4/DZVP+aux. model chemistry gives the best overall performance if one takes into account both the computational time and accuracy of the resulting VO_2^+ dissociation energy. Therefore, the PLAP4/DZVP+aux. model chemistry is chosen to investigate the structural and electronic properties of vanadium oxide clusters $V_xO_y^+$ and V_xO_y (x=1-4, y=1-10) over a wide range of cluster sizes in this contribution.

3.3.2. Minimum-Energy Structures and Relative Energies of $V_xO_y^+$ and V_xO_y (x=1-4, y=1-10)

VO_y^+ and VO_y (y=1-3)

Geometric parameters for the minimum-energy structures of VO_y^+ and VO_y (y=1-3) and their relative energies in different electronic states are collected in Table 3.3. The ground states of VO^+ and VO are the $^3\Sigma$ and $^4\Sigma$ high-spin states, respectively. The $^3\Sigma$ VO^+ species is 24.4 kcal/mol lower in energy than $^1\Delta$ VO^+, while the neutral $^4\Sigma$ VO species is more stable than $^2\Sigma$ VO by 13.8 kcal/mol. The V-O bond lengths of VO^+ and VO in the high-spin ground states are larger than those in the low-spin states. Our calculated results are essentially in agreement with previous work reported by Calatayud *et al.*, who employed the B3LYP/6-31G* model chemistry.[65] Our calculated relative energy differences between the high-spin and low-spin states of VO^+ and VO compare well to the values of 26.3 kcal/mol and 12.5 kcal/mol previously reported for VO^+ and VO, respectively. However, our calculated V-O bond lengths of 1.546 Å for $^3\Sigma$ VO^+ and 1.590 Å for $^4\Sigma$ VO are closer to experimental values (1.540 Å, 1.589 Å)[90] than those previously reported (1.530 Å, 1.569 Å) by Calatayud *et al.*[65]

Both VO_2^+ and VO_2 have a bent geometry and their corresponding ground states are the $^1A_1$ and $^2A_1$ low-spin states, respectively. The C_{2v}-symmetry $^1A_1$ VO_2^+ and $^2A_1$ VO_2 species are more stable than the C_s-symmetry $^3A'$ VO_2^+ and $^4A''$ VO_2 by 41.9 kcal/mol and 43.8 kcal/mol, respectively. The high-spin $^3A'$ VO_2^+ and $^4A''$ VO_2 species are characterized by lengthening of one V-O bond by ~0.2 Å and loss of symmetry. Even though this finding is in agreement with previous work reported by Calatayud *et al.*,[65] our geometric parameters for VO_2 are closer to those reported by Chertihin *et al.*,[7] who employed the B3LYP/6-311+G* model chemistry.

Both VO_3^+ and VO_3 have a pyramidal geometry with C_s symmetry. The ground states of VO_3^+ and VO_3 are the $^1A'$ and $^2A'$ low-spin states. The low-spin $^1A'$ VO_3^+ and $^2A'$ VO_3 species are more stable than the high-spin $^3A''$ VO_3^+ and $^4A''$ VO_3 ones by 11.0 kcal/mol and 36.6 kcal/mol, respectively. Inspection of geometric parameters reveals that VO_3^+ and VO_3 have two different V-O bond lengths and O-V-O bond angles. The V-O bond length of the cation only decreases slightly (by less than 0.071 Å), while the bond angles decrease by as much as 13°, compared to the neutral cluster. Our results are in agreement with Calatayud's report that the ground states of VO_3^+ and VO_3 are the $^1A'$ and $^2A'$ low-spin states according to B3LYP/6-31G* calculations.

<u>$V_2O_4^+$ and V_2O_4</u>

Geometric parameters for the minimum-energy structures of the $V_2O_4^+$ and V_2O_4 isomers and their relative energies in different electronic states are shown in Figs. 3.1a and 3.1b, respectively. Both $V_2O_4^+$ and V_2O_4 have three geometric isomers: a linear-open structure without symmetry, a trans-four-membered ring structure and a cis-four-membered ring structure. The ground states of $V_2O_4^+$ and V_2O_4 are the $^2A'$ low-spin and

^3B_u high-spin states, respectively. The ground states of other isomers remain the low-spin state for the cation and the high-spin state for the neutral cluster. The C_s-symmetry $^2A'$ trans-$V_2O_4^+$ and the C_{2h}-symmetry ^3B_u trans-V_2O_4 are more stable than the C_s-symmetry $^2A'$ cis-$V_2O_4^+$ and the C_{2v}-symmetry $^3B_2$ cis-V_2O_4 by 4.5 kcal/mol and 3.8 kcal/mol, respectively. The ^2A linear-$V_2O_4^+$ and the ^3A linear-V_2O_4 are less stable than the corresponding minimum-structure of the cis-isomers by 22.6 kcal/mol and 33.1 kcal/mol, respectively. The relative energies point out that the trans-four-membered ring structure is the most stable structure for both $V_2O_4^+$ and V_2O_4. Our findings about the ground states of $V_2O_4^+$ and V_2O_4 are in good agreement with previously reported results by Justes *et al.*[32] The bridged V-O bond lengths are larger than the terminal V-O bond lengths for both $V_2O_4^+$ and V_2O_4 ground-state species. The bridged V-O bond lengths in the high-spin $^4A''$ $V_2O_4^+$ species do not change significantly, compared with the low-spin species, but one terminal V-O bond length is elongated by ~0.2 Å. Each of the bridged V-O bonds in the high-spin ^3B_u V_2O_4 species is elongated by ~0.08 Å and the terminal V-O bond lengths do not change significantly, compared with the low-spin ^1A_g V_2O_4 species. Our DFT calculation predicts a triplet ground state, in disagreement with the singlet ground state obtained by multireference averaged coupled-pair functional (MR-ACPF) calculations by Pykavy *et al.*,[60] but in agreement with previous DFT studies by Calatayud *et al.*[29] However, Calatayud *et al.* did not investigate the trans-isomers of $V_2O_4^+$ and V_2O_4, and they concluded that the most stable structure was the cis-four-membered ring structure of $V_2O_4^+$ and V_2O_4 with the $^2A'$ low-spin and $^3B_2$ high-spin ground states, respectively.

<u>$V_2O_5^+$ and V_2O_5</u>

Geometric parameters for the minimum-energy structures of $V_2O_5^+$ and V_2O_5 and their relative energies in different electronic states are shown in Fig. 3.2. Based on the aforementioned structures of $V_2O_4^+$ and V_2O_4, both four-membered-ring structures with C_s symmetry and open structures with no symmetry were investigated for both $V_2O_5^+$ and V_2O_5. The ground states of the $V_2O_5^+$ and V_2O_5 four-membered-ring structures correspond to $^2A'$ and $^1A'$ low-spin states, respectively, while the ground states of open structures also remain low spin states. The energies of C_s-symmetry $^2A'$ $V_2O_5^+$ and $^1A'$ V_2O_5 species are lower than those of C_1-symmetry ^2A $V_2O_5^+$ and ^1A V_2O_5 species by 9.4 kcal/mol and 6.4 kcal/mol, respectively, which indicates that four-membered-ring structures are the most stable. Geometric parameters do not change significantly between the low-spin $^2A'$ state and the high-spin $^4A''$ state of $V_2O_5^+$, with the exception of the V1-O3 bond, which is elongated by ~0.2 Å in the high-spin state. Recently, Asmis *et al.*[71] reported gas-phase infrared spectroscopy of $V_2O_5^+$, which support our finding that the ground-state of $V_2O_5^+$ is the $^2A'$ state, and not the $^2A''$ ground-state of $V_2O_5^+$ reported in previous theoretical studies.[29,32] The main difference in four-memebered-ring V_2O_5 geometric parameters between the low-spin $^1A'$ and the high-spin $^3A''$ states lies in the elongation of the terminal V2-O4 bond for the high-spin $^3A''$ state, in agreement with the previous work by Calatayud *et al.*[29] again.

$V_2O_6^+$ and V_2O_6

Geometric parameters for the minimum-energy structures of $V_2O_6^+$ and V_2O_6 and their relative energies in different electronic states are shown in Figs. 3.3a and 3.3b. Open structure and two kinds of four-membered ring structures, **2** with C_s symmetry and **1** with no symmetry, were investigated. The ground states of $V_2O_6^+$ and V_2O_6 of structures **1** are

the ^2A low-spin and ^3A high-spin states, respectively. The ^2A $V_2O_6^+$ structure **1** is the most stable structure, and is more stable than the ^2A $V_2O_6^+$ open structure and the $^4A''$ $V_2O_6^+$ structure **2** by 34.6 kcal/mol and 52.1 kcal/mol, respectively. Similarly, in the neutral cluster, the most stable structure is the ^3A V_2O_6 structure **1**, which is more stable than the ^3A V_2O_6 structure **2** and the ^3A V_2O_6 open structure by 13.6 kcal/mol and 46.6 kcal/mol, respectively. In the cations, the energy differences between the doublet and quartet states are no larger than 10.8 kcal/mol. In the neutral cluster, the energy difference between the singlet and triplet states of the most stable structure **1** is 6.7 kcal/mol, which is smaller than the energy difference of 18.1 kcal/mol between the singlet and triplet states for structure **2**. Structure **1** can be considered as a complex of the trans-four-membered ring structure $V_2O_4^+$ with O_2. The geometric parameters of **1** indicate that the bond lengths of the terminal V2-O4 and V2-O5 bonds are larger than other terminal V-O bonds of $V_2O_4^+$ by ~0.4 Å, and the calculated binding energy of O_2 (O4-O5) to the trans-four-membered ring $V_2O_4^+$ is only 1.20 eV, which indicates that O_2 detaches easily from $V_2O_6^+$ to form $V_2O_4^+$. This finding could rationalize the experimental observation[8] that the main product ions of collision-induced dissociation (CID) of $V_2O_6^+$ clusters are $V_2O_4^+$ cluster ions. For V_2O_6, the V2-O4 and V2-O5 bonds of structure **1** are elongated by ~0.2 Å and the O4-O5 bond is shortened by ~0.1 Å in the triplet state, compare to the structure in the singlet state.

$V_3O_6^+$ and V_3O_6

Geometric parameters for the minimum-energy structures of $V_3O_6^+$ and V_3O_6 and their relative energies in different electronic states are shown in Fig. 3.4. An open structure with no symmetry and a six-membered ring structure with C_{3v} symmetry were

investigated. The ground states of $V_3O_6^+$ and V_3O_6 are the $^3A''$ and $^4A'$ high-spin states, respectively. In the cation, the energy difference between the singlet and triplet states for the open structure is only 2.9 kcal/mol, while the energy difference between the singlet and triplet states is 13.2 kcal/mol for the six-membered ring structure. For neutral V_3O_6, the energy differences between the doublet and quartet states for the open and six-membered ring structures are 1.6 kcal/mol and 18.8 kcal/mol, respectively. The ^3A $V_3O_6^+$ and ^4A V_3O_6 species are less stable than the $^3A''$ $V_3O_6^+$ and $^4A'$ V_3O_6 ones by 31.5 kcal/mol and 44.0 kcal/mol, which indicates that the six-membered ring structures are the most stable ones. The difference in the V-O bond lengths in the singlet and triplet states of the open structures is rather small (~0.02 Å). The high-spin C_s-symmetry $^3A''$ $V_3O_6^+$ is characterized by lengthening the bridged V-O bonds and one terminal V-O bond around 0.2 Å, compared to the low-spin structure. Geometric parameters do not change significantly between low-spin and high-spin states for both the open structure and the six-membered ring structure of the neutral cluster.

$V_3O_7^+$ and V_3O_7

Geometric parameters for the minimum-energy structures of $V_3O_7^+$ and V_3O_7 and their relative energies in different electronic states are shown in Fig. 3.5. The open structure with no symmetry and the six-membered ring structure with C_s symmetry were investigated. The ground states of $V_3O_7^+$ and V_3O_7 correspond to $^3A''$ and $^4A'$ high-spin states, respectively. In the cation, the energy difference between the singlet and triplet states of the six-membered ring and the open structures are 10.0 kcal/mol and 12.2 kcal/mol, respectively. In the neutral cluster, the energy differences between the doublet and quartet states of the six-membered ring and open structures are 6.6 kcal/mol and 8.4

kcal/mol, respectively. The ^3A $V_3O_7^+$ and ^4A V_3O_7 species are more stable than the $^3A''$ $V_3O_7^+$ and t $^4A'$ V_3O_7 species by 30.3 kcal/mol and 14.9 kcal/mol, respectively, which points out that the six-membered-ring structures are more stable than the open structures. The geometric parameters of $V_3O_7^+$ and V_3O_7 in different electronic states are not significantly different.

$V_3O_8^+$ and V_3O_8

Geometric parameters for the minimum-energy structures of $V_3O_8^+$ and V_3O_8 and their relative energies in different electronic states are displayed in Fig. 3.6. The open structure with no symmetry and the six-membered ring structure with C_s symmetry were investigated. The ground states of $V_3O_8^+$ and V_3O_8 are the $^3A'$ high-spin and the $^2A'$ low-spin states, respectively. In the cation, the energy difference between the singlet and triplet states for the six-membered ring and open structures are 13.1 kcal/mol and 8.6 kcal/mol, respectively, while in the neutral cluster the energy difference between the doublet and quartet states for the six-membered ring and open structures are 14.2 kcal/mol and 9.3 kcal/mol, respectively. The $^3A'$ $V_3O_8^+$ and $^2A'$ V_3O_8 species are more stable than the ^3A $V_3O_8^+$ and ^2A V_3O_8 ones by 56.3 kcal/mol and 21.4 kcal/mol, respectively, which indicates that six-membered-ring structures are more stable than the open ones. The V1-O2 and V2-O2 bonds are elongated by ~0.05 Å in the $^3A'$ $V_3O_8^+$, compared to the $^1A'$ $V_3O_8^+$. The geometric parameters of $V_3O_8^+$ and V_3O_8 species in different electronic states are not significantly different.

$V_4O_8^+$ and V_4O_8

Geometric parameters for the minimum-energy structures of $V_4O_8^+$ and V_4O_8 and their relative energies in different electronic states are shown in Figs. 3.7a and 3.7b. The open

structure with no symmetry and the cage-like structure with C_s symmetry were investigated. The ground states of $V_4O_8^+$ and V_4O_8 correspond to the $^2A'$ low-spin state and the $^3A'$ high-spin state, respectively. In the cation, the energy difference between the doublet and quartet states for the cage-like and open structures are 7.5 kcal/mol and 13.5 kcal/mol, respectively, while in the neutral cluster, the energy difference between singlet and doublet states for the cage-like and open structures are 7.0 kcal/mol and 9.6 kcal/mol, respectively. The cage-like $^2A'$ $V_4O_8^+$ and $^3A'$ V_4O_8 species are much more stable than the ^4A $V_4O_8^+$ and ^3A V_4O_8 open structures by 84.4 kcal/mol and 100.7 kcal/mol, respectively. The geometric parameters of $V_4O_8^+$ and V_4O_8 in different electronic states are not significantly different.

$V_4O_9^+$ and V_4O_9

Geometric parameters for the minimum-energy structures of $V_4O_9^+$ and V_4O_9 and their relative energies in different electronic states are shown in Fig. 3.8. Only cage-like structures are reported since the open structures are very unstable. The ground states of $V_4O_9^+$ and V_4O_9 are the $^2A_1$ low-spin and $^3A_2$ high-spin states, respectively. The C_{3v}-symmetry $^2A_1$ $V_4O_9^+$ is more stable than the C_s-symmetry $^4A'$ $V_4O_9^+$ by 43.9 kcal/mol, while the C_{3v}-symmetry $^1A_1$ V_4O_9 is less stable than the C_{3v}-symmetry $^3A_2$ V_4O_9 by 10.1 kcal/mol. The geometric parameters of $V_4O_9^+$ and V_4O_9 in different electronic states are not significantly different.

$V_4O_{10}^+$ and V_4O_{10}

Geometric parameters for the minimum-energy structures of $V_4O_{10}^+$ and V_4O_{10} and their relative energies in different electronic states are shown in Fig. 3.9. Cage-like structures with C_{3v} symmetry were investigated. The ground states of $V_4O_{10}^+$ and V_4O_{10} correspond

to the $^2A_1$ and $^1T_2$ low-spin states. The C_{3v}-symmetry $^2A_1$ $V_4O_{10}^+$ is more stable than the C_s-symmetry $^4A'$ $V_4O_{10}^+$ by 31.2 kcal/mol, while the T_d-symmetry $^1T_2$ V_4O_{10} is more stable than the C_{3v}-symmetry $^3A_2$ V_4O_{10} by 5.2 kcal/mol. The geometric parameters of $V_4O_{10}^+$ and V_4O_{10} in different electronic states are not significantly different.

3.3.3. Charge Distributions for Selected $V_xO_y^+$

Charge distributions and spin densities for the most stable structures of $V_2O_y^+$ (y=4-6) cations are calculated, based on the Mulliken population analysis and natural population analysis, and collected in Table 3.4. Results of the Mulliken population analysis indicate that the cation excess positive charge is always located on the vanadium atoms and almost equally distributed over all the vanadium atoms of $V_2O_y^+$ (y=4-6) cluster cations. The same trend is observed from the result of natural population analysis. Spin densities show that the unpaired electron is located on the vanadium atom V1 of $^2A'$ $V_2O_4^+$ and it occupies a d-orbital of the vanadium atom. However, the unpaired electron is found on the terminal oxygen atom O4 of $^2A'$ $V_2O_5^+$, which results in weakening of the terminal V2-O4 bond, and explains why the V2-O4 bond is larger than the other terminal V-O bonds by ~0.1 Å. For ^2A $V_2O_6^+$, the unpaired electron is delocalized on the terminal oxygen atoms O4 and O5, which explains why the V2-O4 and V2-O5 bonds are weaker and longer than the other terminal V-O bonds, and why $V_2O_6^+$ is prone to fragmentation into $V_2O_4^+$ and O_2.

Charge distributions for the most stable structures of polyvanadium oxide $V_xO_y^+$ (x=3-4, y=6-10) clusters are calculated, based on Mulliken population analysis, and shown in Table 3.5. The excess positive charge is again almost equally distributed over all the vanadium atoms in $V_xO_y^+$ (x=3-4, y=6-10) clusters. The vanadium atoms of $V_3O_y^+$ (y=6-

8) and of the larger $V_4O_y^+$ (y=8-10) clusters have a positive Mulliken charge in the range 1.12-1.21 e and 1.14-1.26 e, respectively, indicating that charge distributions on vanadium atoms do not change significantly with cluster size. In the most stable structures of $V_3O_y^+$ (y=6-8) and $V_4O_y^+$ (y=8-10), the vanadium atoms always coordinated to three or four oxygen atoms, resulting in similar formal oxidation states and charge distributions for the vanadium atoms.

3.3.4. Ionization Potentials and Binding Energies

We now turn our attention to the ionization potential (IP) of neutral vanadium oxide clusters. We report both the adiabatic and vertical IPs, which are calculated as the energy difference between the optimized neutral and cationic ground-state structures, and as the energy difference between the neutral ground-state structure and the cation in the same geometry, respectively. Adiabatic and vertical IPs are shown in Fig. 3.10 for neutral V_2O_y (y=4-6) clusters. Both the adiabatic and vertical IPs increase as a function of the cluster oxygen-to-vanadium ratio, i.e. neutral clusters with a larger oxygen content have larger IPs, in good agreement with previous work by Calatayud *et al.* [29] As can be seen from Table 3.4, the unpaired electron is located on two terminal oxygen atoms for $V_2O_6^+$ and one terminal oxygen atom for $V_2O_5^+$. However, it is located on one vanadium atom for $V_2O_4^+$, which indicates that neutral V_2O_6 and V_2O_5 clusters lose an electron from the oxygen atoms, while the neutral V_2O_4 loses an electron from the vanadium atom upon ionization. The oxygen atom is more electronegative and binds its electrons more tightly than the vanadium atom, therefore neutral clusters with a larger oxygen content have larger IP values. The adiabatic and vertical IPs for VO_2, V_2O_4, V_3O_6 and V_4O_8 clusters, which have the same oxygen-to-vanadium ratio of 2, are shown in Fig. 3.11. The

adiabatic and vertical IPs for these clusters are in the range 7.51-8.59 eV and 8.27-9.08 eV, respectively. The IPs of vanadium oxide clusters are not found to change significantly as a function of size for cluster with a constant oxygen-to-vanadium ratio, except for VO_2.

The binding energies per atom of $V_xO_y^+$ (x=1-4, y=1-10) vanadium oxide cluster cations are calculated and collected in Table 3.6. The binding energies per atom are calculated for the most stable structure of $V_xO_y^+$ with the following formula: [32]

$$E_{b/n}=[E(V_xO_y^+)-E(V^+)-(x-1)E(V)-yE(O)]/(x+y)$$

The binding energies per atom increase with cluster size, and they are especially large for the larger $V_4O_y^+$ (y=8-10) clusters. Inspection of these larger clusters reveals that they all possess cage-like compact structures, with stronger V-O bonds. We note the exception of $V_2O_6^+$ and $V_3O_8^+$, which have lower binding energies than other bivanadium and trivanadium oxide clusters, most likely due to weaker and longer V-O bonds (many in the range 1.910-2.141 Å for $V_2O_6^+$ and $V_3O_8^+$).

3.4. Conclusions

In the present work, we tested and compared the reliability and efficiency of various functionals and basis sets to investigate vanadium oxide clusters via DFT calculations. The molecular geometry and electronic structure of vanadium oxide clusters $V_xO_y^+$ and V_xO_y (x=1-4, y=1-10) were then investigated with the model chemistry seemed most appropriate. Our results can be summarized as follows: (1) The B3LYP/TZVP model chemistry seems appropriate to investigate vanadium oxide clusters as the VO_2^+ dissociation energy calculated with this model chemistry lies in the range of experimental data. However, the less computationally intensive PLAP4/DZVP+aux. model chemistry

yields a similar accuracy as B3LYP/TZVP, but for half the computational cost, based on single-point calculations for VO_2^+ and $V_3O_6^+$. The PLAP4/DZVP+aux. model chemistry is thus more suitable for investigating large vanadium oxide clusters. (2) Geometric parameters for VO^+ and VO predicted by the PLAP4/DZVP+aux. model chemistry are in good agreement with experimental data.[90] Our results for the molecular structures and electronic properties of bivanadium oxide $V_2O_y^+$ and V_2O_y (y=4-6) clusters are essentially in agreement with previously reported B3LYP/6-31G* results, except for the ground-state of $V_2O_5^+$, which remains difficult to characterize because of the numerous almost degenerate electronic states. The minimum-energy structures of larger polyvanadium oxide $V_xO_y^+$ and V_xO_y (x=3, 4; y=6-10) clusters were also predicted by the PLAP4/DZVP+aux. model chemistry. (3) For vanadium oxide cluster cations, the excess charge is delocalized and almost equally distributed over the vanadium atoms. Charge distributions do not change significantly with cluster size. (4) Both the adiabatic and vertical IPs of neutral vanadium oxide clusters increase as a function of the cluster oxygen-to-vanadium ratio as the electron tends to be removed from the more electronegative oxygen atom upon the ionization of clusters with a higher oxygen content. On the other hand, the IPs of vanadium oxide clusters are not found to change significantly as a function of cluster size for clusters with a constant oxygen-to-vanadium ratio. The binding energies per atom of vanadium oxide cluster cations increase with cluster size, due to the more compact structure of larger clusters.

Table 3.1.Comparison of Experimental and Calculated VO_2^+ Dissociation Energies[a]

	Number of basis functions for VO_2^+	Type of functional	D_0 (eV)
Experiment[8]	-	-	3.51±0.36
B3LYP/6-31G*	51	hybrid	4.36
B3LYP/DZVP	38	hybrid	4.25
B3LYP/TZVP	56	hybrid	3.84
B3PW91/TZVP	56	hybrid	3.81
B3PW86/TZVP	56	hybrid	4.04
SVWN/TZVP	56	LDA	6.09
BLYP/TZVP	56	GGA	5.10
PW91PW91/TZVP	56	GGA	5.30
BLAP1/DZVP+aux.	38	meta-GGA	4.95
BLAP3/DZVP+aux.	38	meta-GGA	5.01
PLAP4/DZVP+aux.	38	meta-GGA	3.84

a. The calculated VO_2^+ dissociation energy is the energy change for the reaction $VO_2^+(^1A) \longrightarrow VO^+(^3\Sigma) + O(^3P_2)$. Zero-point energy corrections are based on harmonic vibrational frequencies.

Table 3.2. Computational Cost of Various Model Chemistries[a]

Model Chemistry	CPU time for VO_2^+ (min)	CPU time for $V_3O_6^+$ (min)
SVWN/TZVP	3.0	248
BLYP/TZVP	1.5	125
PW91PW91/TZVP	2.9	230
B3LYP/TZVP	1.7	156
B3PW91/TZVP	2.8	207
B3PW86/TZVP	2.9	212
BLAP1/DZVP+aux.	0.6	53
BLAP3/DZVP+aux.	0.6	52
PLAP4/DZVP+aux.	0.6	60

a. Based on CPU (Intel PIV 2.0GHz) time required to run a single-point calculation for VO_2^+ and $V_3O_6^+$

Table 3.3. PLAP4/DZVP+aux. Geometric Parameters and Relative Energies for VO_y^+ and VO_y (y=1-3)

Electronic state	Bond length (Å) V-O1	V-O2 V-O3	Bond angle (°) O1-V-O2 O1-V-O3	Dihedral angle (°) O1-V-O2-O3	Expt. bond length (Å)	Relative energy (kcal/mol)
$VO^+(^3\Sigma)$	1.546	-	-	-	1.54	0.0
$VO^+(^1\Delta)$	1.526	-	-	-		24.4
$VO(^4\Sigma)$	1.590	-	-	-	1.589	0.0
$VO(^2\Sigma)$	1.578	-	-	-		13.8
$VO_2^+(^1A_1)$	1.545	1.545	105.17	-	-	0.0
$VO_2^+(^3A')$	1.539	1.746	109.13	-	-	41.9
$VO_2(^2A_1)$	1.589	1.589	107.36	-	-	0.0
$VO_2(^4A'')$	1.584	1.864	116.64	-	-	43.8
$VO_3^+(^1A')$	1.541	1.744	112.28	99.58	-	0.0
$VO_3^+(^3A'')$	1.571	1.711	115.20	105.98	-	11.0
$VO_3(^2A')$	1.576	1.786	123.68	106.49	-	0.0
$VO_3(^4A')$	1.596	1.782	128.79	111.12	-	36.6

Table 3.4. PLAP4/DZVP+aux. Atomic Charge Distributions for $V_2O_y^+$(y=4-6)

	Population analysis	Atomic charges			
		V1	V2	O4	O5
$V_2O_4^+$ ($^2A'$)	Mulliken	+1.41 (1.10)	+1.45 (0.04)	-	-
	natural	+1.52 (1.11)	+1.48 (0.12)	-	-
$V_2O_5^+$ ($^2A'$)	Mulliken	+1.36 (-0.09)	+1.48 (-0.02)	-0.21(0.99)	-
	natural	+1.36 (-0.06)	+1.52 (-0.04)	-0.21(0.96)	-
$V_2O_6^+$ (^2A)	Mulliken	+1.23 (-0.11)	+1.46 (0.01)	-0.05(0.51)	-0.01(0.58)
	natural	+1.25 (-0.04)	+1.51 (-0.07)	-0.06(0.50)	0.02(0.57)

a. Based on Mulliken and natural population analyses (spin density in parentheses).

Table 3.5. PLAP4/DZVP+aux. Atomic Charge Distributions for $V_xO_y^+$(x=3-4, y=6-10)[a]

	Atomic Charges			
	V1	V2	V3	V4
$V_3O_6^+(^3A'')$	+1.18	+1.18	+1.18	-
$V_3O_7^+(^3A'')$	+1.12	+1.12	+1.14	-
$V_3O_8^+(^3A')$	+1.21	+1.21	+1.12	-
$V_4O_8^+(^2A')$	+1.18	+1.18	+1.14	+1.14
$V_4O_9^+(^2A_1)$	+1.21	+1.21	+1.21	+1.18
$V_4O_{10}^+(^2A_1)$	+1.26	+1.26	+1.26	+1.26

a. Based on Mulliken population analysis

Table 3.6. PLAP4/DZVP+aux. Binding Energies per Atom for $V_xO_y^+$ (x=1-4, y=1-10)[a]

	VO^+	VO_2^+	VO_3^+	$V_2O_4^+$	$V_2O_5^+$	$V_2O_6^+$
$E_{b/n}$ (eV)	2.78	3.48	3.55	4.40	4.51	4.10
	$V_3O_6^+$	$V_3O_7^+$	$V_3O_8^+$	$V_4O_8^+$	$V_4O_9^+$	$V_4O_{10}^+$
$E_{b/n}$ (eV)	4.58	4.65	4.53	4.99	5.09	5.21

a. Calculated according to the formula
$E_{b/n}=[E(V_xO_y^+)-E(V^+)-(x-1)E(V)-yE(O)]/(x+y)$

$V_2O_4^+$

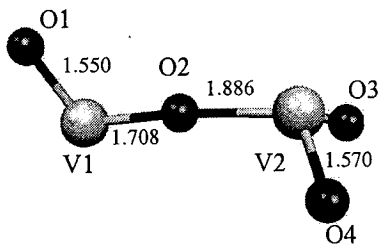

^2A (27.1)

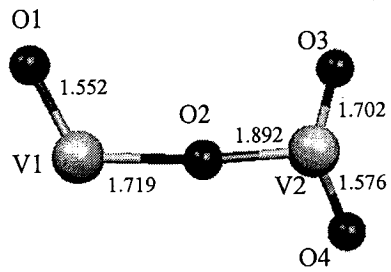

^4A (62.8)

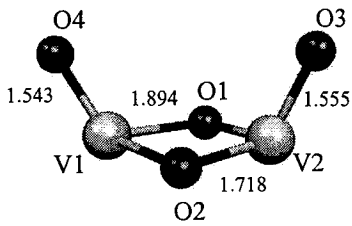

$^2A'$ (4.5)

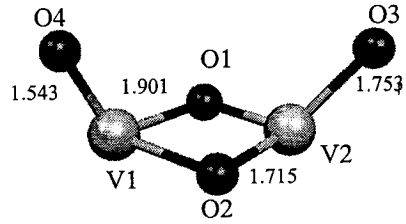

$^4A''$ (42.4)

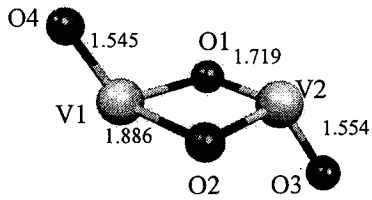

$^2A'$ (0.0)

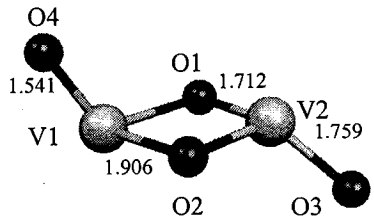

$^4A''$ (46.5)

Fig. 3.1a. PLAP4/DZVP+aux. geometric parameters (bond lengths in Å) and relative energies (in kcal/mol) for $V_2O_4^+$

V_2O_4

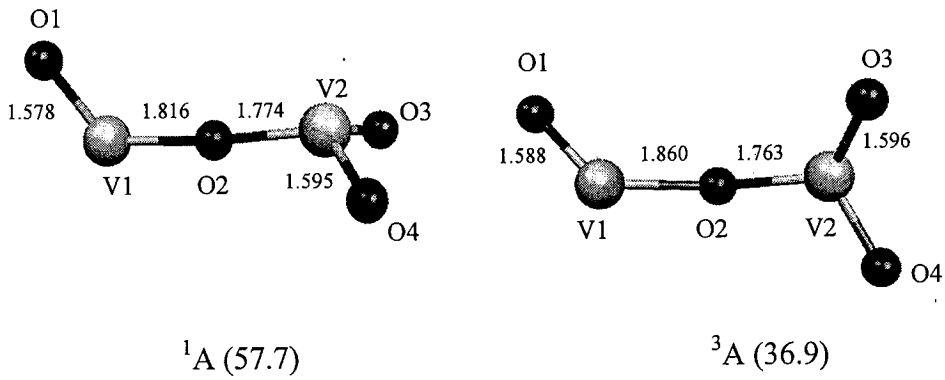

^1A (57.7) ^3A (36.9)

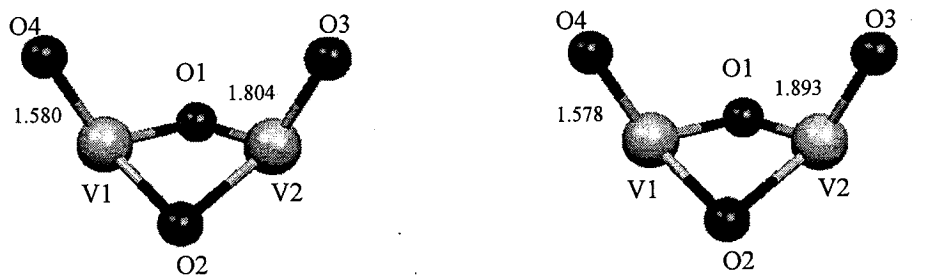

$^1A_1$ (13.2) $^3B_2$ (3.8)

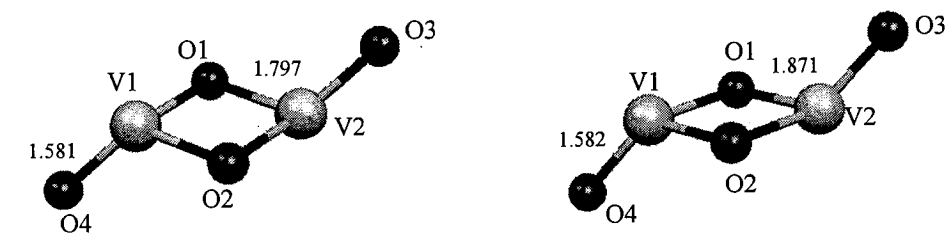

^1A_g (22.0) ^3B_u (0.0)

Fig. 3.1b. PLAP4/DZVP+aux. geometric parameters (bond lengths in Å) and relative energies (in kcal/mol) for V_2O_4

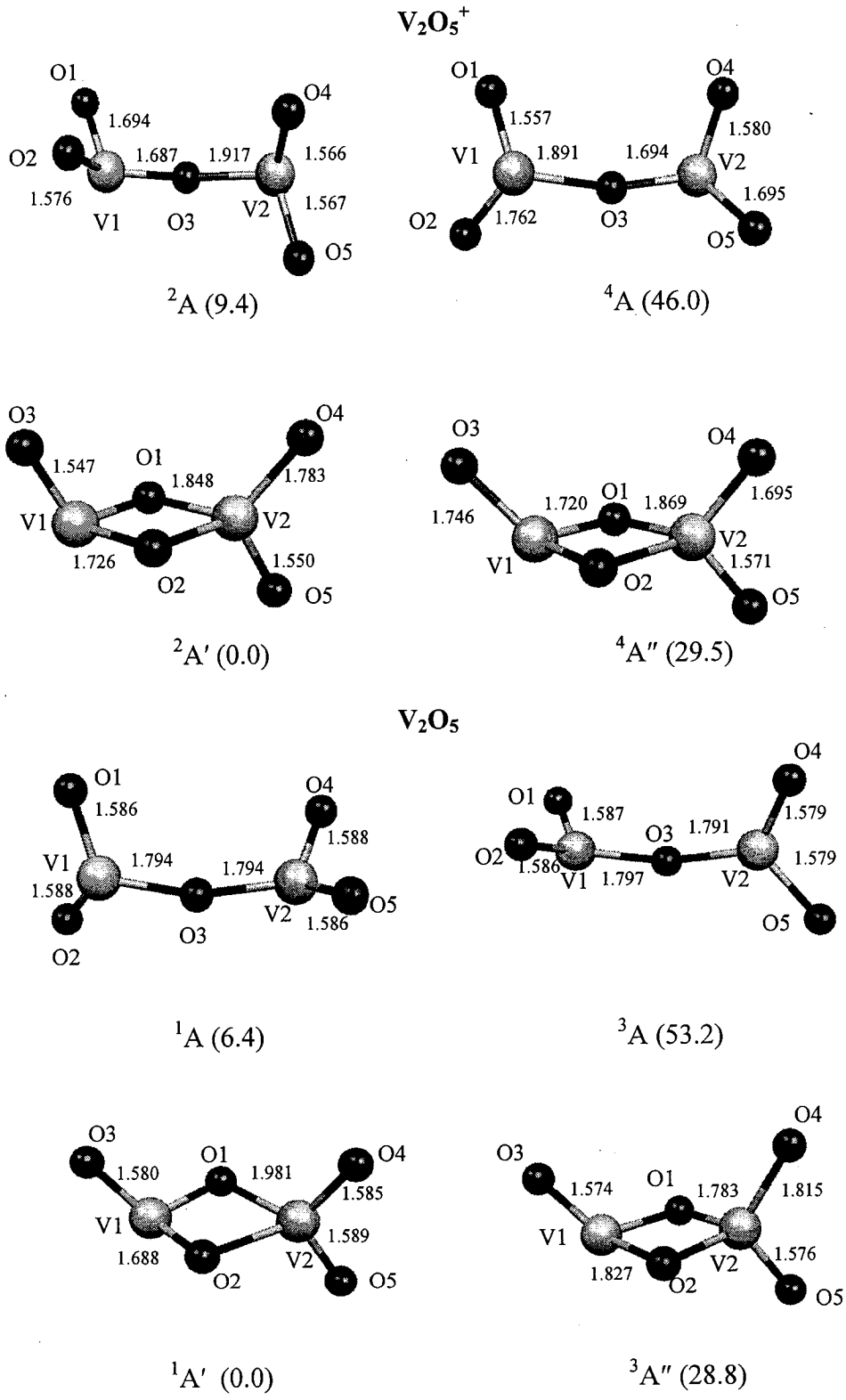

Fig. 3.2. PLAP4/DZVP+aux. geometric parameters (bond lengths in Å) and relative energies (in kcal/mol) for $V_2O_5^+$ and V_2O_5

$V_2O_6^+$

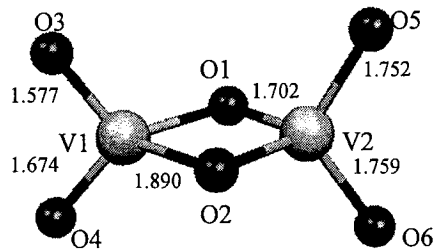

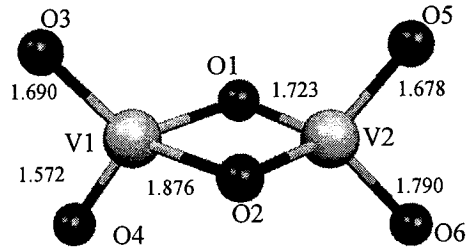

2 $^2A'$ (58.2)

$^4A''$ (52.1)

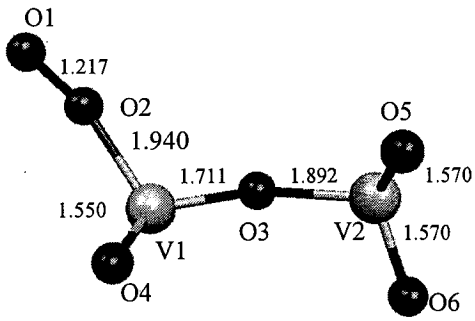

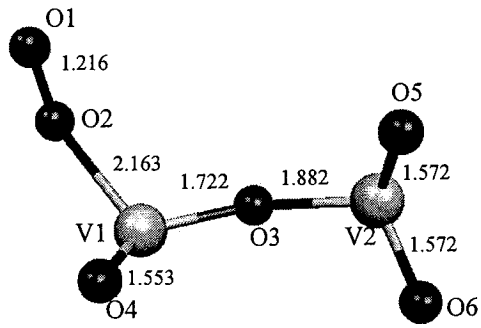

^2A (34.6)

^4A (39.5)

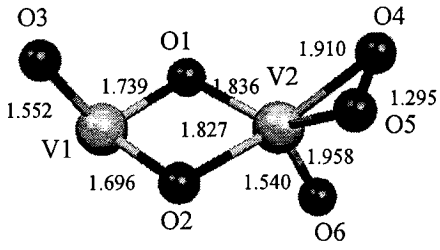

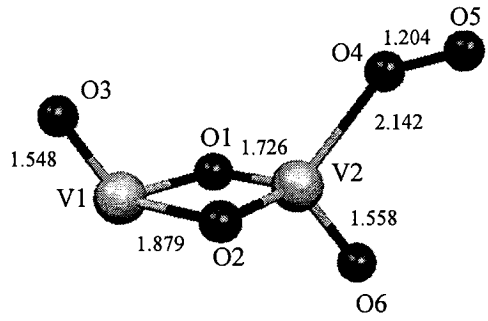

1 ^2A (0.0)

^4A (10.8)

Fig. 3.3a. PLAP4/DZVP+aux. geometric parameters (bond lengths in Å) and relative energies (in kcal/mol) for $V_2O_6^+$

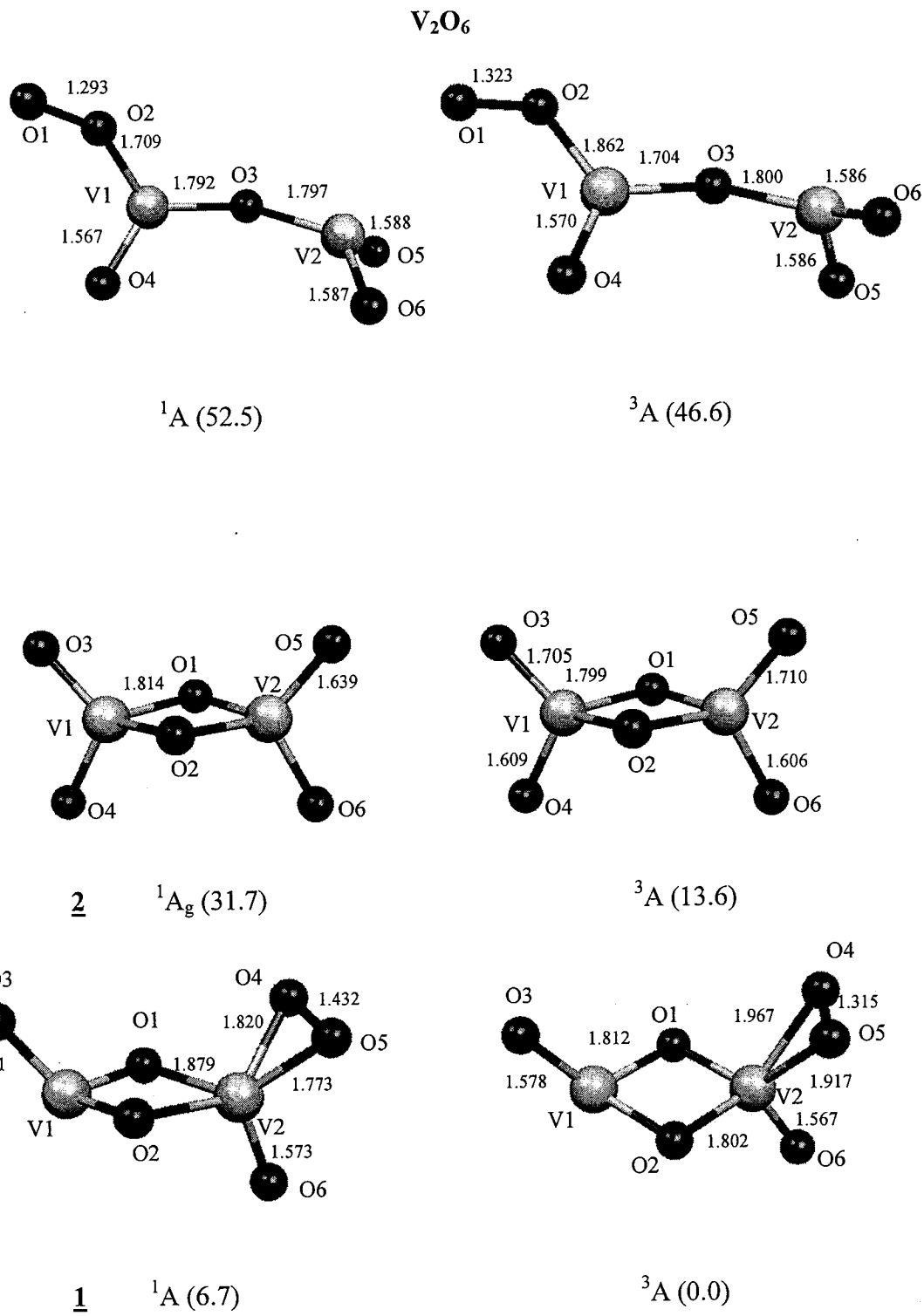

Fig. 3.3b. PLAP4/DZVP+aux. geometric parameters (bond lengths in Å) and relative energies (in kcal/mol) for V_2O_6

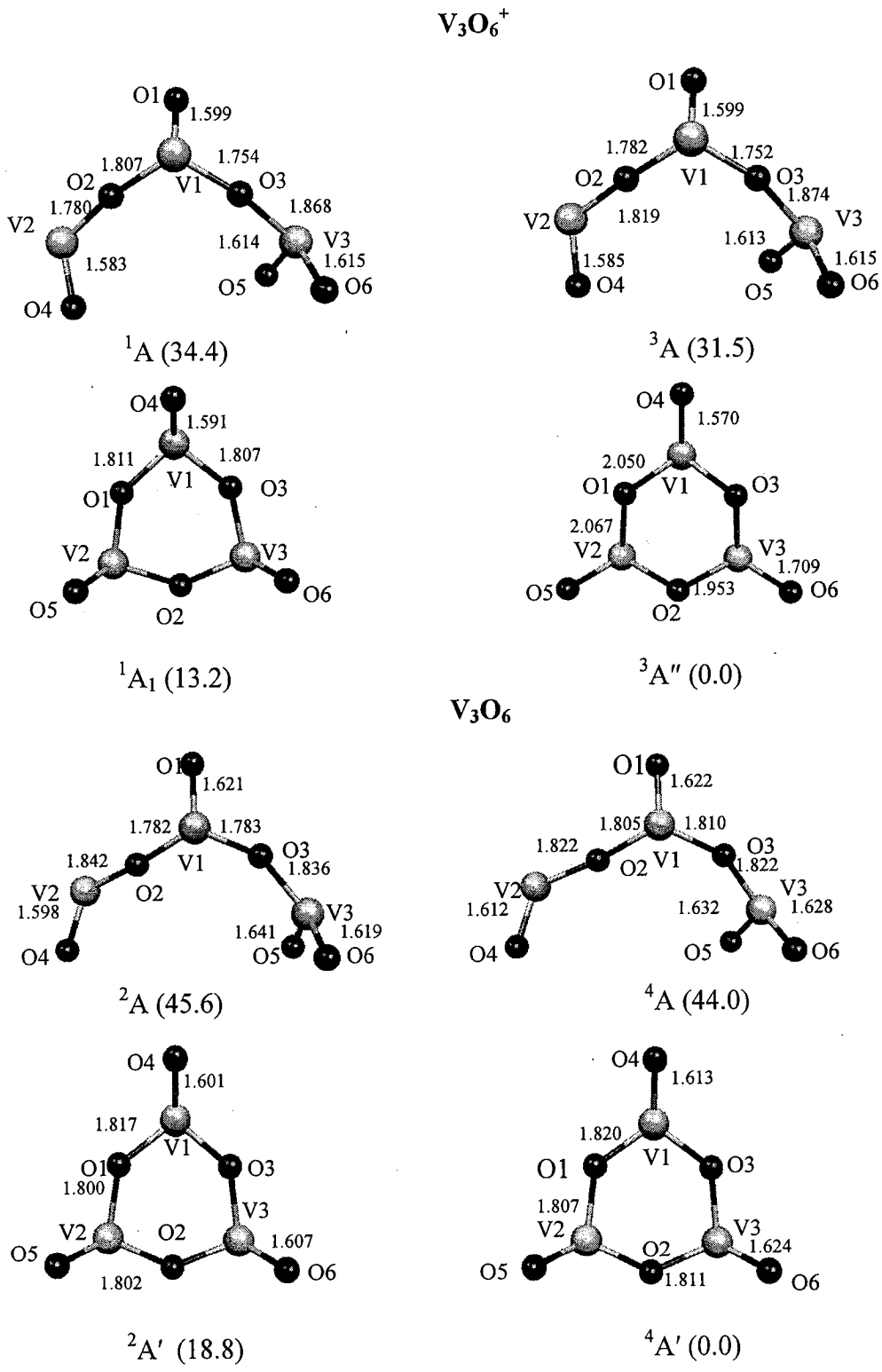

Fig. 3.4. PLAP4/DZVP+aux. geometric parameters (bond lengths in Å) and relative energies (in kcal/mol) for $V_3O_6^+$ and V_3O_6

$V_3O_7^+$

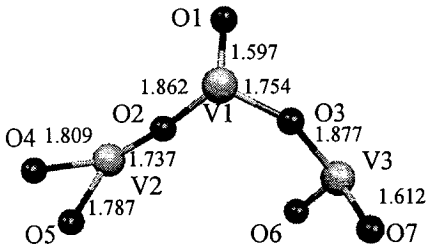

^1A (42.5)

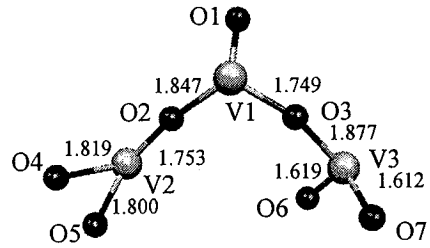

^3A (30.3)

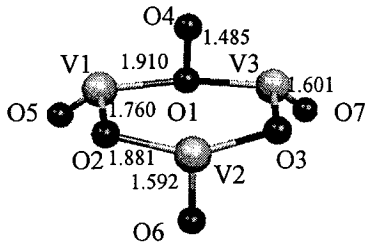

$^1A'$ (10.0)

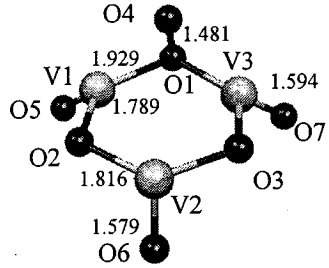

$^3A''$ (0.0)

V_3O_7

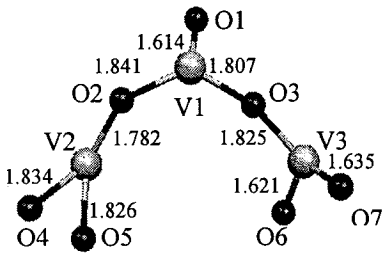

^2A (23.3)

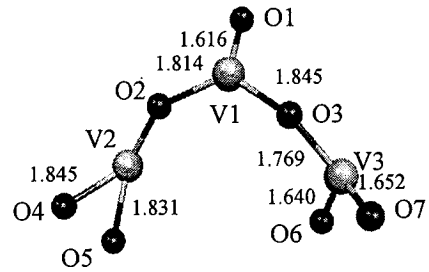

^4A (14.9)

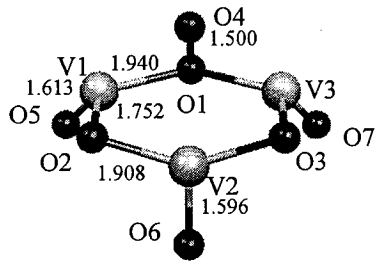

$^2A'$ (6.6)

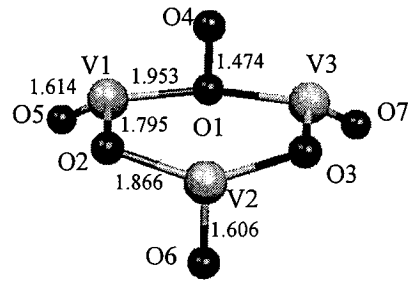

$^4A'$ (0.0)

Fig. 3.5. PLAP4/DZVP+aux. geometric parameters (bond lengths in Å) and relative energies (in kcal/mol) for $V_3O_7^+$ and V_3O_7

$V_3O_8^+$

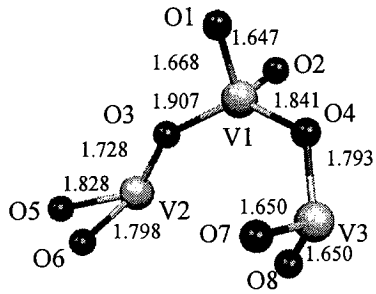

^{1}A (64.9)

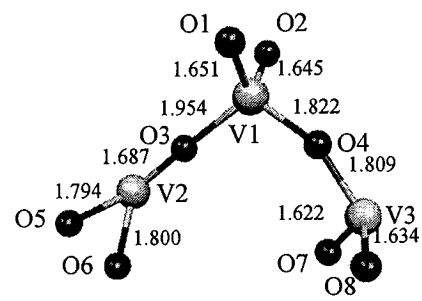

^{3}A (56.3)

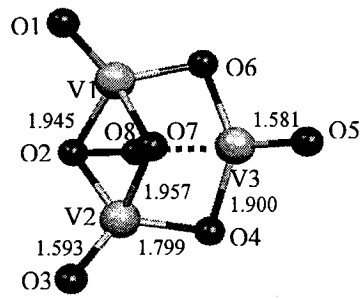

^{1}A′ (13.1)

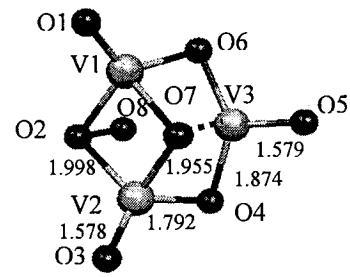

^{3}A′ (0.0)

V_3O_8

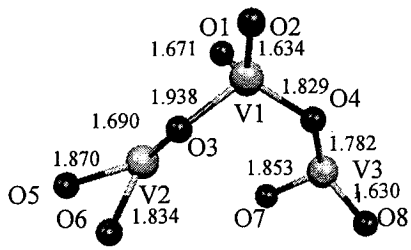

^{2}A (21.4)

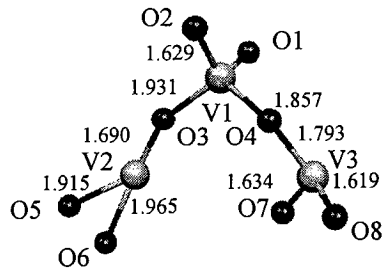

^{4}A (30.7)

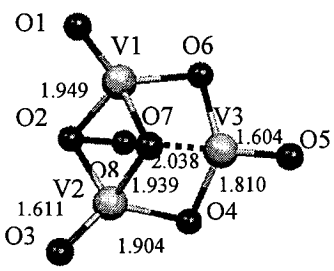

^{2}A′ (0.0)

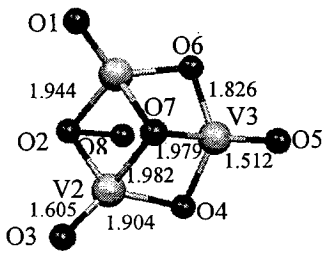

^{4}A′ (14.2)

Fig. 3.6. PLAP4/DZVP+aux. geometric parameters (bond lengths in Å) and relative energies (in kcal/mol) for $V_3O_8^+$ and V_3O_8

$V_4O_8^+$

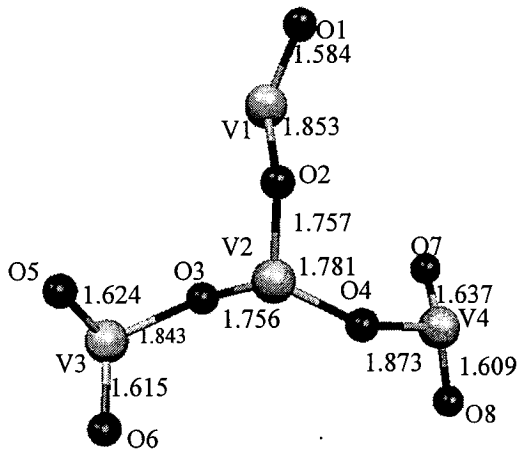

^2A (97.9)

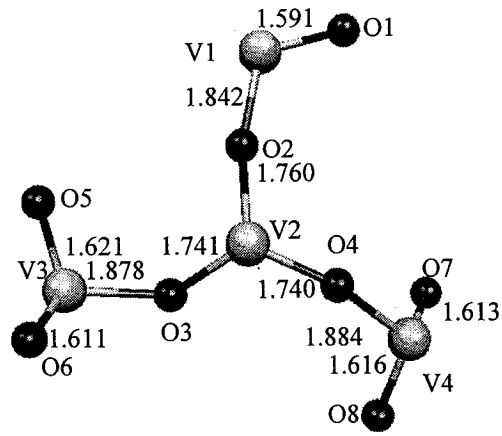

^4A (84.4)

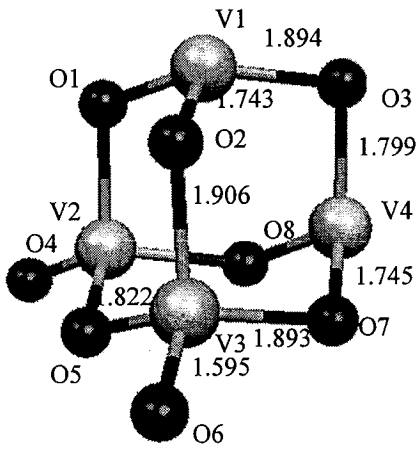

$^2A''$ (0.0)

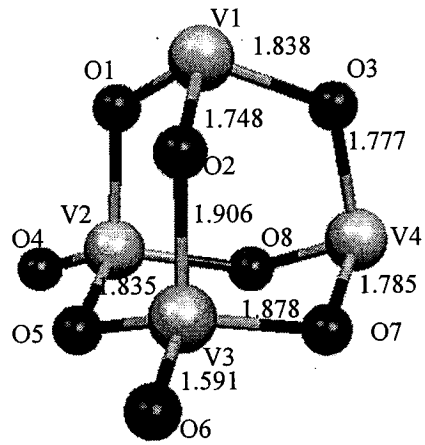

$^4A'$ (7.5)

Fig. 3.7a. PLAP4/DZVP+aux. geometric parameters (bond lengths in Å) and relative energies (in kcal/mol) for $V_4O_8^+$

V_4O_8

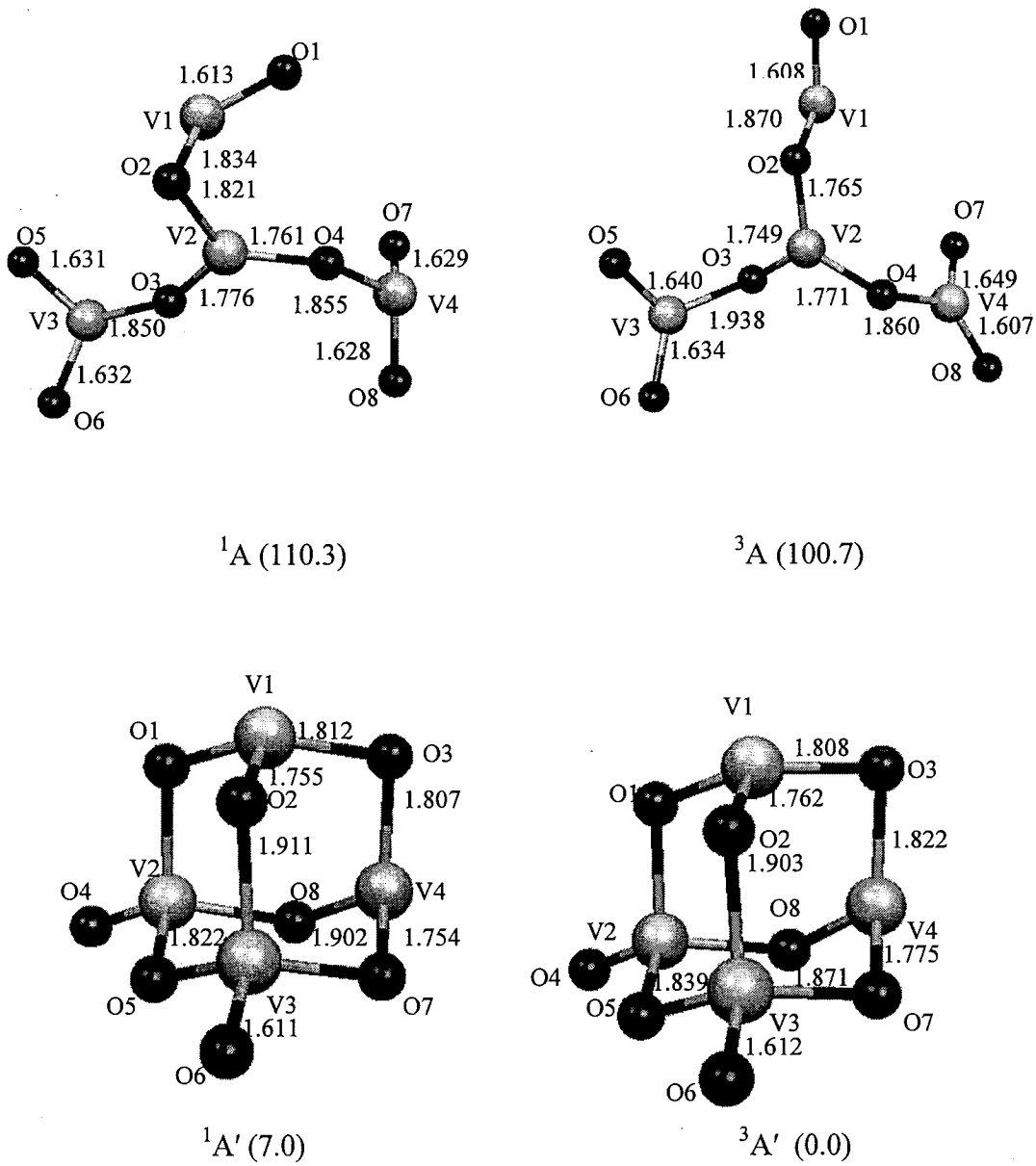

^{1}A (110.3) ^{3}A (100.7)

^{1}A′ (7.0) ^{3}A′ (0.0)

Fig. 3.7b. PLAP4/DZVP+aux. geometric parameters (bond lengths in Å) and relative energies (in kcal/mol) for V_4O_8

$V_4O_9^+$

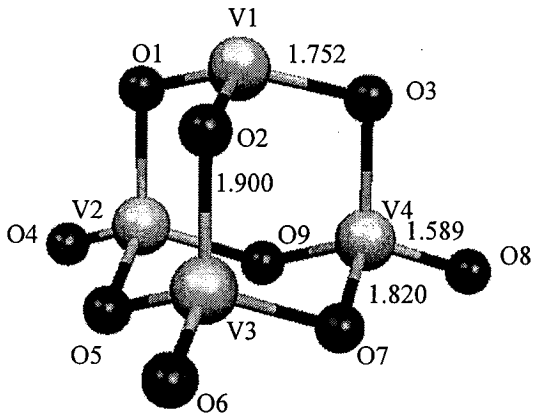

$^2A_1$ (0.0)

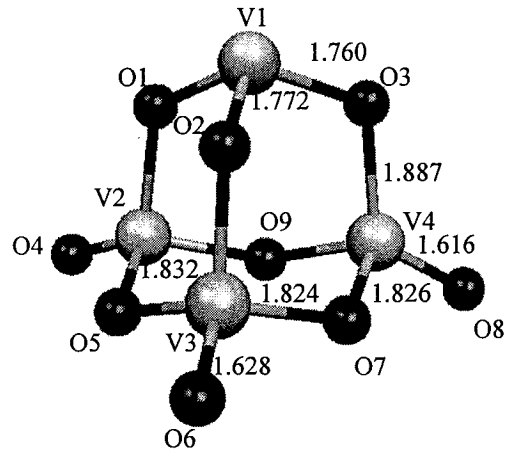

$^4A'$ (43.9)

V_4O_9

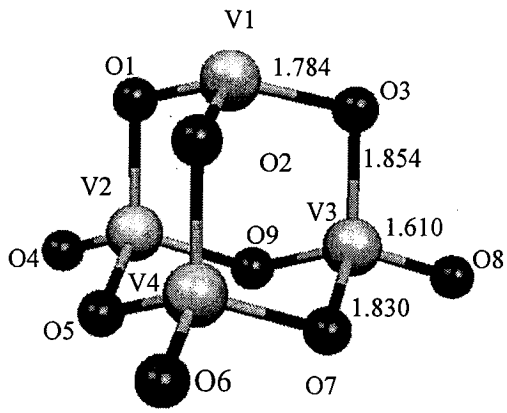

$^1A_1$ (10.1)

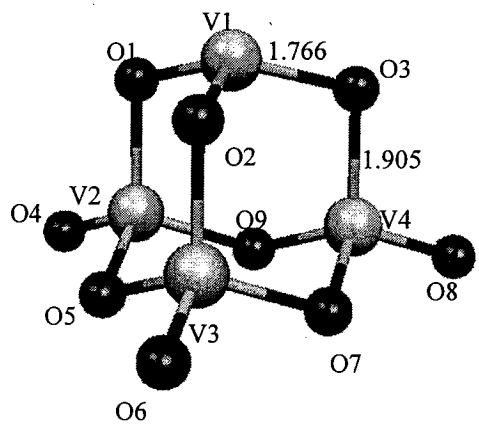

$^3A_2$ (0.0)

Fig. 3.8. PLAP4/DZVP+aux. geometric parameters (bond lengths in Å) and relative energies (in kcal/mol) for $V_4O_9^+$ and V_4O_9

$V_4O_{10}^+$

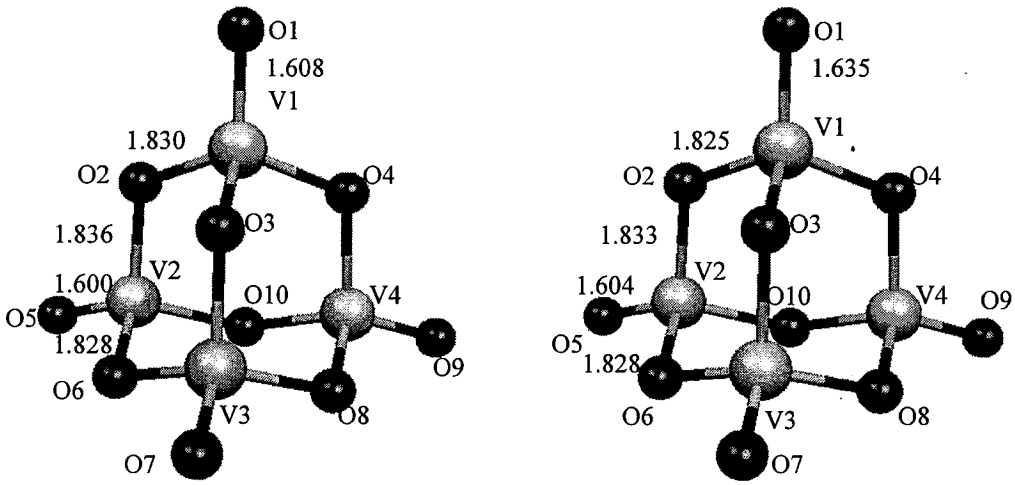

$^2A_1$ (0.0) $^4A'$ (31.2)

V_4O_{10}

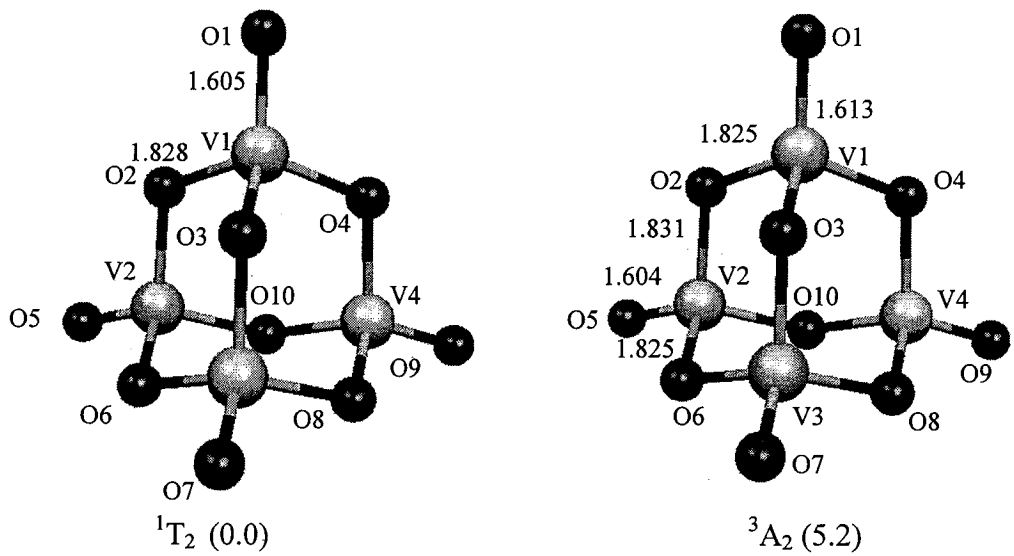

$^1T_2$ (0.0) $^3A_2$ (5.2)

Fig. 3.9. PLAP4/DZVP+aux. geometric parameters (bond lengths in Å) and relative energies (in kcal/mol) for $V_4O_{10}^+$ and V_4O_{10}

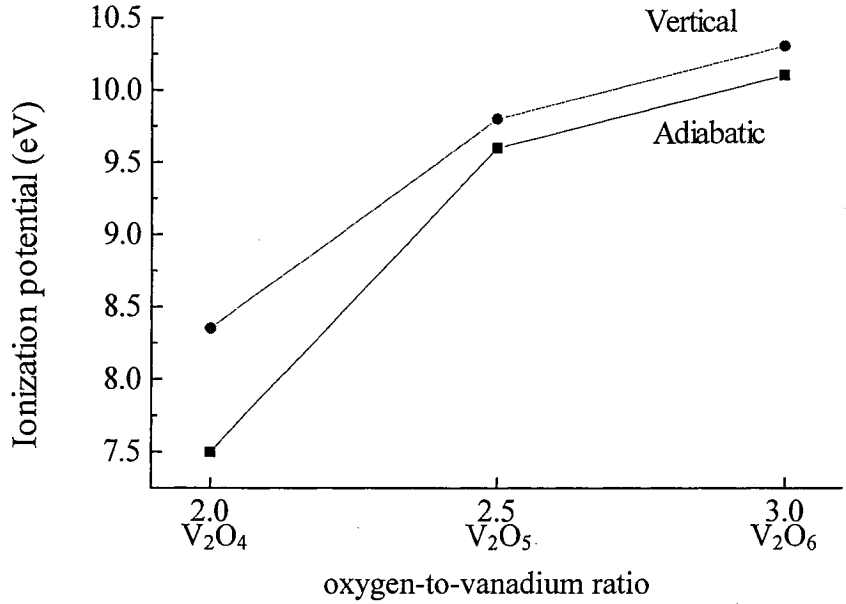

Fig. 3.10. Ionization Potentials for V_2O_y (y=4-6)

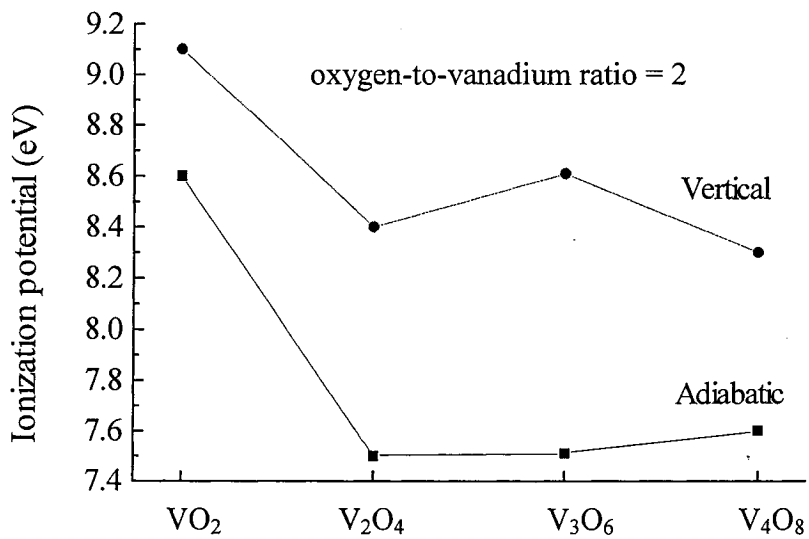

Fig. 3.11. Ionization Potentials for selected V_xO_y with a constant oxygen-to-vanadium ratio

Chapter 4.

Density-Functional Theory Studies of the Reactions of Vanadium Oxide Cluster Cations with Fluorocarbons

(Y. Wei & G. H. Peslherbe, *Journal of Physical Chemistry* A, to be submitted)

4.1. Introduction

Vanadium oxides have been used extensively as catalysts or catalytic supports in a variety of industrial processes, which include the selective oxidation and functionalization of hydrocarbons as well as the selective reduction of NO_x.[72] The molecular design and preparation of highly active catalysts requires a profound knowledge of the reaction mechanisms involved in these catalytic processes. Modern *in-situ* spectroscopic techniques can be used to probe the reactive sites on the surface of catalysts and help understand reaction mechanisms, but they are rather expensive and have a number of limitations.[1] On the other hand, theoretical studies of relevant cluster models provide an alternative for investigating catalytic reaction mechanisms and understanding elementary reaction steps at the molecular level. Gas-phase metal oxide clusters can be regarded as the simplest model for describing the interaction of catalytic active sites with molecules, since the surface of transition metal oxides can be envisioned as a collection of clusters.[26]

Vanadium oxide clusters have been the focus of many experimental and theoretical studies. A considerable amount of experimental work has been reported by Castleman and co-workers, who investigated the properties of vanadium oxide cluster ions through collision-induced dissociation (CID) reactions[12] and their reactivity towards various organic molecules, which include industrially important hydrocarbons[26] and environmentally-relevant halocarbons.[9-11] In the reactions of vanadium oxide cluster ions with hydrocarbons, the clusters were found to lose an oxygen atom by specifically reacting with the hydrocarbons, and not because of collisions. Several theoretical studies of the reactions of vanadium oxide cluster ions with hydrocarbons have been reported

recently. Justes *et al.* [32] investigated the reactions between $V_xO_y^+$ (x=2,4; y=4-10) and ethylene (C_2H_4) through density-functional theory (DFT) calculations to identify possible structure-reactivity relationships, and they confirmed that the oxygen transfer reaction pathway is the most energetically favorable for the reactions of $V_xO_y^+$ (x=2,4; y=4-10) with ethylene. Andres and co-workers[33] reported a DFT study of the reaction of VO_2^+ with C_2H_6, and suggested a four-step (insertion, two consecutive hydrogen transfers, and abstraction) reaction mechanism as the most thermodynamically and kinetically favorable reaction pathway. The latter reaction pathway was also shown to involve multiple electronic states and spin inversion during the reaction, in agreement with previous work on the reaction of VO_2^+ with C_2H_4,[63] and with the work of Engeser *et al.*[70] on the reaction of VO_2^+ with C_3H_8.

Castleman and co-workers found experimental evidence that the reactions of vanadium oxide cluster cations with hexafluoroethane (C_2F_6), 1,1,1-trifluoroethane (CH_3CF_3), difluoromethane (CH_2F_2) and carbon tetrachloride (CCl_4) followed different pathways.[9-11] Experimental results suggest that vanadium oxide cluster cations are chemically inert towards C_2F_6, and only minor association channels between $V_2O_y^+$ (y=4-7) and C_2F_6 were observed. Several different product ions were detected by mass spectrometry in the reaction of vanadium oxide clusters with CH_3CF_3, and the main product ions observed were the so-called HF-elimination product ions. As for the reaction of $V_2O_4^+$ with CH_2F_2, stable $V_xO_y{\cdot}CH_2F_2^+$ ion-molecule complexes were observed upon association with vanadium oxide clusters and the dominant reaction pathway was found to involve the transfer of a single oxygen atom from the cluster to the neutral reactant CH_2F_2, along with abstraction of two fluorine atoms, to form the $V_xO_{y-1}F_2^+$ and CH_2O products.

Interestingly, while the reactivity of vanadium oxide clusters towards CH_3CF_3 seems to be independent of cluster size, the (oxygen transfer) reaction of $V_xO_y^+$ with CH_2F_2 was found to be very sensitive to cluster size and no such reaction was observed between CH_2F_2 and large clusters such as $V_4O_8^+$. Finally, the reaction of vanadium oxide cluster cations with carbon tetrachloride (CCl_4) was shown to involve transfer of a chloride ion for smaller clusters with three or fewer vanadium atoms, and the abstraction of two chlorine atoms with oxygen transfer to the neutral reactant molecule for the larger clusters. Although Castleman and co-workers have reported a large amount of experimental data on the reaction of vanadium oxide clusters towards environmentally important halocarbons, no theoretical studies have been reported on this topic to date, even though such studies could provide critical evidence in understanding the cluster-size dependence of the reactivity of vanadium oxide cluster cations towards halocarbons.

In this chapter, we focus on DFT studies of the mechanism of the reactions of $V_2O_4^+$ with CH_2F_2 and CH_3CF_3, paying particular attention to possible cluster structure-reactivity relationships. The outline of this article is as follows: A brief description of the computational procedure is given in Sec. 4.2. Results about the reactivity of $V_2O_4^+$ towards the fluorocarbons predicted by our calculations are then presented and discussed in Sec. 4.3, along with a connection to experimental data. A brief discussion of the cluster size dependence of the reactivity of cluster ions towards fluorocarbons and concluding remarks follow in Sec. 4.4.

4.2. Computational Methods

Density-functional theory (DFT) calculations were carried out with the Gaussian98 suite of programs.[73] All calculations employ Becke's hybrid three-parameter nonlocal exchange functional combined with the Lee-Yang-Parr gradient-corrected correlation functional (B3LYP),[48,91] along with a triple-zeta valence plus polarization function basis set (TZVP) developed by Ahlrichs and co-workers.[92] This level of theory and basis set were chosen to investigate reactions of $V_2O_4^+$ cluster cations with fluorocarbons, because this combination was shown to properly describe the structure and energetics of vanadium oxide clusters,[93] and the reaction of vanadium oxide cluster cations with such species as ethylene[32] in previous theoretical studies. Gradient-based minimization methods were used for minimum-energy geometry optimization,[81] while transition states were optimized with the synchronous transit quasi-Newton (STQN) method developed by Schlegel and co-workers.[94,95] All stationary points were characterized by a vibrational analysis. Furthermore, intrinsic reaction coordinate (IRC) calculations[96,97] were performed to confirm the nature of transition states and characterize reaction pathways. All electronic energies were corrected for zero-point energy based on harmonic vibrational frequencies. The natural population analysis (NPA)[88,89] was carried out with the NBO program version 3.1, as implemented in Gaussian98 to determine charge distributions.

The quantum theory of atoms in molecules (AIM)[98] was used to further characterize the electronic structure of stationary points using the AIMPAC suite of programs.[98,99] The AIM analysis provides means of mapping topological properties of the electronic density $\rho(r)$ to Lewis-structure representations of molecules.[98] Critical points correspond to

maxima, minima and saddle points in the electron density $\rho(r)$, i.e., points where the density gradient $\nabla\rho(r)$ is zero. These critical points are classified according to their rank ω and signature σ as (ω, σ), where the rank ω is the number of nonzero curvatures in $\rho(r)$ and the signature σ is the sum of the signs of the curvatures at the critical point. For instance, a (3, -1) or bond critical point (BCP) has two negative curvatures and one positive curvature. The Laplacian of the electronic density $\nabla^2\rho(r)$ identifies regions of local charge concentration ($\nabla^2\rho(r) < 0$) and local charge depletion ($\nabla^2\rho(r) > 0$) in the topology of the electron density. The nature of bonding between atoms can be characterized by the value of the electronic density ρ_b and the sign and magnitude of the Laplacian of the electronic density $\nabla^2\rho_b$ at the BCP. We also investigated the topology of the Laplacian of the electron density by characterizing the critical points of L= $-\nabla^2\rho(r)$. The critical points in L are classified according to their rank ω and signature σ as (ω, σ), very much like critical points in $\rho(r)$. The positions of (3, +1) critical points in L function identify regions of maximum local charge depletion.

4.3. Results and Discussion

4.3.1. Structure of $V_2O_4^+$ and Cluster Ion-Molecule Complexes

Minimum-energy structures for the $V_2O_4^+$ isomers and their relative energies are depicted in Fig. 4.1. Three distinct isomers, which include the trans-four-membered ring structure **1**, the cis-four-membered ring structure **2** and the linear-open structure **3** were found with the B3LYP/TZVP model chemistry. The $V_2O_4^+$ lowest energy structure is the trans-four-membered ring structure **1**[93] with C_s symmetry and a $^2A'$ ground electronic state, in agreement with previous work.[32] The ground state of the cis-four-membered ring

structure **2** and the linear-open structure **3** correspond to the $^2A'$ and ^2A electronic states with C_s and C_1 symmetry, respectively, in agreement with previous B3LYP/6-31G* results.[29] Four-membered ring structures are more stable than the linear-open structure, which is higher in energy than the most stable isomer **1** by 26.2 kcal/mol, while the energy difference between the trans-isomer **2** and the cis-isomer **3** is only 4.4 kcal/mol. The binding energies per atom for the three $V_2O_4^+$ isomers were calculated according to the formula[32]

$$E_{b/n}=[E(V_xO_y^+)-E(V^+)-(x-1)E(V)-yE(O)]/(x+y)$$

The calculated binding energies per atom for **1**, **2** and **3** are 4.39 eV, 4.37 eV and 4.21 eV respectively, and further reflect the higher stability of the trans-isomer **1.**

Various ion-molecule complexes formed upon association of $V_2O_4^+$ with CH_2F_2 were investigated and characterized. The structure and relative energies of the six isomers of the $V_2O_4{\cdot}CH_2F_2^+$ complex shown in Fig. 4.2 reveal that the ion-molecule complex isomers **a**, formed upon association of the most stable trans-$V_2O_4^+$ **1** with CH_2F_2, are more stable than the isomers **d**, formed upon association of cis-$V_2O_4^+$ **2** with CH_2F_2 by 4.2 kcal/mol, and complex **b** and **c** are more stable than complex **e** and **f** by 4.6 and 4.5 kcal/mol, respectively. The main geometric difference between the $V_2O_4{\cdot}CH_2F_2^+$ complexes **a** and **b** lies in the 33.30° difference in the V2-F1-C1-F2 dihedral angle, which indicates that rotation around the V2-F1 bond in complex **b** results in another complex **a**, which is slightly lower in energy (by 0.6 kcal/mol). Interestingly, two fluorine atoms of CH_2F_2 point to the V1 atom of $V_2O_4^+$ in the complex $V_2O_4{\cdot}CH_2F_2^+$ **c**, but not to the V2 atom of $V_2O_4^+$. Gillespie *et al.* pointed out that the electron pairs of the ligands are generally attracted toward regions of maximum local charge depletion of a transition

metal atom, which are characterized by (3, +1) critical points in L.[100] In the present case, CH_2F_2 can be considered as a ligand that is attracted to the vanadium atom. Through analysis of the valence-shell charge concentration of the vanadium atoms in the trans-$V_2O_4^+$ isomer **1**, two maximum local charge depletion regions were identified and around the V1 atom above the V1-O1-V2 plane depicted in Fig. 4.3, while only one maximum local charge depletion region was found around the V2 atom under the V1-O1-V2 plane also depicted in Fig. 4.3. This suggests that two fluorine atoms of CH_2F_2 can be attracted to the V1 atom of $V_2O_4^+$, while only one fluorine atom of CH_2F_2 can bind to the V2 atom of $V_2O_4^+$. The energy of complex $V_2O_4{\cdot}CH_2F_2^+$ **c**, which seems to involve two V-F bonds, based on geometric consideration, is higher than that of the single V-F bonded $V_2O_4{\cdot}CH_2F_2^+$ complex **a** by 6.1 kcal/mol. In complex **c**, electronic repulsion between the electrons of two fluorine atoms and the core electrons of vanadium atom most likely raises the energy of complex **c** even though two V-F bonds are formed.

Various ion-molecule complexes formed upon association of $V_2O_4^+$ and CH_3CF_3 were also investigated and characterized. The structure and relative energies of four isomers of the $V_2O_4{\cdot}CH_3CF_3^+$ complex are shown in Fig. 4.4. The complex isomers **A** and **C** formed upon association of the trans-$V_2O_4^+$ **1** with CH_3CF_3 are more stable than the isomers **B** and **D** formed upon association of cis-$V_2O_4^+$ **2** with CH_3CF_3 by 4.3 to12.1 kcal/mol. These findings are similar to what was observed for $V_2O_4{\cdot}CH_2F_2^+$ complexes. Similarly, two fluorine atoms of CH_3CF_3 can bind to the V1 atom of $V_2O_4^+$ to form complexes **C** and **D**, however only one fluorine atom of CH_3CF_3 appears to be bound to the V2 atom of $V_2O_4^+$ in complexes **A** and **B**.

An AIM analysis was carried out in order to further understand the nature of the V-F bonds and the formation of $V_2O_4{\cdot}CH_2F_2^+$ and $V_2O_4{\cdot}CH_3CF_3^+$ complexes. V-F bond critical paths were found and the properties of selected V-F BCPs are presented in Table 4.1. In the quantum theory of AIM, the bond characterized by the low electron density ρ_b and the positive values of the Laplacian of the electron density $\nabla^2\rho_b$ at a BCP is defined as a closed-shell interaction with ionic character.[98] Inspection of the properties of selected V-F BCPs reveals that the V-F bonds in $V_2O_4{\cdot}CH_2F_2^+$ and $V_2O_4{\cdot}CH_3CF_3^+$ complexes are indeed closed-shell interaction with ionic character. One could expect that hydrogen bonding between the positively charged hydrogen and negatively charged oxygen plays a role in the formation of the $V_2O_4{\cdot}CH_2F_2^+$ and $V_2O_4{\cdot}CH_3CF_3^+$ complexes. However, no hydrogen bonding interaction was found in the stable structures of the ion-molecule complexes shown in Figs. 4.2 and 4.4 through AIM analysis.

4.3.2. Thermodynamics of Ion-Molecule Complex Formation

Upon collision with CH_2F_2 and CH_3CF_3, $V_2O_4^+$ could either dissociate into fragments or associate with the reactant molecules to form ion-molecule complexes. Accordingly, we have calculated the enthalpies of $V_2O_4^+$ fragmentation and ion-molecule complexation with the B3LYP/TZVP model chemistry:

$$V_2O_4^+ (^2A') \longrightarrow V_2O_3^+ (^2A') + O (^3P) \qquad \Delta H_{298} = 117.2 \text{ kcal/mol}$$

$$V_2O_4^+ (^2A') + CH_2F_2 (^1A_1) \longrightarrow V_2O_4{\cdot}CH_2F_2^+ (^2A) \qquad \Delta H_{298} = -34.3 \text{ kcal/mol}$$

$$V_2O_4^+ (^2A') + CH_3CF_3 (^1A_1) \longrightarrow V_2O_4{\cdot}CH_3CF_3^+ (^2A) \qquad \Delta H_{298} = -34.8 \text{ kcal/mol}$$

Calculated reaction enthalpies at 298 K show that the loss of a single atomic oxygen from $V_2O_4^+$ is a highly endothermic process, which is thermodynamically unfavorable, in good agreement with previous theoretical studies.[29,32] On the other hand, the association reactions of $V_2O_4^+$ with CH_2F_2 and CH_3CF_3 are exothermic by 34-35 kcal/mol, and are therefore thermodynamically favorable.

These results are consistent with the experimental observation by Castleman and co-workers[10] of the $V_2O_4{\cdot}CH_2F_2^+$ complex and not the product of ion fragmentation $V_2O_3^+$ in the reaction of $V_2O_4^+$ with CH_2F_2. Although the complexation of $V_2O_4^+$ with CH_3CF_3 is also thermodynamically favorable, the $V_2O_4{\cdot}CH_3CF_3^+$ complex was not detected experimentally, which could be indicative of the high reactivity and short lifetime of the $V_2O_4{\cdot}CH_3CF_3^+$ complex.

4.3.3. Charge Distributions of Ions, Molecules and Ion-Molecule Complexes

Charge distributions derived from natural population analysis for the trans-four-membered ring structure $V_2O_4^+$ **1**, CH_2F_2, CH_3CF_3, and their most stable ion-molecule complexes are collected in Table 4.2. The positive charges are almost evenly distributed over the two vanadium atoms of $V_2O_4^+$ with a difference of only 0.04 e, but the unpaired electron is located on the V1 atom of $V_2O_4^+$ based on the analysis of spin densities. The fluorine atoms of CH_2F_2 have a significant negative charge (–0.33 e) and they can interact easily with the positively charged vanadium atom of $V_2O_4^+$ to produce stable ion-molecule complexes. Charge distributions of the cluster ions and molecules do not change dramatically upon complexation of $V_2O_4^+$ with CH_2F_2. The positive charge of the carbon atom increases from +0.40 e to +0.44 e in $V_2O_4{\cdot}CH_2F_2^+$ complex **a**, and is larger than the positive charges of the hydrogen atoms (+0.19 e) in complex **a**. The charge distributions are consistent with a possible attack of the negatively charged oxygen atom on the positively charged carbon atom and weakening of the V-O bond, thus inducing oxygen transfer. The electronic repulsion between the bridged oxygen atoms O1 and O2 and the fluorine atom F2 in complex **b** (cf. Fig. 4.2) may explain why the rotation around C-F2 bond allows formation of the more stable complex **a**, since charges on the bridged oxygen atoms are higher than those on the terminal oxygen atoms.

Charge distributions of the cluster ions and molecules do not change dramatically upon complexation of $V_2O_4^+$ and CH_3CF_3, except that the negative charge of the F1 atom bound to $V_2O_4^+$ increases from –0.32 e to –0.48 e, while the negative charges of the other fluorine atoms are slightly reduced (by ~0.1 e). The methyl carbon atom C2 has a negative charge of –0.71 e and the hydrogen atoms have positive charges in the range of

0.27–0.29 e, which are consistent with an attack of positively charged hydrogen atom on the negatively charged oxygen atom, but not with an attack of the oxygen atom on the carbon atom as what was observed for CH_2F_2. The charge distributions in the $V_2O_4{\cdot}CH_3CF_3^+$ complexes suggest a reaction pathway involving abstraction by the $V_2O_4^+$ oxygen atom. This may explain why stepwise HF abstraction and not oxygen transfer, is observed in the reaction of $V_2O_4^+$ with CH_3CF_3.[9]

4.3.4. Mechanisms of the Reactions of $V_2O_4^+$ with CH_2F_2 and CH_3CF_3

Two possible reaction pathways were investigated for the reaction of $V_2O_4^+$ with CH_2F_2 on the doublet (ground-state) potential energy surface. The energy profile and the structures of stationary points along reaction pathway 1 are shown in Fig. 4.5, while the topological properties of the electron density ρ_b at selected BCPs for stationary point structures are given in Table 4.3. The first reaction step involves the approach of $V_2O_4^+$ towards CH_2F_2 to form the $V_2O_4{\cdot}CH_2F_2^+$ ion-molecule complex through a barrierless process. In reaction pathway 1, the most stable $V_2O_4{\cdot}CH_2F_2^+$ complex **a** is considered as the starting point to investigate the next reaction steps. The geometry of the $V_2O_4{\cdot}CH_2F_2^+$ complex **a** suggests formation of a V2-F1 bond, with a bond length of 1.994 Å, while the C1-F1 bond is elongated to 1.521 Å. The BCP electron density ρ_b for the C1-F1 bond decreases from 1.63 e/Å^3 to 1.06 e/Å^3, revealing that the C1-F1 bond is weakened upon the formation of the V2-F1 bond. The next reaction step involves attack of the terminal oxygen atom O3 on the positively charged carbon atom C1 of the vanadium oxide cluster via transition state $\mathbf{TS_{ag}}$ to yield an intermediate complex **g**, and results in simultaneous cleavage of the C1-F1 bond and formation of the C1-O3 bond. Low values of ρ_b and

positive values of $\nabla^2\rho_b$ for the C1-F1 bond in $\mathbf{TS_{ag}}$ further indicate that the shared interaction between the C1 and F1 atoms has changed into a close d-shell interaction. A new BCP point is also found between the C1 and O3 atoms in $\mathbf{TS_{ag}}$, which is consistent with formation of the new C1-O3 bond. The BCP for the C1-F1 bond vanishes and the value of ρ_b for the C1-O3 bond increases in complex **g**, consistent with C1-F1 bond cleavage and C1-O3 bond formation, while the value of ρ_b for the V2-O3 bond decreases slightly, consistent with weakening and lengthening of the V2-O3 bond (from 1.559 Å to 1.698 Å). Cleavage of the C1-F1 bond is more facile than cleavage of the V2-O3 bond because the energy required for cleavage of the C-F bond is 116.8 kcal/mol, which is less than that required for cleavage of the terminal V-O bond (129.1 kcal/mol) according to our B3LYP/TZVP calculations.

$$CH_2F_2\ (^1A_1) \longrightarrow CH_2F\ (^2A) + F\ (^2P) \qquad \Delta E=116.8 \text{ kcal/mol}$$

$$V_2O_4^+\ (^2A') \longrightarrow V_2O_3^+\ (^2A') + O\ (^3P) \qquad \Delta E=129.1 \text{ kcal/mol}$$

The next reaction step involves attack of the F2 fluorine atom on the V2 vanadium atom, thereby significantly weakening the terminal V2-O3 bond and affording oxygen atom transfer to produce a complex **h** via transition state $\mathbf{TS_{gh}}$. In complex **h**, low values of ρ_b and positive values of $\nabla^2\rho_b$ for the BCP between the V2 and O3 atoms indicate that a weak electrostatic interaction remains between the vanadium and oxygen atoms. The $V_2O_3F_2{\cdot}CH_2O^+$ ion-molecule complex **h** further dissociates to form the four-membered ring structure $V_2O_3F_2^+$ and CH_2O products via a barrierless process. From the energy profile for reaction pathway 1 shown in Fig. 4.5, the complex **a** is more stable than the reactants $V_2O_4^+$ and CH_2F_2 by 34.7 kcal/mol, due to the formation of one V-F bond. The first energy barrier is 21.0 kcal/mol from the starting complex **a** to the intermediate

complex **g**. The second energy barrier from complex **g** to complex **h** is 21.8 kcal/mol, while only 18.8 kcal/mol is required to fragment complex **h** to form the $V_2O_3F_2^+$ and CH_2O products.

The energy profile and the structures of stationary points along reaction pathway 2 are shown in Fig. 4.6, while the topological properties of the electron density ρ_b at selected BCPs for stationary point structures are given in Table 4.4. Reaction pathway 2 starts with formation of the $V_2O_4{\cdot}CH_2F_2^+$ complex **b**, upon association of $V_2O_4^+$ with CH_2F_2. In complex **b**, a BCP was found between the F1 and V2 atoms, while the electron density ρ_b for the C1-F1 bond decreases from 1.63 to 0.88 e/Å^3, which indicates V2-F1 bond formation along with C1-F1 bond weakening. The geometry of complex **b**, with a shorter C1-O1 distance (4.181 Å) than C1-O3 distance (4.419 Å) suggests that the bridged oxygen atom O2 will attack the positively charged carbon atom C1 more readily than the terminal oxygen atom O3. Complex **b** is converted to intermediate complex **i** via transition state $\mathbf{TS_{bi}}$, which involves cleavage of the C1-F1 bond along with strengthening the V2-F1 bond, and formation of the C1-O2 bond. The BCP between the C1 and F1 atoms vanishes in complex **i**, indicative of C1-F1 bond cleavage. As can be seen from Table 4.4, the electron density ρ_b for the C1-O2 bond increases from 0.12 to 1.75 e/Å^3, which reveals that the C1-O2 bond strengthens significantly in going from the transition state to complex **i**. The next step involves the attack of the F2 fluorine atom on the V1 vanadium atom, along with V1-O2 bond cleavage to produce a very stable complex **j** via transition state $\mathbf{TS_{ij}}$. From the energy profile for reaction pathway 2 shown in Fig. 4.6, the $V_2O_4{\cdot}CH_2F_2^+$ complex **b** is more stable than the reactants by 34.1kcal/mol. The first energy barrier to form intermediate complex **i** from the starting complex **b** is

22.8 kcal/mol, while only 6.6 kcal/mol is required to form complex **j** from intermediate complex **i.** The resulting complex **j** that is much more stable than other complexes (it is more stable than the $V_2O_3F_2{\cdot}CH_2O^+$ complex **h** found in reaction pathway 1 by 21.6 kcal/mol) and it may not readily dissociate to form the $V_2O_3F_2^+$ and CH_2O products.

Both pathways for the reaction of $V_2O_4^+$ with CH_2F_2 involve two energy barriers. The first energy barrier is very similar in magnitude for both reaction pathways, but the second energy barrier of reaction pathway 2 is lower than that of reaction pathway 1 by 15.2 kcal/mol. This suggests that formation of the very stable $V_2O_3F_2{\cdot}CH_2O^+$ complex **j** along pathway 2, (which involves bridged oxygen transfer along with fluorine abstraction from the fluorocarbon) is relatively easy, and this could explain why the complex was observed experimentally.[10] As for reaction pathway1, both barriers and the energy required to dissociate the complex **h** are of similar magnitude (~20 kcal/mol), and thus the reaction of $V_2O_4^+$ with CH_2F_2 via pathway 2, which involves transfer of the terminal oxygen, along with abstraction of the fluorine atoms from CH_2F_2, may proceed completely to form the $V_2O_4F_2^+$ and CH_2O products that are also observed experimentaly.[10]

Let us now turn our attention to the reaction of $V_2O_4^+$ with CH_3CF_3. The energy profile and the structures of stationary points along the reaction of $V_2O_4^+$ with CH_3CF_3 are shown in Fig. 4.7, while the topological properties of the electron density ρ_b at selected BCPs for stationary point structures are given in Table 4.5. In complex **A** formed upon association of $V_2O_4^+$ with CH_3CF_3, a BCP is found between the V2 and F1 atoms, which are only separated by 1.943 Å, while the C1-F1 bond is elongated to 1.669 Å and the electron density ρ_b decreases from 1.74 to 0.80 e/Å^3, which indicates significant C1-F1

bond weakening upon formation of the V2-F1 bond. The next reaction step involves the rotation of the methyl group around the C1-C2 bond to approach the terminal oxygen atom O3 to produce complex **E** via transition state $\mathbf{TS_{AE}}$. As can be seen from Table 4.5, the BCP between C1 and F1 vanishes and a BCP between O3 and H1 appears in $\mathbf{TS_{AE}}$, consistent with C1-F1 bond cleavage and initial O3-H1 bond formation. Large ρ_b value (1.77 e/Å^3) and negative $\nabla^2\rho_b$ value (-38.32 e/Å^5) for the O3-H1 bond in complex **E** suggests that a strong (covalent) bond is formed between the O3 and H1 atoms. The final reaction step is the dissociation of the product complex **E** via a barrierless reaction, resulting in the $V_2O_4{\cdot}HF^+$ and CH_2CF_2 products. As discussed in section 4.3.3, the hydrogen atoms in complex **A** are positively charged and the methyl carbon atom C2 is negatively charged. It is thus not surprising that the methyl group rotates in the course of the reaction so that one of the positively charged hydrogen atoms can attack the terminal oxygen atom O3 (which carries a much more negative charge than O2) and cleave the V-O bond. From the energy profile shown in Fig. 4.7, the $V_2O_4{\cdot}CH_2F_2^+$ complex **A** is more stable than the reactants $V_2O_4^+$ and CH_3CF_3 by 35.1 kcal/mol. The low energy barrier (6.2 kcal/mol) for complex **A** isomerization to **E** along with the low fragmentation energy (7.8 kcal/mol) of complex **E** suggests that the reaction of $V_2O_4^+$ and CH_3CF_3 proceeds readily to form the $V_2O_4{\cdot}HF^+$ and CH_2CF_2 products. This reaction mechanisms and the low barriers association with it may explain why Castleman and co-workers only observed with reaction products $V_2O_4{\cdot}HF^+$ (and CH_2CF_2) and not the highly reactive, short-lived $V_2O_4{\cdot}CH_3CF_3$.

4.4. Conclusions

In this chapter, we have reported the results of a DFT investigation of the reactions of $V_2O_4^+$ clusters with CH_2F_2 and CH_3CF_3 using the B3LYP/TZVP model chemistry. The ion-molecule complexes formed upon association of the most stable trans-$V_2O_4^+$ **1** cluster with CH_2F_2 and CH_3CF_3 are more stable than those formed upon association of cis-$V_2O_4^+$ **2** with CH_2F_2 and CH_3CF_3. The association of $V_2O_4^+$ with fluorocarbons to form ion-molecule complexes was shown to be thermodynamically favorable, and governed by the formation of V-F bonds. The reaction of $V_2O_4^+$ with CH_2F_2 may proceed via two pathways. The first one involves transfer of the terminal oxygen, along with abstraction of fluorine atoms from CH_2F_2, to form the $V_2O_4F_2^+$ and CH_2O products, which is consistent with experimental observations. The second pathway involves transfer of the bridged oxygen atom and leads to a very stable $V_2O_4{\cdot}CH_2F_2^+$ ion-molecule product complex, which was also observed experimentally. In contrast, stepwise HF abstraction from the halocarbon prevails in the reaction of $V_2O_4^+$ with CH_3CF_3, to yield the $V_2O_4HF^+$ product, which was again observed experimentally. Thus, our DFT calculations provide mechanisms for the reactions of $V_2O_4^+$ with CH_2F_2 and CH_3CF_3 that are fully consistent with the experimental observations of the reaction products.

In order to elucidate the difference in the reactivity of $V_xO_y^+$ towards CH_2F_2 and CH_3CF_3 observed as a function of cluster size, the structure of larger clusters such as $V_4O_8^+$ was also investigated, and minimum-energy structures predicted by the B3LYP/TZVP model chemistry for two $V_4O_8^+$ isomers and their relative energies are shown in Fig. 8. The ground state of the cage-like C_s-symmetry $V_4O_8^+$ **I** corresponds to a

$^2A''$ state, while that of **II** corresponds to a ^2A state. The cage-like structure **I** is much more stable than the open structure **II** by 99.5 kcal/mol. The calculated binding energies per atom for the most stable $V_2O_4^+$ and $V_4O_8^+$ cluster ions are 4.39 eV and 4.99 eV, respectively, which indicates that the V-O bond strength increases as a function of cluster size. Assuming the same reaction mechanisms as that for $V_2O_4^+$, oxygen transfer in the reaction of $V_xO_y^+$ with CH_2F_2 requires cleavage of a V-O bond, and the strong V-O bonds found for larger clusters such as $V_4O_8^+$ may explain the difficulty of achieving oxygen transfer for larger clusters, and thus the experimental observation that large vanadium oxide clusters are chemically inert towards CH_2F_2. However, the reaction of $V_2O_4^+$, and presumably of the larger clusters, with CH_3CF_3 does not involve cleavage of V-O bonds, and this may explain why the reactivity of vanadium oxide cluster ions was not observed to depend on cluster size experimentally.

Table 4.1. Topological Properties of the Electron Density at Selected Bond Critical Points in $V_2O_4 \cdot CH_2F_2^+$ and $V_2O_4 \cdot CH_3CF_3^+$ Complexes[a]

Ion-Molecule Complex	Bond	ρ_b (e/Å^3)	$\nabla^2\rho_b$ (e/Å^5)
Complex **a**	V2-F1	0.48	10.12
Complex **b**	V2-F1	0.45	9.83
Complex **c**	V1-F1	0.25	4.92
Complex **c**	V1-F2	0.25	4.92
Complex **A**	V2-F1	0.54	11.68
Complex **C**	V1-F1	0.24	4.97
Complex **C**	V1-F2	0.24	4.97

a. Obtained from AIM analysis of B3LYP/TZVP wavefunctions

Table 4.2. Charge Distributions of CH_2F_2, CH_3CF_3, $V_2O_4^+$ and their Complexes[a]

	$V_2O_4^+$ **1**	$V_2O_4 \cdot CH_2F_2^+$ **a**	CH_2F_2	$V_2O_4 \cdot CH_3CF_3^+$ **A**	CH_3CF_3
V1	1.52	1.50	-	1.49	-
V2	1.48	1.38	-	1.37	-
O1	-0.67	-0.67	-	-0.68	-
O2	-0.67	-0.67	-	-0.67	-
O3	-0.30	-0.33	-	-0.34	-
O4	-0.36	-0.40	-	-0.40	-
C1	-	0.44	0.40	1.03	0.94
C2	-	-	-	-0.71	-0.67
H1	-	0.19	0.13	0.29	0.23
H2	-	0.19	0.13	0.27	0.23
H3	-	-	-	0.27	0.23
F1	-	-0.39	-0.33	-0.48	-0.32
F2	-	-0.25	-0.33	-0.22	-0.32
F3	-	-	-	-0.22	-0.32

a. Charges in fraction of electron obtained from natural population analysis of B3LYP/TZVP wavefunctions

Table 4.3. Topological Properties of the Electron Density at Selected Bond Critical Points along Pathway 1 of the Reaction of $V_2O_4^+$ with CH_2F_2 (Terminal Oxygen Transfer and Fluorine Abstraction)[a]

Separated $V_2O_4^+$ and CH_2F_2	V2-O3	C1-F1	C1-F2	V2-F1	V2-F2	C1-O3
ρ_b (e/Å^3)	2.00	1.63	1.63	-	-	-
$\nabla^2\rho_b$ (e/Å^5)	26.12	-7.27	-7.27	-	-	-
Complex **a**	V2-O3	C1-F1	C1-F2	V2-F1	V2-F2	C1-O3
ρ_b (e/Å^3)	1.97	1.06	1.85	0.45	-	-
$\nabla^2\rho_b$ (e/Å^5)	25.87	-1.59	-5.06	10.11	-	-
TS_{ag}	V2-O3	C1-F1	C1-F2	V2-F1	V2-F2	C1-O3
ρ_b (e/Å^3)	1.76	0.14	2.09	0.89	-	0.13
$\nabla^2\rho_b$ (e/Å^5)	24.14	2.19	8.16	17.45	-	1.95
Complex **g**	V2-O3	C1-F1	C1-F2	V2-F1	V2-F2	C1-O3
ρ_b (e/Å^3)	1.95	-	1.70	1.95	-	1.48
$\nabla^2\rho_b$ (e/Å^5)	22.97	-	-7.31	23.03	-	-7.70
TS_{gh}	V2-O3	C1-F1	C1-F2	V2-F1	V2-F2	C1-O3
ρ_b (e/Å^3)	0.62	-	0.40	1.19	0.70	2.34
$\nabla^2\rho_b$ (e/Å^5)	10.03	-	3.95	22.50	13.09	-10.94
Complex **h**	V2-O3	C1-F1	C1-F2	V2-F1	V2-F2	C1-O3
ρ_b (e/Å^3)	0.37	-	-	1.19	1.04	2.49
$\nabla^2\rho_b$ (e/Å^5)	5.15	-	-	22.25	20.27	2.65

a. Obtained from AIM analysis of B3LYP/TZVP wavefunctions

Table 4.4. Topological Properties of the Electron Density at Selected Bond Critical Points along Pathway 2 of the Reaction of $V_2O_4^+$ with CH_2F_2 (Bridged Oxygen Transfer and Fluorine Abstraction)[a]

Separated $V_2O_4^+$ and CH_2F_2	V1-O2	V2-O2	C1-F1	C1-F2	V2-F1	V1-F2	C1-O2
ρ_b (e/Å^3)	0.77	1.27	1.63	1.63	-	-	-
$\nabla^2\rho_b$ (e/Å^5)	12.76	18.93	-7.27	-7.27	-	-	-
Complex **b**	V1-O2	V2-O2	C1-F1	C1-F2	V2-F1	V1-F2	C1-O2
ρ_b (e/Å^3)	0.81	1.22	0.88	1.82	0.44	-	-
$\nabla^2\rho_b$ (e/Å^5)	13.19	18.25	-1.89	-5.19	9.84	-	-
TS_{bi}	V1-O2	V2-O2	C1-F1	C1-F2	V2-F1	V1-F2	C1-O2
ρ_b (e/Å^3)	0.82	1.02	0.13	2.10	0.89	-	0.12
$\nabla^2\rho_b$ (e/Å^5)	13.39	15.51	2.14	7.92	17.97	-	1.72
Complex **i**	V1-O2	V2-O2	C1-F1	C1-F2	V2-F1	V1-F2	C1-O2
ρ_b (e/Å^3)	0.51	0.67	-	1.23	1.14	0.33	1.75
$\nabla^2\rho_b$ (e/Å^5)	8.66	11.22	-	-4.19	22.25	7.03	-13.19
TS_{ij}	V1-O2	V2-O2	C1-F1	C1-F2	V2-F1	V1-F2	C1-O2
ρ_b (e/Å^3)	0.18	0.79	-	1.02	1.15	0.47	1.91
$\nabla^2\rho_b$ (e/Å^5)	2.74	2.74	-	1.19	22.25	8.93	-13.86
Complex **j**	V1-O2	V2-O2	C1-F1	C1-F2	V2-F1	V1-F2	C1-O2
ρ_b (e/Å^3)	-	0.57	-	-	1.03	1.12	2.42
$\nabla^2\rho_b$ (e/Å^5)	-	10.83	-	-	21.31	22.07	-14.61

a. Obtained from AIM analysis of B3LYP/TZVP wavefunctions

Table 4.5. Topological Properties of the Electron Density at Selected Bond Critical Points along the Pathway of the Reaction of $V_2O_4^+$ with CH_3CF_3[a]

Separated $V_2O_4^+$ and CH_3CF_3	V2-O3	C1-F1	C2-H1	V2-F1	O3-H1
ρ_b (e/Å^3)	2.00	1.74	1.80	-	-
$\nabla^2\rho_b$ (e/Å^5)	26.12	-11.25	-22.35	-	-
Complex **A**	V2-O3	C1-F1	C2-H1	V2-F1	O3-H1
ρ_b (e/Å^3)	1.96	0.80	1.81	0.54	-
$\nabla^2\rho_b$ (e/Å^5)	25.73	1.63	-22.98	11.68	-
TS_{AE}	V2-O3	C1-F1	C2-H1	V2-F1	O3-H1
ρ_b (e/Å^3)	1.67	-	1.42	1.03	0.36
$\nabla^2\rho_b$ (e/Å^5)	23.97	-	-15.72	20.21	2.92
Complex **E**	V2-O3	C1-F1	C2-H1	V2-F1	O3-H1
ρ_b (e/Å^3)	1.29	-	0.30	1.16	1.77
$\nabla^2\rho_b$ (e/Å^5)	23.90	-	1.03	22.44	-38.32

a. Obtained from AIM analysis of B3LYP/TZVP wavefunctions

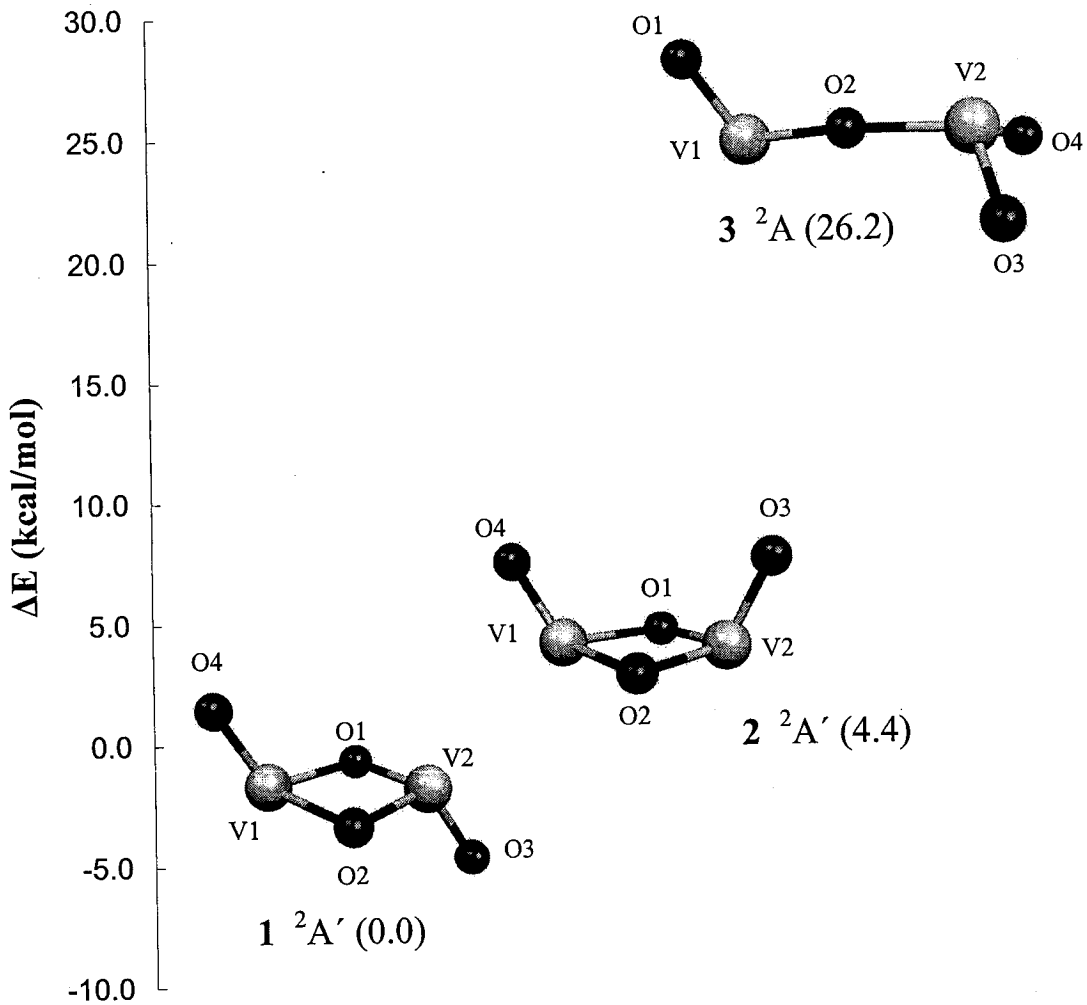

Fig. 4.1. B3LYP/TZVP minimum-energy structures and relative energies of trans-$V_2O_4^+$ **1**, cis-$V_2O_4^+$ **2** and linear-$V_2O_4^+$ **3**

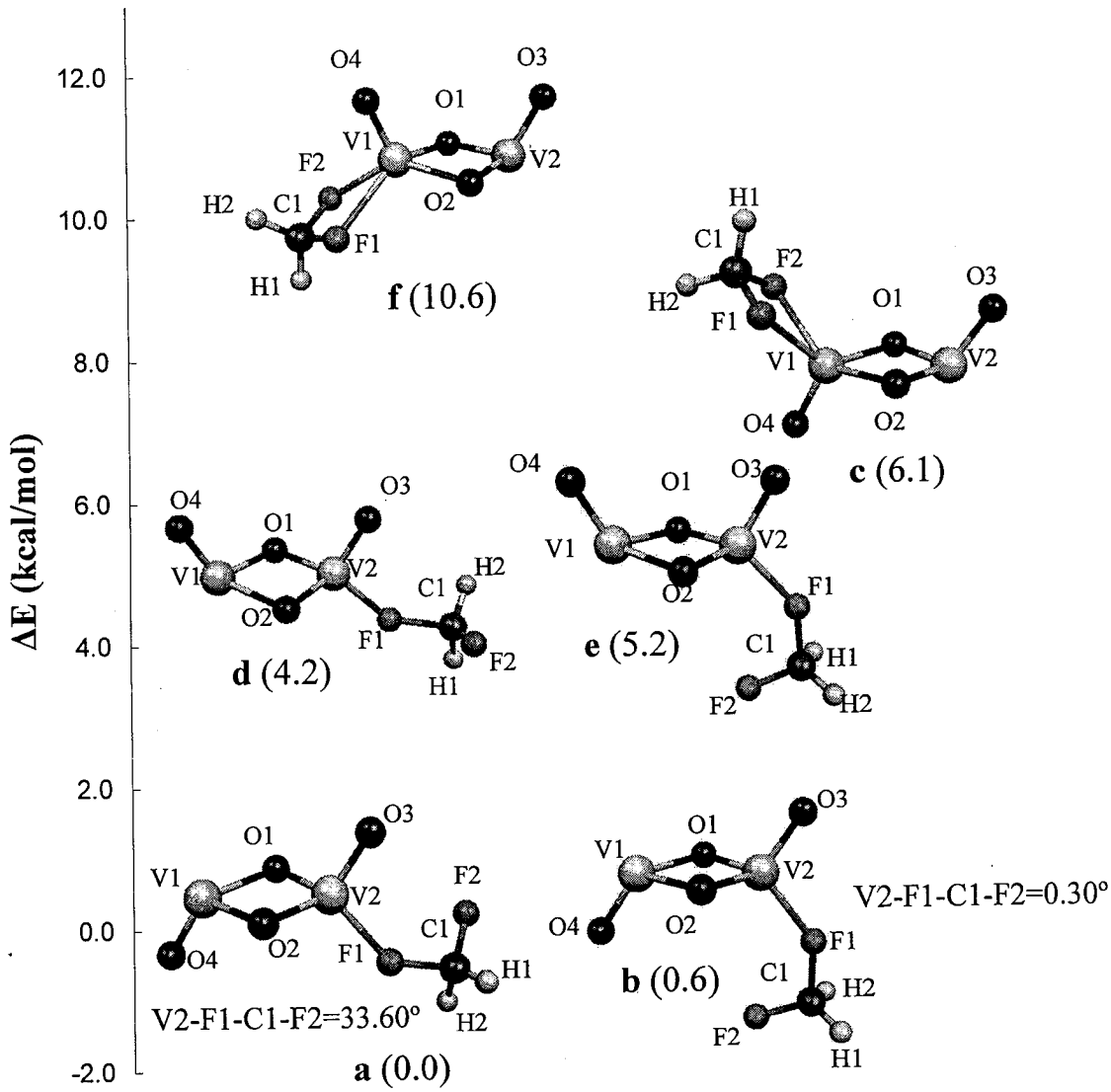

Fig. 4.2. B3LYP/TZVP minimum-energy structures and relative energies of the $V_2O_4 \cdot CH_2F_2^+$ complex isomers

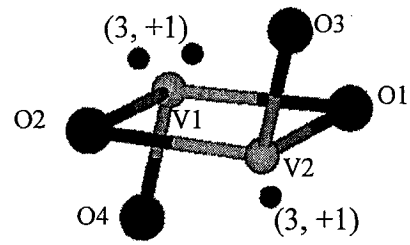

Fig. 4.3. Positions of (3, +1) critical points in $L=-\nabla^2\rho(r)$ around the vanadium atoms of $V_2O_4^+$

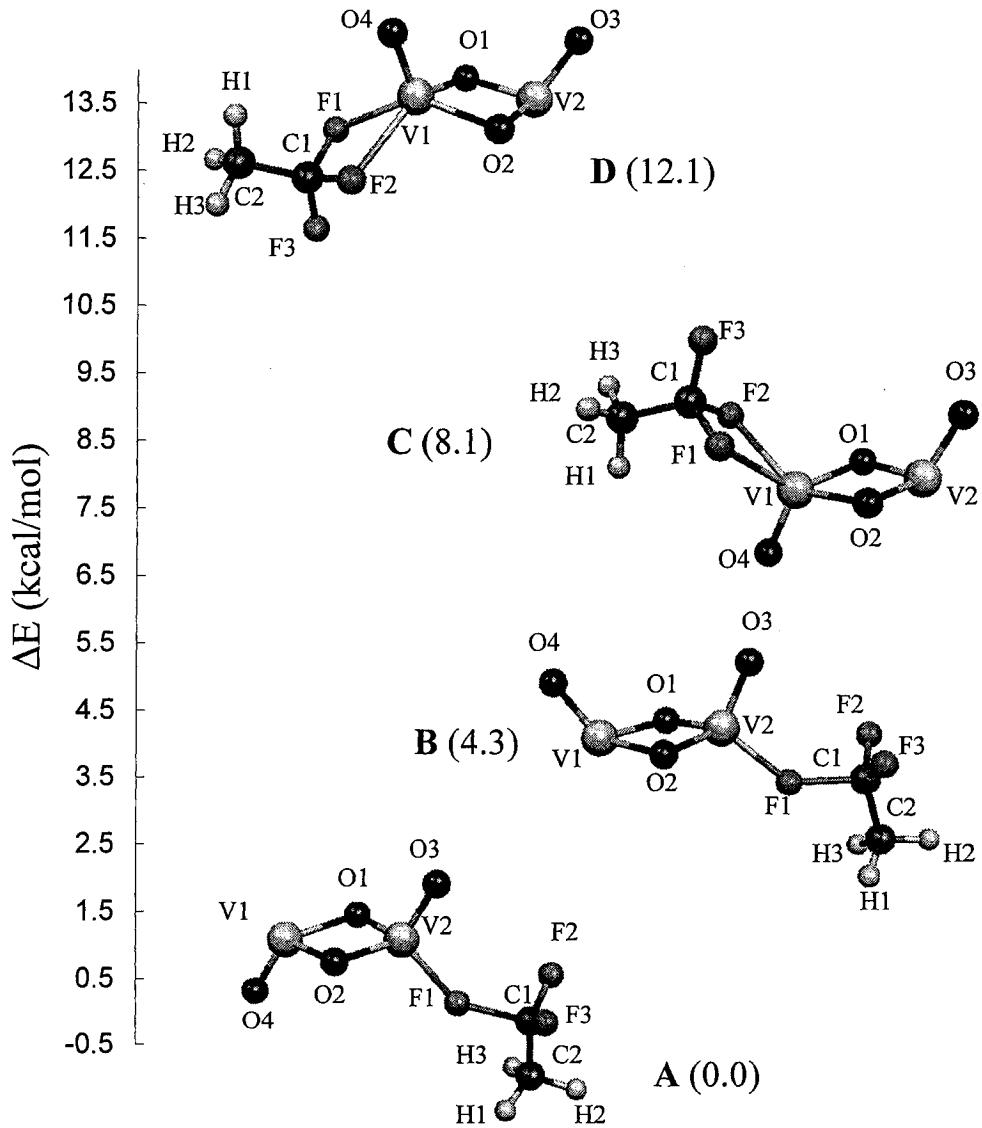

Fig. 4.4. B3LYP/TZVP minimum-energy structures and relative energies of the $V_2O_4{\cdot}CH_3CF_3^+$ complex isomers

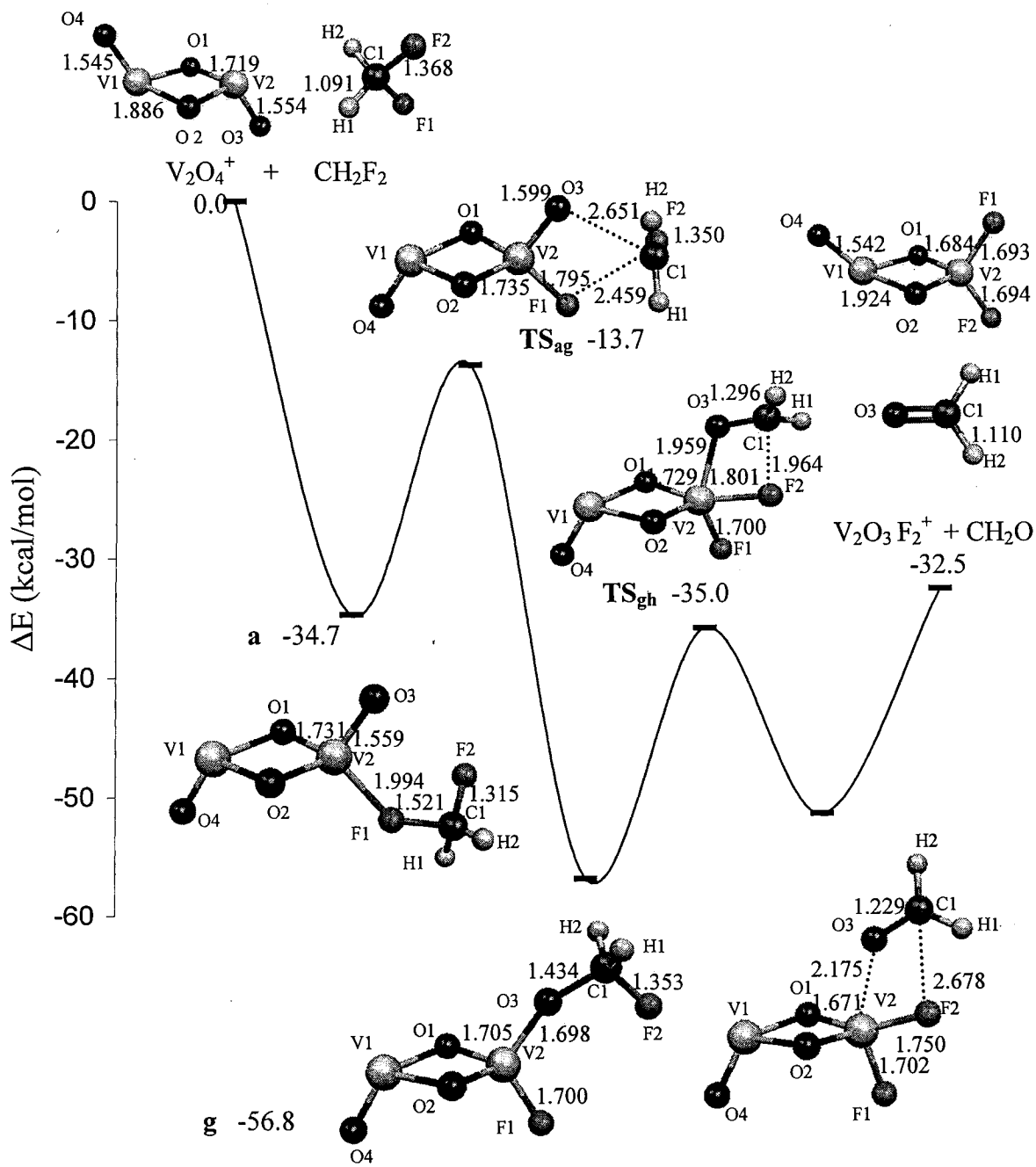

Fig. 4.5. Energy profile and structure of stationary points (with selected geometric parameters) along pathway 1 for the reaction of $V_2O_4^+$ with CH_2F_2 (terminal oxygen transfer and fluorine abstraction). Bond lengths in Å

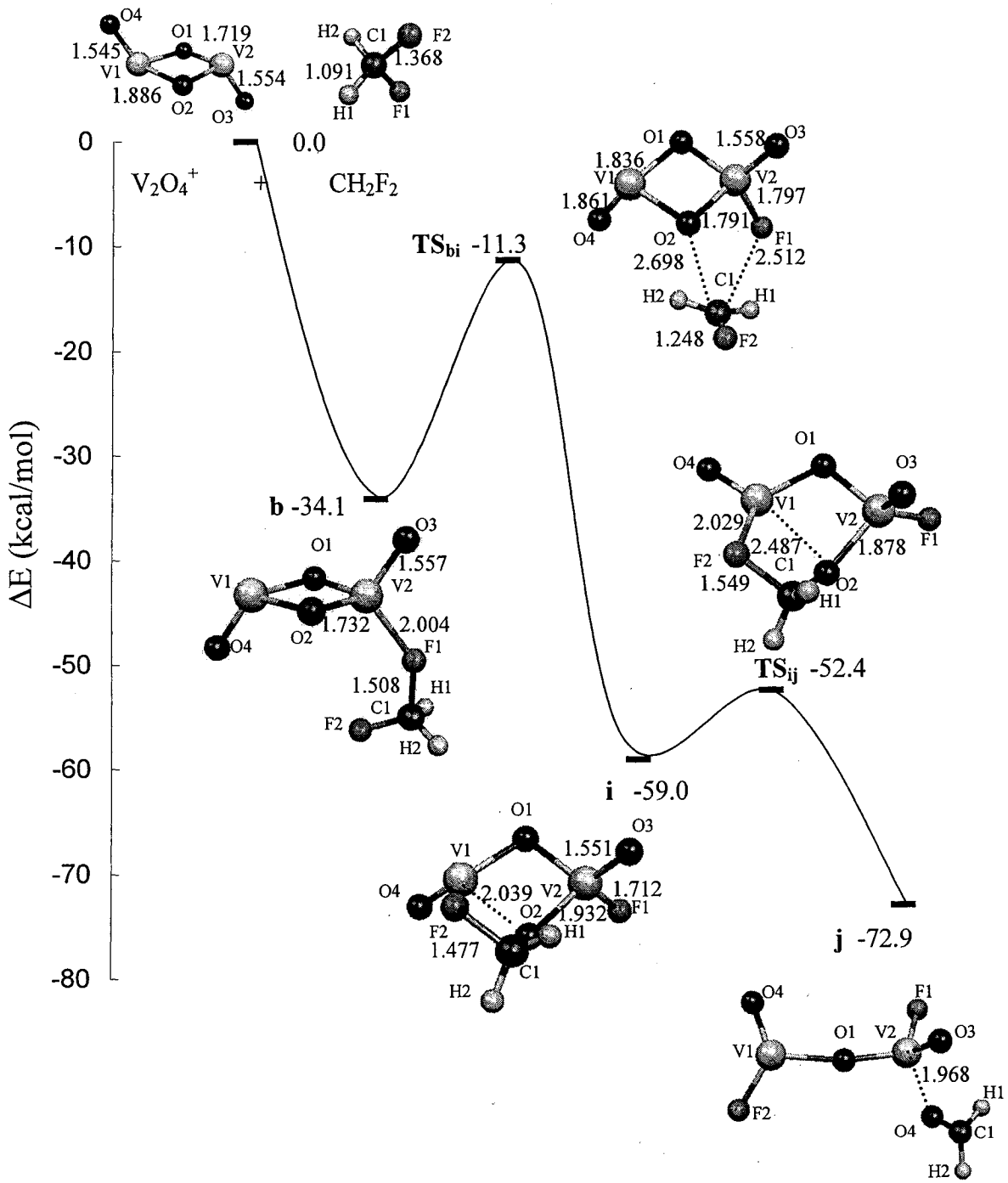

Fig. 4.6. Energy profile and structure of stationary points (with selected geometric parameters) along pathway 2 for the reaction of $V_2O_4^+$ with CH_2F_2 (bridged oxygen transfer and fluorine abstraction). Bond lengths in Å

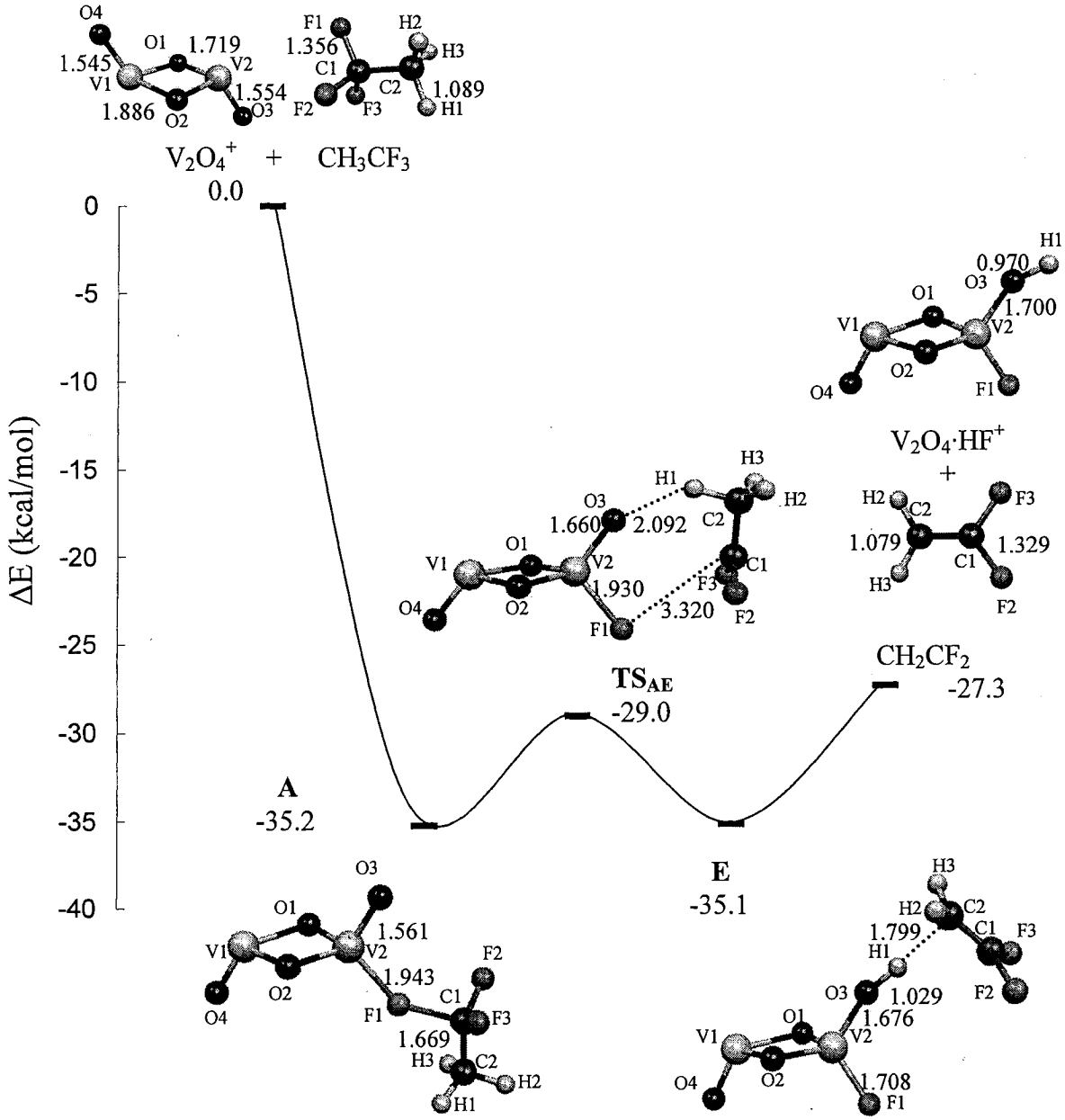

Fig. 4.7. Energy profile and structure of stationary points (with selected geometric parameters) along pathway for the reaction of $V_2O_4^+$ with $CH_3 CF_3$. Bond lengths in Å

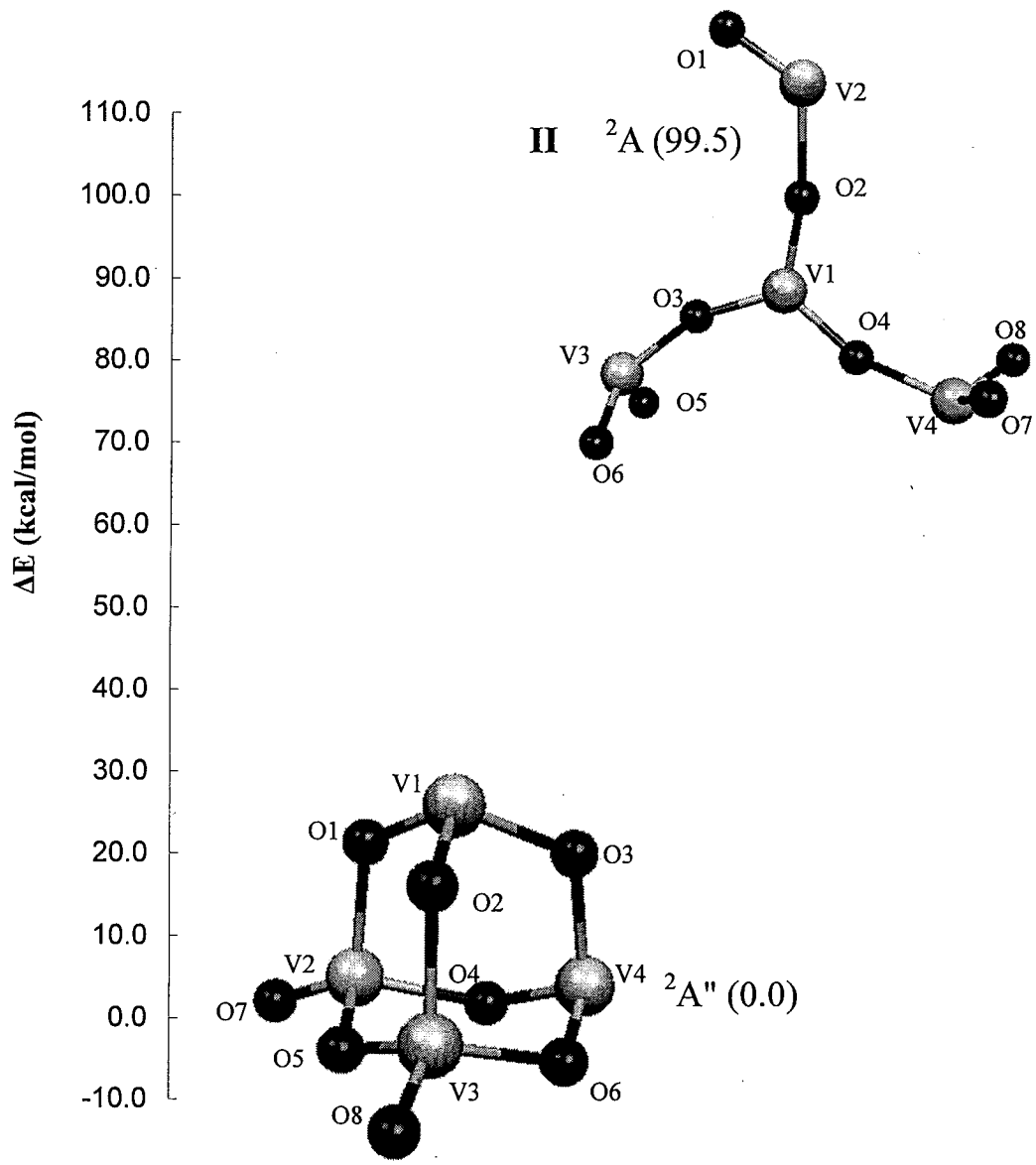

Fig. 4.8. B3LYP/TZVP minimum-energy structures and relative energies of cage-like $V_4O_8^+$ **I** and open-structure $V_4O_8^+$ **II**

Chapter 5.

General Conclusions

In the present work, the molecular geometry and electronic structure of vanadium oxide clusters $V_xO_y^+$ and V_xO_y (x=1-4, y=1-10), and the reactivity of selected $V_xO_y^+$ towards halocarbons were investigated by density-functional theory (DFT) calculations. The key results can be summarized as follows:

(1) The B3LYP/TZVP model chemistry seems appropriate to investigate vanadium oxide clusters as the VO_2^+ dissociation energy calculated with this model chemistry lies in the range of experimental data.[12] However, the less computational intensive PLAP4/DZVP+aux. model chemistry yields a similar accuracy as B3LYP/TZVP, but for half the computational cost of B3LYP/TZVP based on single-point calculations for VO_2^+ and $V_3O_6^+$. The PLAP4/DZVP+aux. model chemistry is thus more suitable for investigating large vanadium oxide clusters.

(2) Geometric parameters for VO^+ and VO predicted by the PLAP4/DZVP+aux. model chemistry are in good agreement with experimental data.[90] Our results for the molecular structures and electronic properties of bivanadium oxide $V_2O_y^+$ and V_2O_y (y=4-6) clusters are essentially in agreement with previously reported B3LYP/6-31G* results. We systematically investigated the molecular structures and electronic properties of polyvanadium oxide $V_xO_y^+$ and V_xO_y (x=3, 4; y=6-10) clusters, which had not been done before. Our results confirm that compact structures are the most stable structures for vanadium oxide clusters.

(3) For vanadium oxide cluster cations, the excess charge is delocalized and almost equally distributed over the vanadium atoms. Charge distributions do not change significantly with cluster size.

(4) Both the adiabatic and vertical ionization potentials (IPs) of neutral vanadium oxide clusters increase as a function of the cluster oxygen-to-vanadium ratio. In high oxygen-to-vanadium ratio clusters, the electron is removed from an oxygen atom upon ionization, since the location of the unpaired electron is found on the oxygen atom in the corresponding cluster cations. thus more energy is required than that of removing an electron from the vanadium atom of the low oxygen-to-vanadium ratio cluster. On the other hand, the IPs of neutral vanadium oxide clusters are not found to change significantly as a function of cluster size for clusters with a constant oxygen-to-vanadium ratio. The binding energies per atom of vanadium oxide cluster cations increase with cluster size, due to the compact structure of larger clusters.

(5) The reactions of $V_2O_4^+$ clusters with CH_2F_2 and CH_3CF_3 were investigated using the B3LYP/TZVP model chemistry. The association of $V_2O_4^+$ with fluorocarbons to form ion-molecule complexes was shown to be thermodynamically favorable and governed by the formation of V-F bonds. Charge distributions of the cluster ions and molecules do not exhibit significant changes upon complexation.

(6) The reaction of $V_2O_4^+$ with CH_2F_2 involves transfer of the terminal oxygen, along with abstraction of fluorine atoms from CH_2F_2, to form the $V_2O_4F_2^+$ and CH_2O products, which is consistent with experimental observations. However, transfer of the bridged oxygen atom leads to a much more stable $V_2O_4{\cdot}CH_2F_2^+$ product complex, which was also observed experimentally. In contrast, stepwise HF abstraction from the fluorocarbon is

predominant in the reaction of $V_2O_4^+$ with CH_3CF_3, to yield the $V_2O_4 \cdot HF^+$ product, which is again consistent with experimental observations.

(7) Oxygen transfer in the reaction of $V_xO_y^+$ with CH_2F_2 requires cleavage of a V-O bond, and the strong V-O bonds found for larger clusters such as $V_4O_8^+$ may explain why the difficulty of achieving oxygen transfer for larger clusters, and thus the experimental observation that large vanadium oxide clusters are chemically inert towards CH_2F_2. However, the reaction of $V_2O_4^+$ with CH_3CF_3 does not involve cleavage of V-O bonds, which may explain why the reactivity of vanadium oxide cluster ions was not observed to depend on cluster size experimentally.

Our findings provide invaluable information on the precise structure of vanadium oxide clusters and their reactivity towards halocarbons, and help gain insight into the molecular-level mechanism of catalysis by transition metal oxide clusters.

References

(1) Thomas, J. M.; Thomas, W. J. *Principles and Practice of Heterogeneous Catalysis*; Weinheim; New York:VCH, 1996.

(2) Council, N. R. *National Academy Press, Washington* **1992.**

(3) Nicholas, J. B. *Top. Catal.* **1997**, *4*, 157.

(4) Shido, T.; Yamaguchi, M.; Imada, Y.; Ichikawa, M. *Nippon Kagaku Kaishi* **1995**, 853.

(5) Ivanenko, S. V.; Dzhoraev, R. R. *J. Appl. Chem.* **1995**, *68*, 849.

(6) Topsoee, N. Y.; Topsoee, H.; Dumesic, J. A. *J. Catal.* **1995**, *151*, 226.

(7) Chertihin, G. V.; Bare, W. D.; Andrews, L. *J. Phys. Chem. A* **1997**, *101*, 5090.

(8) Bell, R. C.; Zemski, K. A.; Kerns, K. P.; Deng, H. T.; Castleman, J. A. W. *J. Phys. Chem. A* **1998**, *102*, 1733.

(9) Bell, R. C.; Zemski, K. A.; Castleman, J. A. W. *J. Phys. Chem. A* **1998**, *102*, 8293.

(10) Bell, R. C.; Zemski, K. A.; Castleman, J. A. W. *J. Phys. Chem. A* **1999**, *103*, 2992.

(11) Bell, R. C.; Zemski, K. A.; Castleman, J. A. W. *J. Phys. Chem. A* **1999**, *103*, 1585.

(12) Bell, R. C.; Zemski, K. A.; Justes, D. R.; Castleman, A. W., Jr. *J. Chem. Phys.* **2001**, *114*, 798.

(13) Kooi, S. E.; Castleman, A. W., Jr. *J. Phys. Chem. A* **1999**, *103*, 5671.

(14) Khan, M. I.; Yohannes, E.; Powell, D. *Inorg. Chem.* **1999**, *38*, 212.

(15) Khan, M. I.; Yohannes, E.; Doedens, R. J. *Angew. Chem. Int. Ed.* **1999**, *38*, 1292.

(16) Khan, M. I.; Yohannes, E.; Powell, D. *Chem. Commun.* **1999**, 23.

(17) Khan, M. I. *J. Solid State Chem.* **2000**, *152*, 105.

(18) Koyanagi, G. K.; Bohme, D. K.; Kretzschmar, I.; Schrolder, D.; Schwarz, H. *J. Phys. Chem. A* **2001**, *105*, 4259.

(19) Melzer, M.; Urban, J.; Sack-Kongehl, H.; Weiss, K.; Freund, H. J.; Schloegl, R. *Catal. Lett.* **2002**, *81*, 219.

(20) Fielicke, A.; Rademann, K. *Phys. Chem. Chem. Phys.* **2002**, *4*, 2621.

(21) Nieman, G. C.; Parks, E. K.; Richtsmeier, S. C.; Liu, K.; Pogo, L. G.; Riley, S. J. *High. Temp. Sci.* **1986**, *22*.

(22) Foltin, M.; Stueber, F. J.; Bernstein, E. R. *J. Chem. Phys.* **1999**, *111*, 9577.

(23) Deo, G.; Wachs, I. E.; Haver, J.; Crit, J. *Rev. Surf. Chem.* **1994**, *4*, 1.

(24) Bond, G. C. *J. Catal.* **1989**, *116*, 531.

(25) Urbanek, A.; Trela, M. *Catal. Rev. Sci. Eng.* **1980**, *21*, 73.

(26) Zemski, K. A.; Justes, D. R.; Castleman, J. A. W. *J. Phys. Chem. B* **2002**, *106*, 6136.

(27) Vyboishchikov, S. F.; Sauer, J. *J. Phys. Chem. A* **2000**, *104*, 10913.

(28) Vyboishchikov, S. F.; Sauer, J. *J. Phys. Chem. A* **2001**, *105*, 8588.

(29) Calatayud, M.; Andres, J.; Beltran, A. *J. Phys. Chem. A* **2001**, *105*, 9760.

(30) Boulet, P.; Baiker, A.; Chermette, H.; Gilardoni, F.; Volta, J. C.; Weber, J. *J. Phys. Chem. B* **2002**, *106*, 9659.

(31) Anstrom, M.; Dumesic, J. A.; Topsoe, N.-Y. *Catal. Lett.* **2002**, *78*, 281.

(32) Justes, D. R.; Mitric, R.; Moore, N. A.; Bonacic-Koutecky, V.; Castleman, A. W., Jr. *J. Am. Chem. Soc.* **2003**, *125*, 6289.

(33) Gracia, L.; Andres, J.; Safont, V. S.; Beltran, A.; Sambrano, J. R. *Organometallics* **2004**, *23*, 730.

(34) Engeser, M.; Weiske, T.; Schroeder, D.; Schwarz, H. *J. Phys. Chem. A* **2003**, *107*, 2855.

(35) Hehre, W. J.; Radom, L.; Schleyer, P.; Pople, J. A. *Ab initio Molecular Orbital Theory*; Wiley: New York, 1986.

(36) Thomas, L. H. *Proc. Cambridge Philos. Soc.* **1927**, *23*, 542.

(37) Fermi, E. Z. *Phys.* **1928**, *48*, 73.

(38) Dirac, P. A. M. *Proc. Cambridge Philos. Soc.* **1930**, *26*, 376.

(39) Car, R. *Quant. Struct.-Act. Relat.*, **2002**, *21*, 97.

(40) Slater, J. C. *Phys. Rev.* **1951**, *81*, 385.

(41) Hohengerg, P.; Kohn, W. *Phys. Rev. B* **1964**, *136*, 864.

(42) Korn, W.; Sham, L. J. *Phys. Rev.* **1965**, *140*, A1133.

(43) Tozer, D. J.; Handy, N. C. *Recent Advances in Density Functional Methods, Part II*; World Scientific: Singapore, 1997.

(44) Slater, J. C. In *Quantum Theory of Molecules and Solids*; McGraw-Hill: New York, 1974; Vol. 4.

(45) Vosko, S. J.; Wilk, L.; Nussair, M. *Can. J. Phys.* **1980**, *58*, 1200.

(46) Koch, W.; Holthausen, M. C. *A Chemist's Guide to Density Functional Theory*; WILEY-VCH: Weinheim, 2001.

(47) Perdew , J. P.; Wang , Y. *Phys. Rev. B* **1986**, *33*, 8800.

(48) Becke, A. D. *Phys. Rev. A* **1988**, *38*, 3098.

(49) Lee, C.; Yang , W.; Parr, R. G. *Phys. Rev. B* **1988**, *37*, 785.

(50) Perdew, J. P.; Chevary, J. A.; Vosko, S. H.; Jackson, K. A.; Pederson, M. R.; Singh, D. J.; Fiolhais, C. *Phys. Rev. B* **1992**, *46*, 6671.

(51) Proynov, E. I.; Vela, A.; Ruiz, E.; Salahub, D. R. *Chem. Phys. Lett.* **1994**, *230*, 419.

(52) Proynov, E. I.; Vela, A.; Ruiz, E.; Salahub, D. R. *Int. J. Quantum Chem.* **1995**, *29*, 61.

(53) Proynov, E. I.; Vela, A.; Salahub, D. R. *Phys. Rev. A* **1994**, *50*, 3766.

(54) Proynov, E. I.; Sirois, S.; Salahub, D. R. *Int. J. Quant. Chem.* **1997**, *64*, 427.

(55) Ziegler, T. *Chem. Rev.* **1991**, *91*, 651.

(56) Shimizu, R.; Fuchikami, T. *Catal. Today* **2001**, *71*, 137.

(57) Chakrabarti, A.; Hermann, K.; Druzinic, R.; Witko, M.; Wagner, F.; Petersen, M. *Phys. Rev. B: Condens. Matter* **1999**, *59*, 10583.

(58) Broclawik, E.; Borowski, T. *Chem. Phys. Lett.* **2001**, *339*, 433.

(59) Anstrom, M.; Topsoe, N.-Y.; Dumesic, J. A. *J. Catal.* **2003**, *213*, 115.

(60) Pykavy, M.; van Wullen, C.; Sauer, J. *J. Chem. Phys.* **2004**, *120*, 4207.

(61) Khaliullin, R. Z.; Bell, A. T. *J. Phys. Chem. B* **2002**, *106*, 7832.

(62) Pykavy, M.; Van Wuellen, C. *J. Phys. Chem. A* **2003**, *107*, 5566.

(63) Gracia, L.; Sambrano, J. R.; Safont, V. S.; Calatayud, M.; Beltran, A.; Andres, J. *J. Phys. Chem. A* **2003**, *107*, 3107.

(64) Calatayud, M.; Berski, S.; Beltran, A.; Andres, J. *Theor. Chem. Acc.* **2002**, *108*, 12.

(65) Calatayud, M.; Silvi, B.; Andres, J.; Beltran, A. *Chem. Phys. Lett.* **2001**, *333*, 493.

(66) Schroder, D.; Engeser, M.; Schwarz, H.; Harvey, J. N. *ChemPhysChem* **2002**, *3*, 584.

(67) Fielicke, A.; Mitric, R.; Meijer, G.; Bonacic-Koutecky, V.; Von Helden, G. *J. Am. Chem. Soc.* **2003**, *125*, 15716.

(68) Khan, M. I.; Yohannes, E.; Doedens, R. J. *Inorg. Chem.* **2003**, *42*, 3125.

(69) Chiodo, S.; Kondakova, O.; Michelini, M. d. C.; Russo, N.; Sicilia, E. *Inorg. Chem.* **2003**, *42*, 8773.

(70) Engeser, M.; Schlangen, M.; Schroeder, D.; Schwarz, H.; Yumura, T.; Yoshizawa, K. *Organometallics* **2003**, *22*, 3933.

(71) Asmis, K. R.; Meijer, G.; Bruemmer, M.; Kaposta, C.; Santambrogio, G.; Woeste, L.; Sauer, J. *J. Chem. Phys.* **2004**, *120*, 6461.

(72) Weckhuysen, B. M.; Keller, D. E. *Catal. Today* **2003**, *78*, 25.

(73) Frisch, M. J.; Trucks, G. W.; Schlegel, H. B.; Scuseria, G. E.; Robb, M. A.; Cheeseman, J. R.; Zakrzewski, V. G.; Montgomery, J. A. J.; Stratmann, R. E.; Burant, J. C. D., S.; Millam, J. M. , Daniels, A. D.; Kudin,K. N.; Strain, M. C.; Farkas, O.; Tomasi, J.; Barone, V.; Cossi, M.; Cammi, R.; Mennucci, B.; Pomelli, C.; Adamo, C.; Clifford, S.; Ocherski,J.; Petersson, G. A.; Ayala.PlY.;Cui, Q.; Morokuma, K.; Malick, D.K.; Rabuck, A. D.; Raghavachari,K.; Foresman, J. B.; Cioslowski,J.; Ortiz, J. V.; Stefanov, B. B.; Liu, G.; Liashenko,A.; Piskorz, P.; Komaromin,I.; Gomperts,R.; Martin,

R. L.; Fox, D.J.; Keith, T.; Al-Laham, M.A.; Peng, C. Y.; Nanayakkara, A.; Gonzalez, C.; Challacombe, M.; Gill, P. M. W.; Johnson, B. G.; Chen, W.; Wong, M. W.; Andres, J.L.; Head-Gordon, M.; Replogle, E. S.; Pople, J. Gaussian 98. In *Gaussian, Inc.;*, 1998; Vol. Pittsburgh, PA.

(74) M.E. Casida, C. D., A. Goursot, A. Koester, L. Pettersson, E. Proynov, A. St-Amant, D. Salahub--principal authors; H. Duarte, N. Godbout, J. Guan, C. Jamorski, M. Leboeuf, V. Malkin, O. Malkina, F. Sim, A. Vela-contributing authors. **1998**.

(75) St-Amant, A. *PhD Thesis*.

(76) St-Amant, A.; Salahub, D. R. *Chem. Phys. Lett.* **1990**, *169*, 387.

(77) Rassolov, V. A. P., J. A. ; Ratner, M. A.; Windus, T. L. *J. Chem. Phys.* **1998**, 1223.

(78) Schafer, A. H. H. A. *J. Chem. Phys.* **1994**, *100*, 5829.

(79) Russo, N.; Andzelm, J.; Salahub, D. R. *J. Chem. Phys.* **1987**, *87*, 6562.

(80) Godbout, N.; Salahub, D. R.; Andzelm, J.; Wimmer, E. *Can. J. Chem.* **1992**, *70*, 560.

(81) Schlegel, H. B. *J. Comput. Chem.* **1982**, *3*, 214.

(82) Broyden, C. G. *J. I. Math. Appl.* **1970**, *6*, 223.

(83) Fletcher, R. *Comput. J.* **1970**, *13*, 317.

(84) Shanno, D. F. *Math. Comput.* **1970**, *24*, 647.

(85) Goldfarb, D. *Math. Comput.* **1970**, *24*, 23.

(86) Shanno, D. F. *J. Optimiz. Theory App.* **1985**, *46*, 87.

(87) Mulliken, R. S. *J. Chem. Phys.* **1962**, *36*, 3428.

(88) Reed, A. E.; Curtiss, L. A.; Weinhold, F. *Chem. Rev.* **1988**, *88*, 899.

(89) Reed, A. E.; Weinstock, R. B.; Weinhold, F. *J. Chem. Phys.* **1985**, *83*, 735.

(90) Harrison, J. F. *Chem. Rev.* **2000**, *100*, 679.

(91) Becke, A. D. *J. Chem. Phys.* **1993**, *98*, 1372.

(92) Ahlrichs, R.; Baer, M.; Haeser, M.; Horn, H.; Koelmel, C. *Chem. Phys. Lett.* **1989**, *162*, 165.

(93) Wei, Y.; Peslherbe, G. H. *J. Phys. Chem. A* **2005**, To be submitted.

(94) Peng, C.; Schlegel, H. B. *Isr. J. Chem.* **1994**, *33*, 449.

(95) Peng, C.; Ayala, P.; Schlegel, H. B.; Frisch, M. J. *J. Comput. Chem.* **1996**, *17*, 49.

(96) Gonzalez, C.; Schlegel, H. B. *J. Chem. Phys.* **1989**, *90*, 2154.

(97) Gonzalez, C.; Schlegel, H. B. *J. Phys. Chem.* **1990**, *94*, 5523.

(98) Bader, R. F. W. *Atoms in Monlecules. A Quantum Theory*; Clarendon Press: Oxford, 1990.

(99) Biegler-Konig, F. W.; Bader, R. F. W.; Tang, T. *J. Comput. Chem.* **1982**, *3*, 317.

(100) Gillespie, R. J.; Bytheway, I.; Tang, T.-H.; Bader, R. F. W. *Inorg. Chem.* **1996**, *35*, 3954.

Appendix A

1. Cartesian Coordinates (Å) and Total Energy (E_h) for the Stationary Points of V_xO_y and $V_xO_y^+$ (x=1-4, y=1-10)

$VO^+ (^3\Sigma)$

O	0.000000,0.000000,1.550000	
V	0.000000,0.000000,0.004003	Total energy = -1019.020827

$VO^+ (^1\Delta)$

O	0.000000,0.000000,1.531025	
V	0.000000,0.000000,0.005001	Total energy = -1019.059711

$VO (^4\Sigma)$

O	0.000000,0.000000,1.591106	
V	0.000000,0.000000,0.000964	Total energy = -1019.284797

$VO (^2\Sigma)$

O	0.000000,0.000000,1.585005	
V	0.000000,0.000000,0.007208	Total energy = -1019.262785

$VO_2^+ (^1A_1)$

O1	0.000000,1.207004,0.745001	
O2	0.000000,1.207004,0.745001	
V1	0.000000,0.000000,-0.220004	Total energy = -1094.349928

$VO_2^+ (^3A')$

V1	-0.016002,0.000000,-0.009003	
O1	1.210001,0.000000, 1.057011	
O2	-1.182997,0.000000, 1.063025	Total energy = -1094.282156

$VO_2 (^2A_1)$

O1	0.000000, 1.280104 0.736977	
O2	0.000000, -1.280104 0.737977	
V1	0.000000, 0.000000 -0.204045	Total energy = -1094.665574

VO_2 ($^4A''$)

V1	-0.0048769,	0.000000,	-0.026014	
O1	1.2352014,	0.000000,	1.060002	
O2	-1.2190078,	0.000000,	1.074899	Total energy = -1094.595774

VO_3^+ ($^1A'$)

V1	-0.005401,	0.000000,	-0.015892	
O1	1.536309,	0.000000,	-0.021005	
O2	-0.642698,	-0.685041,	-1.488000	
O3	-0.642698,	0.685041,	-1.488000	Total energy = -1169.514954

VO_3^+ ($^3A''$)

V1	0.001219,	0.000000,	0.119023	
O1	1.516902,	0.000000,	-0.073001	
O2	-0.762047,	-0.640014	-1.488911	
O3	-0.762047,	0.640014	-1.488911	Total energy = -1169.531258

VO_3 ($^2A'$)

V1	0.112721,	0.000000,	-0.178500	
O1	1.646097,	0.000000,	0.184042	
O2	-0.548780,	-0.699330,	-1.682810	
O3	-0.548780,	0.699330,	-1.682810	Total energy = -1169.865217

VO_3 ($^4A'$)

V1	0.080068,	0.000000,	-0.213801	
O1	1.817050,	0.000000,	0.263911	
O2	-0.699007,	-0.700794,	-1.630004	
O3	-0.699007,	-0.700794,	-1.630004	Total energy = -1169.806890

trans-$V_2O_4^+$ ($^2A'$)

O1	0.047691,	0.084369,	1.217090	
V1	-0.069665,	-1.350972,	0.000000	
O2	0.047691,	0.084369,	-1.217090	
V2	0.047691,	1.297746,	0.000000	
O3	1.390168,	2.081142,	0.000000	
O4	-1.422373,	-2.096853,	0.000000	Total energy=-2188.9314642

trans-$V_2O_4^+$ ($^4A''$)

O1	0.005635,	0.058302,	1.215075	
V1	0.013340,	-1.410164,	0.000000	
O2	0.005635,	0.058302,	-1.215075	
V2	0.005635,	1.263725,	0.000000	
O3	1.232367,	2.524090,	0.000000	
O4	-1.298189,	-2.219680,	0.000000	Total energy= -2188.857280

cis-$V_2O_4^+$ ($^2A'$)

O1	0.351607,	0.082505,	1.215623	
V1	0.172814,	-1.359121,	0.000000	
O2	0.351607,	0.082505,	-1.215623	
V2	0.351607,	1.295979,	0.000000	
O3	-1.002061,	2.061929,	0.000000	
O4	-1.208864,	-2.045405,	0.000000	Total energy= -2188.924284

cis-$V_2O_4^+$ ($^4A''$)

O1	0.324689,	0.037885,	1.207153	
V1	0.183924,	-1.424311,	0.000000	
O2	0.324689,	0.037885,	-1.207153	
V2	0.324689,	1.255425,	0.000000	
O3	-0.906006,	2.504289,	0.000000	
O4	-1.205633,	-2.094511,	0.000000	Total energy=-2188.857457

Linear-open $V_2O_4^+$ (^2A)

O1	-2.961173,	0.018120,	0.783707	
V1	-1.958495,	-0.007829,	-0.398003	
O2	-0.307546,	-0.013344,	0.038836	
V2	1.556114,	0.003152,	0.328655	
O3	2.201868,	1.278749,	-0.320575	
O4	2.223698,	-1.270078,	-0.302592	Total energy= -2188.888360

Linear-open $V_2O_4^+$ (^4A)

O1	2.860373,	0.904909,	-0.073275	
V1	1.995820,	-0.368222,	0.128397	
O2	0.143366,	-0.270880,	-0.243030	
V2	-1.532983,	0.008813,	-0.330128	
O3	-1.984761,	1.480772,	0.434807	
O4	-2.349636,	-1.081499,	0.461475	Total energy= -2188.831446

trans-V_2O_4 (^1A_g)

O1	0.000000,	0.000000,	1.271219	
V1	0.000000,	1.270761,	0.000000	
O2	0.000000,	0.000000,	-1.271219	
V2	0.000000,	-1.270761,	0.000000	
O3	1.047873,	-2.454758,	0.000000	
O4	-1.047873,	2.454758,	0.000000	Total energy=-2189.206788

trans-V_2O_4 (^3B_u)

O1	0.000000,	0.000000,	1.250787	
V1	0.000000,	1.318050,	0.000000	
O2	0.000000,	0.000000,	-1.250787	
V2	0.000000,	-1.318050,	0.000000	
O3	1.142516,	-2.411796,	0.000000	
O4	-1.142516,	2.411796,	0.000000	Total energy=-2189.241868

cis-V_2O_4 ($^1A_1$)

O1	0.685758,	-0.353765,	0.764677	
V1	-0.595531,	-1.670535,	0.000000	
O2	0.685758,	-0.353765,	-0.764677	
V2	0.685758,	1.530609,	0.000000	
O3	0.514551,	3.113651,	0.000000	
O4	-2.145469,	-2.003834,	0.000000	Total energy=-2189.220834

cis-V_2O_4 ($^3B_2$)

O1	-0.759977,	0.000000,	-0.916231	
V1	0.000000,	1.661668,	-0.106896	
O2	0.759977,	0.000000,	-0.916231	
V2	0.000000,	-1.661668,	-0.106896	
O3	0.000000,	-2.522376,	1.223557	
O4	0.000000,	2.522376,	1.223557	Total energy=-2189.041921

linear-open V_2O_4 (^1A)

V1	2.008044,	-0.000655,	-0.367189	
O1	0.206784,	-0.000953,	-0.132595	
V2	-1.527328,	0.000181,	0.241625	
O2	3.060718,	0.001525,	0.808788	
O3	-2.324046,	1.323376,	-0.158374	
O4	-2.325514,	-1.322585,	-0.156823	Total energy=-2189.149962

linear-open V_2O_4 (^3A)

V1	-1.978515,	-0.290212,	0.182529
O1	-0.163056,	-0.262898,	-0.222221
V2	1.570944,	0.057391,	-0.242852
O2	-3.202743,	0.635491,	-0.225452
O3	2.041565,	1.448574,	0.381715
O4	2.496001,	-1.151808,	0.239385

Total energy= -2189.183004

four-membered ring $V_2O_5^+$ ($^2A'$)

O1	0.121334,	-0.293009,	1.192862
V1	0.121334,	1.117976,	0.000000
O2	0.121334,	-0.293009,	-1.192862
V2	0.132323,	-1.540385,	0.000000
O3	-1.224146,	-2.285099,	0.000000
O4	1.500404,	1.825196,	0.000000
O5	-1.248190,	2.260346,	0.000000

Total energy=-2264.113058

four-membered ring $V_2O_5^+$ ($^4A''$)

O1	0.188932,	-0.274435,	1.205328
V1	0.060648,	1.148524,	0.000000
O2	0.188932,	-0.274435,	-1.205328
V2	0.188932,	-1.502103,	0.000000
O3	-1.037437,	-2.744887,	0.000000
O4	1.255197,	2.168962,	0.000000
O5	-1.313166,	2.141337,	0.000000

Total energy=-2264.066084

open structure $V_2O_5^+$ (^2A)

V1	1.773037,	-0.066997,	-0.334809
O1	-0.096502,	-0.490348,	-0.297501
V2	-1.712219,	-0.332491,	0.162895
O2	2.516646,	-0.853492,	0.798673
O3	-1.924000,	0.825984,	1.210517
O4	-2.681396,	0.203654,	-1.118216
O5	2.010399,	1.462730,	-0.099221

Total energy=-2264.098097

open structure $V_2O_5^+$ (^4A)

V1	-1.742406,	-0.024485,	0.307987	
O1	0.087750,	-0.301156,	-0.077424	
V2	1.747350,	-0.102098,	-0.354436	
O2	-2.807320,	-1.142872,	-0.541237	
O3	2.231863,	1.367134,	-0.035183	
O4	2.677975,	-0.997696,	0.742465	
O5	-2.204480,	1.438517,	0.044918	Total energy=-2264.039739

four-membered ring V_2O_5 ($^1A'$)

O1	0.061614,	-0.356594,	1.238216	
V1	0.061614,	1.190311,	0.000000	
O2	0.061614,	-0.356594,	-1.238216	
V2	0.172183,	-1.499215,	0.000000	
O3	-0.994247,	-2.564312,	0.000000	
O4	1.409885,	2.030259,	0.000000	
O5	-1.211035,	2.135340,	0.000000	Total energy=-2264.505763

four-membered ring V_2O_5 ($^3A''$)

O1	0.193039,	-0.164242,	1.232132	
V1	0.064053,	1.117633,	0.000000	
O2	0.193039,	-0.164242,	-1.232132	
V2	0.193039,	-1.513119,	0.000000	
O3	-0.935125,	-2.610347,	0.000000	
O4	1.324989,	2.063576,	0.000000	
O5	-1.515081,	2.012275,	0.000000	Total energy=-2264.459897

open structure V_2O_5 (^1A)

V1	1.762687,	-0.147725,	-0.205848	
O1	-0.000018,	-0.408659,	-0.000205	
V2	-1.762630,	-0.147636,	0.205831	
O2	2.679065,	-0.649549,	0.990240	
O3	-2.226297,	1.278654,	0.722802	
O4	-2.679414,	-0.649720,	-0.989829	
O5	2.226499,	1.278439,	-0.722959	Total energy=-2264.479688

open structure V_2O_5 (^3A)

V1	1.724847,	0.041581,	-0.100620
O1	-0.017782,	-0.372943,	-0.081040
V2	-1.808096,	-0.271640,	0.041569
O2	3.025127,	-1.147832,	0.239154
O3	-2.393417,	0.450396,	1.327081
O4	-2.578102,	0.186255,	-1.268389
O5	2.203513,	1.545542,	-0.047032

Total energy=-2264.420986

Model 1 four-membered ring $V_2O_6^+$ (^2A)

V1	0.471683,	0.184925,	-1.157962
O1	1.737445,	-0.204525,	-0.098502
O2	0.551805,	-0.574799,	1.119121
V2	-0.932208,	-0.258306,	0.085938
O3	-2.303242,	0.923704,	0.695831
O4	-1.977149,	1.288827,	-0.503167
O5	2.538800,	1.075811,	0.258932
O6	-1.596953,	-1.567830,	-0.376633

Total energy=-2339.356379

Model 1 four-membered ring $V_2O_6^+$ (^4A)

O1	-0.517564,	0.282560,	-1.220780
V1	-1.923690,	0.031221,	0.000256
O2	-0.516995,	0.281047,	1.220925
V2	0.697461,	0.394189,	-0.000137
O3	2.264845,	-1.066283,	-0.000511
O4	3.466972,	-1.131497,	0.000091
O5	-2.555384,	-1.381806,	-0.000508
O6	1.383533,	1.792925,	0.000443

Total energy=-2339.339150

Model 2 four-membered ring $V_2O_6^+$ ($^2A'$)

O1	0.060269,	0.101228,	1.202023
V1	0.576685,	1.189996,	0.000000
O2	0.060269,	0.101228,	-1.202023
V2	-0.576745,	-1.210121,	0.000000
O3	-2.131208,	-1.477722,	0.000000
O4	2.319351,	1.425992,	0.000000
O5	0.060269,	-2.757955,	0.000000
O6	-0.368776,	2.665088,	0.000000

Total energy=-2339. 263597

Model 2 four-membered ring $V_2O_6^+$ ($^4A''$)

O1	-0.034531,	0.068684,	1.203329

V1	0.036299,	-1.368190,	0.000000	
O2	-0.034531,	0.068684,	-1.203329	
V2	-0.034531,	1.301776,	0.000000	
O3	1.253431,	2.545003,	0.000000	
O4	-1.409110,	2.264491,	0.000000	
O5	-1.156404,	-2.565167,	0.000000	
O6	1.376062,	-2.190756,	0.000000	Total energy=-2339.273372

open structure $V_2O_6^+$ (^2A)

V1	0.273164,	0.645560,	-0.220707	
O1	-0.259714,	-0.007277,	-0.612001	
V2	-2.077322,	-0.377064,	-0.238415	
O2	2.717416,	-0.645383,	-0.319181	
O3	-2.242062,	-1.167496,	1.107964	
O4	-2.930214,	0.938412,	-0.155874	
O5	1.366512,	1.365955,	1.148835	
O6	3.660015,	-1.256135,	0.150234	Total energy=-2339.301242

open structure $V_2O_6^+$ (^4A)

V1	-1.257131,	-0.741797,	-0.215066	
O1	0.260794,	-0.044939,	-0.635991	
V2	2.054190,	0.377092,	-0.253077	
O2	-2.947995,	0.597445,	-0.375986	
O3	2.173782,	1.287525,	1.022634	
O4	2.938563,	-0.904685,	-0.045970	
O5	-1.359827,	-1.449895,	1.163454	
O6	-3.356860,	1.563074,	0.217770	Total energy=-2339.293451

Model 1 four-membered ring V_2O_6 (^1A)

O1	0.517003,	0.454109,	1.184621	
V1	1.677267,	0.224389,	-0.053272	
O2	0.561578,	-0.195029,	-1.208934	
V2	-1.025747,	0.193972,	0.076357	
O3	-1.778533,	-1.366355,	-0.481311	
O4	-2.380825,	-0.778583,	0.677891	
O5	2.761867,	-0.893728,	0.216757	
O6	-1.554209,	1.576801,	-0.455394	Total energy=-2339.678382

Model 1 four-membered ring V_2O_6 (^3A)

O1	0.386225,	-0.255170,	-1.233456	
V1	1.711517,	-0.191594,	0.000172	
O2	0.386070,	-0.254088,	1.233664	
V2	-0.927169,	-0.258087,	0.000047	
O3	-2.042860,	1.223038,	0.657118	
O4	-2.041635,	1.223476,	-0.657617	
O5	2.798777,	0.952684,	-0.000312	
O6	-1.741578,	-1.597107,	-0.000028	Total energy=-2339.689077

Model 2 four-membered ring V_2O_6 (^1A_g)

O1	0.000000 ,	0.000000,	1.232315	
V1	1.330587,	0.000000,	0.000000	
O2	0.000000,	0.000000 ,	-1.232315	
V2	1.330587,	0.000000 ,	0.000000	
O3	-2.317545,	1.308468,	0.000000	
O4	-2.317545,	-1.308468,	0.000000	
O5	2.317545,	-1.308468,	0.000000	
O6	2.317545 ,	1.308468 ,	0.000000	Total energy=-2339.638584

Model 2 four-membered ring V_2O_6 (^3A)

O1	0.000225,	-0.007138,	1.219000	
V1	1.322518,	-0.007635,	0.000000	
O2	0.000226,	-0.007139,	-1.219870	
V2	-1.322116,	-0.006540,	0.000000	
O3	-2.404646,	1.311744,	0.000000	
O4	-2.303162,	-1.281590,	0.000000	
O5	2.296010,	-1.285528,	0.000000	
O6	2.410192,	1.310406,	0.000000	Total energy=-2339.683290

open structure V_2O_6 (^1A)

V1	1.361142,	0.353219,	-0.353572	
O1	-0.326276,	-0.245402,	-0.283297	
V2	-2.081895,	-0.358221,	0.082810	
O2	2.558000,	-0.818912,	-0.016954	
O3	-2.566184,	0.272047,	1.455879	
O4	-3.057043,	0.042032,	-1.105232	
O5	1.716086,	1.747720,	0.266244	
O6	3.747580,	-0.983107,	0.461800	Total energy=-2339.605406

open structure V_2O_6 (^3A)

V1	-1.345306,	0.279644,	-0.007663	
O1	0.341954,	-0.298811,	-0.039701	
V2	2.140779,	-0.360823,	-0.013854	
O2	-2.739285,	-0.953874,	-0.033488	
O3	2.887244,	0.243164,	-1.276406	
O4	2.844385,	0.092254,	1.333609	
O5	-1.589031,	1.828271,	0.075055	
O6	-4.032250,	-0.677614,	0.002794	Total energy=-2339.614814

open structure $V_3O_6^+$ (^1A)

V1	-3.358028,	-1.033101,	-0.566091	
O1	-2.816909,	-2.488002,	-0.876298	
O2	-2.262291,	-0.056090,	0.440401	
V2	-0.906226,	0.818377,	1.255034	
O3	0.715439,	0.289989,	0.843000	
O4	-1.089087,	2.383312,	0.984098	
V3	2.230001,	-0.317355,	-0.065301	
O5	2.842129,	-1.611959,	0.678012	
O6	1.783108,	-0.762000,	-1.552356	Total energy=-3284.607707

open structure $V_3O_6^+$ (^3A)

V1	-3.344219,	-1.044996,	-0.560705	
O1	-2.840590,	-2.494827,	-0.954627	
O2	-2.162126,	-0.113808,	0.461000	
V2	-0.880013,	0.834307,	1.253525	
O3	0.773796,	0.393846,	0.881058	
O4	-1.118637,	2.390985,	0.976654	
V3	2.216631,	-0.322690,	-0.075124	
O5	2.805285,	-1.619101,	0.682198	
O6	1.688832,	-0.799786,	-1.524359	Total energy=-3284.612326

six-membered ring $V_3O_6^+$ ($^1A_1$)

V1	1.947011,	0.000000,	0.000000	
V2	-0.973506,	1.686161,	0.000000	
V3	-0.973506,	-1.686161,	0.000000	
O1	2.929205,	0.000000,	1.249542	
O2	-1.464603,	2.536766,	1.249542	
O3	-1.464603,	-2.536766,	1.249542	
O4	0.813139,	1.425102,	0.057766	
O5	-1.640744,	-0.008352,	0.057766	
O6	0.827605,	-1.416750,	0.057766	Total energy=-3284.641489

six-membered ring $V_3O_6^+$ ($^3A''$)

V1	1.947012,	0.000000,	0.000000	
V2	-0.973506,	1.686161,	0.000000	
V3	-0.973506,	-1.686161,	0.000000	
O1	2.929206,	0.000000,	1.249542	
O2	-1.464603,	2.536766,	1.249542	
O3	-1.464603,	-2.536766,	1.249542	
O4	0.813139,	1.425102,	0.057766	
O5	-1.640744,	-0.008352,	0.057766	
O6	0.827605,	-1.416750,	0.057766	Total energy=-3284.662481

open structure V_3O_6 (^2A)

V1	-2.755476,	-0.145630,	-0.287176	
O1	-2.051826,	-1.385629,	-1.046504	
O2	-2.509910,	-0.425531,	1.540800	
V2	-1.076409,	0.592026,	1.105581	
O3	0.606185,	0.074269,	0.926361	
O4	-1.836049,	1.712547,	0.003696	
V3	2.034452,	-0.558162,	-0.151070	
O5	3.276134,	-1.378197,	0.548183	
O6	1.451858,	-1.261762,	-1.500251	Total energy=-3284.881728

open structure V_3O_6 (^4A)

V1	-3.517082,	-1.025601,	-0.563055	
O1	-3.555461,	-2.596934,	-0.919613	
O2	-2.108968,	-0.239828,	0.286067	
V2	-0.816542,	0.818843,	0.968893	
O3	0.960953,	0.497635,	0.867250	
O4	-1.252067,	2.353734,	1.255253	
V3	2.335381,	-0.310002,	-0.012826	
O5	3.090782,	-1.500502,	0.799220	
O6	2.001961,	-0.773416,	-1.541570	Total energy=-3284.882622

six-membered ring V_3O_6 ($^2A'$)

V1	1.928311,	0.000000,	0.000000	
V2	-0.964155,	1.669966,	0.000000	
V3	-0.964155,	-1.669970,	0.000000	
O1	3.182726,	0.000000,	1.011317	
O2	-1.591363,	2.756322,	1.011317	
O3	-1.591363,	-2.756322,	1.011317	
O4	0.813182,	1.408170,	0.237303	
O5	-1.626102,	0.000151,	0.237303	
O6	0.812919,	-1.408322,	0.237303	Total energy=-3284.922796

six-membered ring V_3O_6 ($^4A'$)

V1	1.910530,	0.000000,	0.000000	
V2	-0.955265,	1.654567,	0.000000	
V3	-0.955265,	-1.654567,	0.000000	
O1	3.245251,	0.000000,	0.905041	
O2	-1.622626,	2.810470,	0.905041	
O3	-1.622626,	-2.810470,	0.905041	
O4	0.850359,	1.472246,	0.133081	
O5	-1.700182,	0.000309,	0.133081	
O6	0.849823,	-1.472555,	0.133081	Total energy=-3284.952758

open structure $V_3O_7^+$ (^1A)

V1	-3.068839,	-1.039557,	-1.003398	
O1	-3.352670,	-2.774836,	-0.686920	
O2	-1.908306,	-0.218584,	-0.006207	
V2	-0.865426,	0.654746,	1.264337	
O3	0.848496,	0.422808,	0.980169	
O4	-1.219894,	2.211322,	1.288257	
V3	2.267368,	-0.173577,	-0.094396	
O5	3.110926,	-1.318270,	0.664778	
O6	1.637432,	-0.826699,	-1.436129	
O7	-4.516420,	-1.935878,	-0.395684	Total energy=-3359.824404

open structure $V_3O_7^+$ (^3A)

V1	-2.988518,	-1.087361,	-3.826719	
O1	-3.264974,	-2.843382,	-0.698554	
O2	-2.077585,	-0.091962,	0.134189	
V2	-0.896972,	0.748800,	1.278940	
O3	0.770391,	0.320000,	0.976565	
O4	-1.076966,	2.336355,	1.250238	
V3	2.244498,	-0.208795,	-0.057421	
O5	2.972847,	-1.479313,	0.614183	
O6	1.692772,	-0.663268,	-1.509500	
O7	-4.442826,	-2.029599,	-0.430546	Total energy=-3359.843874

six-membered ring $V_3O_7^+$ ($^1A'$)

O1	-0.159544,	0.000000,	-1.415752	
O2	-0.592763,	0.000000,	0.000000	
O3	3.681929,	0.000000,	1.479292	
V1	3.130525,	0.000000,	0.000000	
O4	2.344860,	1.628692,	-0.161947	
O5	2.344860,	-1.628692,	-0.161947	
O6	0.000000,	2.537132,	1.107043	
O7	0.000000,	-2.537132,	1.107043	
V2	0.567217,	1.540331,	0.000000	
V3	0.567217,	-1.540331,	0.000000	Total energy=-3359.876245

six-membered ring $V_3O_7^+$ ($^3A'$)

O1	0.000000,	0.000000,	-1.406080	
O2	-0.622917,	0.000000,	0.000000	
O3	3.688700,	0.000000,	1.525556	
V1	3.226076,	0.000000,	0.000000	
O4	2.339059,	1.560866,	-0.222490	
O5	2.339059,	-1.560866,	-0.222490	
O6	0.000000,	2.665161,	1.001224	
O7	0.000000,	-2.665161,	1.001224	
V2	0.543925,	1.552894,	0.000000	
V3	0.543925,	-1.552894,	0.000000	Total energy=-3359.892143

open structure V_3O_7 (^2A)

V1	-3.195148,	-0.960900,	-0.585360	
O1	-2.949874,	-2.691271,	-1.098477	
O2	-2.470957,	0.089590,	0.659561	
V2	-0.912261,	0.952261,	1.123410	
O3	0.742750,	0.270797,	0.892909	
O4	-0.983264,	2.562972,	1.110678	
V3	2.141552,	-0.408957,	-0.054311	
O5	3.019035,	-1.571780,	0.676478	
O6	1.827712,	-0.804866,	-1.595510	
O7	-4.286879,	-2.436373,	-0.554570	Total energy=-3360.109699

open structure V_3O_7 (^4A)

V1	-3.154093,	-0.974407,	-0.607422	
O1	-2.973938,	-2.734103,	-1.077149	
O2	-2.428081,	0.041232,	0.644719	
V2	-0.898493,	0.987734,	1.051200	
O3	0.764509,	0.276640,	0.931791	
O4	-1.014370,	2.596087,	1.146386	
V3	2.147398,	-0.405159,	-0.036756	
O5	2.993274,	-1.611742,	0.656029	
O6	1.800758,	-0.765145,	-1.587257	
O7	-4.304296,	-2.409663,	-0.546734	Total energy=-3360.122908

six-membered ring V_3O_7 ($^2A'$)

O1	0.000000,	0.000000,	-1.466798	
O2	-0.314016,	0.000000,	0.000000	
O3	3.178215,	0.000000,	1.303659	
V1	2.257344,	0.000000,	0.000000	
O4	1.980539,	1.815321,	-0.514089	
O5	1.980539,	-1.815321,	-0.514089	
O6	0.000000,	2.667230,	1.348478	
O7	0.000000,	-2.667230,	1.348478	
V2	0.306183,	1.837684,	0.000000	
V3	0.306183,	-1.837684,	0.000000	Total energy=-3360.136123

six-membered ring V_3O_7 ($^4A'$)

O1	0.000000,	0.000000,	-1.461090	
O2	0.193000,	0.000000,	0.000000	
O3	3.307803,	0.000000,	1.407258	
V1	2.533839,	0.000000,	0.000000	
O4	2.215211,	1.762897,	-0.521005	
O5	2.215211,	-1.762897,	-0.521005	
O6	0.000000,	2.975794,	1.119210	
O7	0.000000,	-2.975794,	1.119210	
V2	0.505219,	1.927988,	0.000000	
V3	0.505219,	-1.927988,	0.000000	Total energy=-3360.146661

open structure $V_3O_8^+$ (^1A)

V1	-3.221356,	-0.894173,	-0.757807	
O1	-2.833504,	-2.631650,	-0.965637	
O2	-2.148785,	-0.017609,	0.155584	
V2	-0.819255,	1.068853,	1.233417	
O3	0.896980,	0.501522,	0.948816	
O4	-1.045278,	2.594310,	0.685914	
V3	2.157229,	-0.355435,	-0.012001	
O5	2.543970,	-1.775416,	0.682309	
O6	1.524328,	-0.707803,	-1.473353	
O7	-3.922294,	-2.377333,	-0.022788	
O8	-1.189237,	1.076314,	2.825240	Total energy=-3435.102501

open structure $V_3O_8^+$ (^3A)

V1	-3.192517,	-0.927647,	-0.733032	
O1	-2.866517,	-2.681856,	-0.982867	
O2	-2.122971,	0.030630,	0.166129	
V2	-0.839086,	1.072160,	1.209759	
O3	0.871375,	0.499558,	0.936966	
O4	-0.997527,	2.631803,	0.726762	
V3	2.154970,	-0.345056,	-0.013738	
O5	2.533477,	-1.764681,	0.685843	
O6	1.533193,	-0.711181,	-1.473248	
O7	-3.958869,	-2.412516,	-0.050932	
O8	-1.172731,	1.090365,	2.828053	Total energy=-3435.119293

six-membered ring $V_3O_8^+$ ($^1A'$)

O1	0.000000,	0.000000,	-0.898892	
O2	1.558971,	0.000000,	1.119573	
O3	1.248215,	0.000000,	-1.676198	
O4	4.430911,	0.000000,	0.981791	
V1	3.192243,	0.000000,	0.000000	
O5	2.651293,	1.797730,	-0.289177	
O6	2.651293,	-1.797730,	-0.289177	
O7	0.000000,	2.611110,	0.634875	
O8	0.000000,	-2.611110,	0.634875	
V2	0.907980,	1.466582,	0.000000	
V3	0.907980,	-1.466582,	0.000000	Total energy=-3435.188274

six-membered ring $V_3O_8^+$ ($^3A'$)

O1	0.000000,	0.000000,	-2.996029	
O2	2.033846,	0.000000,	1.942096	
O3	2.523812,	0.000000,	-3.834098	
O4	7.414820,	0.000000,	1.968895	
V1	5.175794,	0.000000,	0.000000	
O5	4.316606,	3.396122,	-0.514651	
O6	4.316606,	-3.396122,	-0.514651	
O7	0.000000,	5.179734,	1.687977	
O8	0.000000,	-5.179734,	1.687977	
V2	1.002294,	2.933905,	0.000000	
V3	1.002294,	-2.933905,	0.000000	Total energy=-3435.209803

open structure V_3O_8 (^2A)

V1	-1.692255,	-1.008337,	-0.286102	
O1	-2.905453,	-2.093492,	-1.063818	
O2	-1.541023,	-1.058349,	1.485519	
V2	-0.835185,	0.699242,	1.595024	
O3	0.984101,	0.635757,	1.282900	
O4	-1.526095,	0.961081,	0.002188	
V3	1.410685,	-0.300879,	-0.203966	
O5	2.665326,	-1.270963,	0.010489	
O6	-0.054127,	-1.173736,	-0.962790	
O7	-3.244067,	-0.687459,	-1.251413	
O8	-1.319109,	1.778713,	2.691663	Total energy=-3435.505724

open structure V_3O_8 (^4A)

V1	-2.735001,	-1.183305,	-0.429313	
O1	-3.120047,	-2.906209,	-1.276040	
O2	-2.220403,	0.152882,	0.484932	
V2	-0.789041,	1.145000,	1.365785	
O3	0.846217,	0.280003,	1.206858	
O4	-0.709390,	2.601990,	0.627201	
V3	1.980233,	-0.295197,	-0.057193	
O5	2.986552,	-1.465001,	0.428909	
O6	1.149223,	-0.793000,	-1.372674	
O7	-4.254429,	-2.429003,	-0.622401	
O8	-1.193893,	1.373836,	2.927007	Total energy=-3435.490955

six-membered ring V_3O_8 ($^2A'$)

O1	0.000000,	0.000000,	-0.955047	
O2	1.732405,	0.000000,	1.174945	
O3	1.265739,	0.000000,	-1.709801	
O4	4.879245,	0.000000,	0.649581	
V1	3.414740,	0.000000,	0.000000	
O5	2.856387,	1.684148,	-0.350565	
O6	2.856387,	-1.684148,	-0.350565	
O7	0.000000,	2.473166,	0.580828	
O8	0.000000,	-2.473166,	0.580828	
V2	1.012642,	1.363478,	0.000000	
V3	1.012642,	-1.363478,	0.000000	Total energy=-3435.539895

six-membered ring V_3O_8 ($^4A'$)

O1	0.857480,	-0.004698,	-1.458718	
O2	1.165548,	0.002711,	1.348314	
O3	-0.921293,	0.013069,	0.011267	
O4	3.951382,	-0.002653,	1.174230	
V1	2.692779,	0.007150,	0.199336	
O5	2.167193,	1.680873,	-0.493282	
O6	2.170055,	-1.672157,	-0.495080	
O7	-0.064118,	2.594847,	1.055475	
O8	-0.072728,	-2.607067,	1.061116	
V2	0.391038,	1.356168,	0.154702	
V3	0.394400,	-1.368243,	0.155729	Total energy=-3435.662364

open structure $V_4O_8^+$ (^2A)

V1	-2.850129,	-1.417928,	-1.768009	
O1	-3.509400,	-2.798025,	-1.260337	
O2	-1.011033,	-1.461738,	-1.389002	
V2	0.004002,	-1.096992,	-0.023026	
O3	1.590329,	-1.798026,	0.119002	
O4	-0.261436,	0.490003,	0.690218	
V3	3.275890,	-2.246923,	-0.591894	
O5	3.133307,	-3.147104,	-1.927007	
O6	4.040030,	-0.884339,	-0.998903	
O7	-3.541363,	-0.208022,	-0.939005	
V4	-0.040193,	2.198001,	1.343992	
O8	1.378999,	2.487003,	2.004374	Total energy=-4379.582301

open structure $V_4O_8^+$ (^4A)

V1	-2.713682,	-1.383237,	-1.814324	
O1	-3.510868,	-2.717250,	-1.380259	
O2	-0.930808,	-1.463176,	-1.222243	
V2	0.131444,	-1.056277,	0.102645	
O3	1.803997,	-1.562375,	0.087505	
O4	-0.328110,	0.376017,	1.030784	
V3	3.368553,	-2.244595,	-0.715267	
O5	3.018344,	-3.476846,	-1.699825	
O6	4.061524,	-1.098227,	-1.612128	
O7	-3.442564,	-0.107589,	-1.126988	
V4	-0.339426,	2.084298,	1.726032	
O8	1.091856,	2.766566,	1.884654	Total energy=-4379.603875

Cage-like structure $V_4O_8^+$ ($^2A'$)

O1	0.000000,	0.000000,	-0.732116	
V1	3.354250,	0.000000,	0.000000	
V2	1.745200,	0.000000,	2.218900	
O2	3.497043,	0.000000,	1.792017	
O3	0.875196,	1.418993,	1.702236	
O4	0.875196,	-1.418993,	1.702236	
V3	0.759696,	1.565400,	-0.193770	
V4	0.759696,	-1.565400,	-0.193770	
O5	2.582781,	1.411216,	-0.675479	
O6	2.582781,	-1.411216,	-0.675479	
O7	-0.006465,	2.823640,	-0.793659	
O8	-0.006465,	-2.823640,	-0.793659	Total energy=-4379.738313

Cage-like structure $V_4O_8^+$ ($^4A'$)

O1	0.000000,	0.000000,	-0.791379	
V1	3.635461,	0.000000,	0.000000	
V2	1.589953,	0.000000,	2.432780	
O2	3.292666,	0.000000,	1.742695	
O3	0.907094,	1.394750,	1.632518	
O4	0.907094,	-1.394750,	1.632518	
V3	0.869126,	1.528450,	-0.267408	
V4	0.869126,	-1.528450,	-0.267408	
O5	2.696618,	1.364224,	-0.663645	
O6	2.696618,	-1.364224,	-0.663645	
O7	0.141589,	2.832194,	-0.816476	
O8	0.141589,	-2.832194,	-0.816476	Total energy=-4379.726401

open structure V_4O_8 (^1A)

V1	-2.569257,	-1.302472,	-1.748090	
O1	-3.326979,	-2.742237,	-1.877298	
O2	-0.947437,	-1.310569,	-0.858659	
V2	0.125392,	-0.885882,	0.487610	
O3	1.833535,	-1.307300,	0.479379	
O4	-0.625222,	0.059967,	1.848880	
V3	3.154025,	-1.774974,	-0.739337	
O5	3.007449,	-3.217519,	-1.478533	
O6	3.542224,	-0.612684,	-1.809875	
O7	-3.601275,	-0.163989,	-1.202967	
V4	0.060682,	1.458820,	0.886165	
O8	1.557122,	1.916150,	1.273313	Total energy=-4379.849995

open structure V_4O_8 (^3A)

V1	-2.553559,	-1.267389,	-1.527698	
O1	-2.854441,	-2.865831,	-1.547384	
O2	-0.737373,	-0.676192,	-1.499979	
V2	-0.058165,	-1.163939,	0.012912	
O3	1.219736,	-2.404601,	0.145717	
O4	-0.023720,	0.105728,	1.213649	
V3	2.845944,	-2.194539,	-0.698413	
O5	3.094692,	-3.100824,	-2.013815	
O6	3.312393,	-0.640118,	-0.886681	
O7	-3.589099,	-0.515512,	-0.520773	
V4	0.826219,	1.755181,	0.848165	
O8	0.727632,	3.085346,	1.734886	Total energy=-4379.854068

Cage-like structure V_4O_8 ($^1A'$)

O1	0.000000,	0.000000,	-0.682284	
V1	3.287909,	0.000000,	0.000000	
V2	1.682055,	0.000000,	2.243384	
O2	3.440009,	0.000000,	1.800659	
O3	0.800274,	1.440757,	1.768247	
O4	0.800274,	-1.440757,	1.768247	
V3	0.723261,	1.579444,	-0.134740	
V4	0.723261,	-1.579444,	-0.134740	
O5	2.543730,	1.439421,	-0.670269	
O6	2.543730,	-1.439421,	-0.670269	
O7	-0.061496,	2.869410,	-0.694381	
O8	-0.061496,	-2.869410,	-0.694381	Total energy=-4380.014669

Cage-like structure V_4O_8 ($^3A'$)

O1	0.000000,	0.000000,	-0.817303	
V1	3.376363,	0.000000,	0.000000	
V2	1.843520,	0.000000,	2.086741	
O2	3.625674,	0.000000,	1.803999	
O3	0.944581,	1.434816,	1.599668	
O4	0.944581,	-1.434816,	1.599668	
V3	0.820052,	1.560641,	-0.295388	
V4	0.820052,	-1.560641,	-0.295388	
O5	2.633343,	1.428495,	-0.746252	
O6	2.633343,	-1.428495,	-0.746252	
O7	0.097765,	2.889955,	-0.849007	
O8	0.097765,	-2.889955,	-0.849007	Total energy=-4380.025724

Cage-like structure $V_4O_9^+$ ($^2A'$)

V1	0.000000,	0.000000,	2.592130	
O1	1.604301,	0.000000,	1.890151	
O2	-0.802150,	1.389365,	1.890151	
O3	-0.802150,	-1.389365,	1.890151	
V2	1.788682,	0.000000,	0.000000	
V3	-0.894341,	1.549044,	0.000000	
V4	-0.894341,	-1.549044,	0.000000	
O4	-1.728382,	0.000000,	-0.464186	
O5	0.864191,	-1.496823,	-0.464186	
O6	0.864191,	1.496823,	-0.464186	
O7	3.287894,	0.000000,	-0.524353	
O8	-1.643947,	2.847399,	-0.524353	
O9	-1.643947,	-2.847399,	-0.524353	Total energy= -4455.083450

Cage-like structure $V_4O_9^+$ ($^4A'$)

O1	0.000000,	0.000000,	-0.323308	
O2	5.036930,	0.000000,	-0.687177	
V1	3.573324,	0.000000,	0.000000	
V2	1.901862,	0.000000,	2.654453	
O3	3.486592,	0.000000,	1.879188	
O4	1.050581,	1.399646,	1.971950	
O5	1.050581,	-1.399646,	1.971950	
V3	0.807549,	1.572217,	0.142575	
V4	0.807549,	-1.572217,	0.142575	
O6	2.521786,	1.411999,	-0.470329	
O7	2.521786,	-1.411999,	-0.470329	
O8	0.064361,	2.947654,	-0.293398	
O9	0.064361,	-2.947654,	-0.293398	Total energy=-4455.153409

Cage-like structure V_4O_9 ($^1A_1$)

V1	0.000000,	0.000000,	2.302523	
O1	1.726383,	0.000000,	1.853612	
O2	-0.863191,	1.495091,	1.853612	
O3	-0.863191,	-1.495091,	1.853612	
V2	1.746375,	0.000000,	0.000000	
V3	-0.873188,	1.512405,	0.000000	
V4	-0.873188,	-1.512405,	0.000000	
O4	-1.685166,	0.000000,	-0.633063	
O5	0.842583,	-1.459397,	-0.633063	
O6	0.842583,	1.459397,	-0.633063	
O7	3.260598,	0.000000,	-0.543740	
O8	-1.630299,	2.823761,	-0.543740	
O9	-1.630299,	-2.823761,	-0.543740	Total energy=-4455.389101

Cage-like structure V_4O_9 ($^3A_2$)

V1	0.000000,	0.000000,	2.544321	
O1	1.642230,	0.000000,	1.897814	
O2	-0.821115,	1.422213,	1.897814	
O3	-0.821115,	-1.422213,	1.897814	
V2	1.807707,	0.000000,	0.000000	
V3	-0.903853,	1.565520,	0.000000	
V4	-0.903853,	-1.565520,	0.000000	
O4	-1.664230,	0.000000,	-0.542435	
O5	0.832115,	-1.441265,	-0.542435	
O6	0.832115,	1.441265,	-0.542435	
O7	3.307386,	0.000000,	-0.570879	
O8	-1.653693,	2.864280,	-0.570879	
O9	-1.653693,	-2.86428,	-0.570879	Total energy=-4455.405228

Cage-like structure $V_4O_{10}^+$ ($^2A_1$)

O1	0.000000,	0.000000,	4.167614	
V1	0.000000,	0.000000,	2.560981	
O2	1.667627,	0.000000,	1.812069	
O3	-0.833814,	1.444208,	1.812069	
O4	-0.833814,	-1.444208,	1.812069	
V2	1.816937,	0.000000,	0.000000	
V3	-0.908468,	1.573513,	0.000000	
V4	-0.908468,	-1.573513,	0.000000	
O5	-1.670264,	0.000000,	-0.516922	
O6	0.835132,	-1.446491,	-0.516922	
O7	0.835132,	1.446491,	-0.516922	
O8	3.342846,	0.000000,	-0.527660	
O9	-1.671423,	2.894990,	-0.527660	
O10	-1.671423,	-2.894990,	-0.527660	Total energy= -4530.330184

Cage-like structure $V_4O_{10}^+$ ($^4A'$)

O1	0.000000,	0.000000,	4.252120	
V1	0.000000,	0.000000,	2.616751	
O2	1.638535,	0.000000,	1.815358	
O3	-0.819267,	1.419013,	1.815358	
O4	-0.819267,	-1.419013,	1.815358	
V2	1.846667,	0.000000,	0.000000	
V3	-0.923334,	1.599261,	0.000000	
V4	-0.923334,	-1.599261,	0.000000	
O5	-1.647526,	0.000000,	-0.505491	
O6	0.823763,	-1.426799,	-0.505491	
O7	0.823763,	1.426799,	-0.505491	
O8	3.388668,	0.000000,	-0.542181	
O9	-1.694334,	2.934672,	-0.542181	
O10	-1.694334,	-2.934672,	-0.542181	Total energy=-4530.282201

Cage-like structure V_4O_{10} ($^1T_2$)

O1	0.000000,	0.000000,	4.135673	
V1	0.000000,	0.000000,	2.531484	
O2	1.685275,	0.000000,	1.823236	
O3	-0.842637,	1.459491,	1.823236	
O4	-0.842637,	-1.459491,	1.823236	
V2	1.792428,	0.000000,	0.000000	
V3	-0.896214,	1.552288,	0.000000	
V4	-0.896214,	-1.552288,	0.000000	
O5	-1.686996,	0.000000,	-0.552379	
O6	0.843498,	-1.460981,	-0.552379	
O7	0.843498,	1.460981,	-0.552379	
O8	3.305397,	0.000000,	-0.533593	
O9	-1.652699,	2.862558,	-0.533593	
O10	-1.652699,	-2.862558,	-0.533593	Total energy=-4530.754494

Cage-like structure V_4O_{10} ($^3A_2$)

O1	0.000000,	0.000000,	4.217842	
V1	0.000000,	0.000000,	2.589183	
O2	1.655369,	0.000000,	1.820482	
O3	-0.827684,	1.433591,	1.820482	
O4	-0.827684,	-1.433591,	1.820482	
V2	1.820988,	0.000000,	0.000000	
V3	-0.910494,	1.577022,	0.000000	
V4	-0.910494,	-1.577022,	0.000000	
O5	-1.702390,	0.000000,	-0.472135	
O6	0.851195,	-1.474313,	-0.472135	
O7	0.851195,	1.474313,	-0.472135	
O8	3.368318,	0.000000,	-0.501969	
O9	-1.684159,	2.917049,	-0.501969	
O10	-1.684159,	-2.917049,	-0.501969	Total energy=-4530.762781

Vibrational Frequency for VO_y^+ and VO_y (y=1-3)

VO_y^+ and VO_y	Frequency (cm^{-1})
VO^+ ($^1\Delta$)	1182.77(96.82)
VO^+($^3\Sigma$)	1141.08 (80.76)
VO ($^2\Sigma$)	1095.95(206.53)
VO ($^4\Sigma$)	1046.44(193.29)
VO_2^+($^1A_1$)	458.09(7.92);1111.60(194.22);1151.10(24.26)
VO_2^+ ($^3A'$)	203.01(16.42);661.54(49.09);1111.77(68.37)
VO_2 ($^2A_1$)	294.81(3.58);1007.96 (367.76);1035.97(40.89)
VO_2 ($^4A''$)	126.97(20.90);558.07(107.91); 1053.62(191.92)
VO_3^+($^3A''$)	224.43(17.60); 248.32 (8.81);514.13(1.77);583.25 (32.85); 1173.98 (122.75);1229.34(60.70)
VO_3^+ ($^1A'$)	198.65(10.98);300.99(20.73);623.63(8.22);680.35(16.16); 1034.73(68.35);1159.52(147.68);
VO_3 ($^2A'$)	217.59(48.50);262.13(19.20);640.00(30.78);651.00(29.24); 943.01(103.66);1081.47 (295.99)
VO_3 ($^4A'$)	187.40(11.45);472.78(16.41);545.08(62.68);576.96(570.43); 1025.51(244.38);1193.82(52.80)

Vibrational Frequency for $V_2O_y^+$ and V_2O_y (y=4-6)

	Frequency (cm^{-1})
trans-$V_2O_4^+$ ($^2A'$)	114.78(23.35);196.11(15.27);210.79(2.54);331.64(0.92);351.80(36.54); 393.62(28.09);443.77(244.37);652.18(3.32);790.18(156.71);861.66 (145.09);1128.53(320.26) ;1148.57(63.51)
trans-$V_2O_4^+$ ($^4A''$)	70.06(11.86);144.89(13.09);155.24(5.10);231.76(0.12);313.49(56.68); 337.57(0.81);339.03(3.15);636.09(298.12);714.85(84.55);742.52(167.6 7);858.85(179.03);1150.57(185.32);
cis-$V_2O_4^+$ ($^2A'$)	106.34(1.07);202.55(46.69);220.01(1.62);316.98(0.01);352.88(5.37); 373.21(39.55);427.53(2.66);655.82(263.98);778.93(172.99);868.29(182 .25);1121.70(203.49);1153.34(142.75)
cis-$V_2O_4^+$ ($^4A''$)	70.84(1.14);168.47(21.66);190.72(0.07);216.87(3.07);328.41(26.61); 359.51(31.92);390.58(0.89);631.40(311.37);697.50(46.03);755.04(154. 41); 848.49(132.90); 1146.37(176.84);
Linear-$V_2O_4^+$(^2A)	42.33(18.27);71.12(29.22);97.79(33.59);171.68(8.21);267.45(36.88); 302.79(85.18);359.52(5.71);451.46(9.14);942.13(827.53);1088.05(244. 83);1106.93(90.22);1129.20(116.19);
Linear-$V_2O_4^+$(^4A)	50.66(10.83);63.46(18.21);105.80(48.52);141.10(78.77);204.20(16.10); 276.1496(61.59);311.26(40.75);326.69(106.52);540.01(276.24);654.74(192.73);1009.74(194.92);1113.70(285.29)
trans-V_2O_4 (^1A_g)	77.19(23.95);170.69(0.00);200.05(12.57);267.60(68.36);297.22(0.00) ;379.00(0.00);463.53(74.57);577.83(0.00);754.34(0.00);785.34(169.93) 1074.31(590.06);1102.80(0.00)
trans-V_2O_4 (^3B_u)	90.81(22.42);177.64(0.00);198.25(18.99);292.82(0.00);311.38(71.84); 359.18(0.00);458.88(0.00);693.74(599.17);720.49(180.28);745.20(0.00) ; 1071.69(667.27);1096.02(0.00);
cis-V_2O_4 ($^1A_1$)	37.33(0.06);95.87(51.48);133.55(0.00);136.37(48.08)210.62(51.29); 370.95(58.24);391.31(11.97);424.26(0.00);539.84(297.27);826.07(14.4 5) ;1064.19(424.12);1092.15(296.51)
cis-V_2O_4 ($^3B_2$)	16.69(45.44);28.88(6.41);99.42(17.45);124.49(60.57);185.18(35.59);35 6.38(13.15);358.93(71.35);455.58(0.80);546.13(327.71);816.46(9.57);1 051.71(546.80);1084.16(214.59)
linear-V_2O_4 (^1A)	43.07(13.00);48.37(23.90);70.61(49.08);147.47(8.02);261.08(103.61); 293.31(20.83);318.84(9.85);444.27(8.18);875.03(535.66);1047.97(418. 85);1059.84(320.88);1085.87(142.19)
linear-V_2O_4 (^3A)	35.25(18.52);42.92(19.94);78.95(39.44);118.29(11.58);249.75(126.58); 302.42(17.20);326.22(1.34);435.38(24.02);896.59(960.30);1040.84(373 .79);1058.54(274.60);1066.20(88.37)
four-membered ring $V_2O_5^+$($^2A'$)	91.88(4.70);161.93(1.17);206.25(13.73);215.20(7.35);260.07(0.49);331. 63(0.04);392.89(16.10);432.95(11.76);489.94(2.79);690.28(163.55) ;752.04(179.24);764.72(129.09);865.35(159.79);1133.75(255.29);1142. 82(61.34)
four-membered	65.41(5.83);135.07(1.62);154.86(8.49);156.28(7.39);211.96(2.01);245.0

rin $V_2O_5^+$ ($^4A''$)	4(0.02);322.56(30.56);375.33(1.21);422.67(0.00);574.44(0.01);661.07(343.97);705.67(27.45);758.65(134.94);834.83(82.12);1011.86(140.91)
Open $V_2O_5^+(^2A)$	26.37(6.94);62.24(3.16);67.31(9.34);164.98(3.20);190.90(43.09);224.86(8.72);300.24(44.24);333.32(26.73);357.80(22.68);453.46(19.13);547.86(6.25);938.15(654.46);995.92(23.10);1089.64(215.35);1114.64(43.36)
Open $V_2O_5^+(^4A)$	26.26(7.89);61.23(2.38);71.67(23.29);130.42(3.70);171.41(13.38);208.61(6.59);218.66(15.22);288.72(60.22);332.78(17.15);349.26(7.75);512.22(26.39);657.47(84.01);812.05(13.48);992.79(168.15);1082.8499(144.73)
four-membered ring $V_2O_5(^1A')$	86.47(7.39);170.31(27.96);179.85(2.36);194.98(11.27);273.50(1.69);323.04(2.31);368.97(33.23);391.54(10.34);431.40(4.77);577.52(171.30);851.67(190.97);913.70(193.60);1066.62(347.00)1073.28(236.80);1097.49(135.64)
four-membered ring $V_2O_5(^3A'')$	83.94(6.22);179.40(13.47);184.55(0.11);205.29(18.78);254.74(3.04);313.50(0.38);350.54(34.92);391.86(1.60);505.47(0.08);677.27(53.81);700.74(442.93);738.06(159.01);774.53(58.91);1086.83(509.04);1103.59(46.88)
V_2O_5 (^1A) Open	44.48(7.38);54.09(11.38);55.25(0.10);169.91(13.78);176.73(68.01);289.87(36.33);300.88(51.89);323.93(5.54);383.27(8.32);483.10(3.68);933.51(1021.21);1058.12(265.06);1072.33(275.63);1072.85(235.26);1083.04(107.94)
V_2O_5 (^3A) Open	30.32(4.64);33.93(11.49);50.33(4.64);102.91(29.30);142.89(8.35);201.81(46.64);280.81(44.49);293.36(22.22);333.53(3.21);450.81(9.92);647.92(53.49);919.41(1098.16);1043.99(171.18);1073.52(260.51);1076.63(151.62)
Model 1 four-membered ring $V_2O_6^+$ (^2A)	84.26(5.43);129.74(2.28);143.73(4.38);205.54(11.12);233.99(4.93);243.27(2.22);330.30(1.09);360.01(7.29);407.39(11.44);426.59(20.29);507.76(0.13);582.35(11.56);689.34(307.08);779.35(115.77);889.33(201.77); 1132.38(232.25);1160.85(103.41);1239.39(84.93)
Model 1 four-membered ring $V_2O_6^+$ (^4A)	48.26(1.21);48.76(0.94);110.69(0.08);114.28(11.03);162.44(11.73);199.46(14.84);215.00(2.95);257.08(4.04);328.29(0.92);354.73(48.20);423.51(33.00);449.51(3.38);658.60(292.96);786.36(149.57);851.00(175.47);1124.23(327.24);1143.72(68.01);1610.91(25.40)
Model 2 four-membered ring $V_2O_6^+$ ($^2A'$)	60.46(6.86);109.19(5.13);124.63(1.62);153.87(19.29);165.74(2.47);212.92(1.80);266.59(0.38);269.01(0.28);335.26(35.11);406.39(0.25);442.89(1.61);475.45(65.05);667.94(186.93);745.01(231.43);761.38(109.11);766.05(68.85);836.0(85.57);1139.15(132.08);
Model 2 four-membered ring $V_2O_6^+$ ($^4A''$)	47.16(14.36);95.53(2.94);119.57(6.12);156.80(11.37);165.04(3.90);184.50(0.29);212.80(0.83);259.94(0.16);307.72(57.45);371.56(0.72);428.67(78.90);431.96(0.74);571.39(0.36)649.81(389.33);720.56(15.09);756.61(103.21);819.91(35.91);1003.27(132.09)
Open $V_2O_6^+(^2A)$	26.09(3.30);43.01(0.97);58.89(3.75);85.52(1.74);111.54(9.35);157.30(7.15);207.30(56.28);239.05(4.82);277.59(33.75);304.83(30.38);326.16(47.87);363.18(34.34);463.93(32.27);910.59(964.85);1089.05(229.11);1105.57(42.77);1130.98(174.58);1442.05(400.52)

Open $V_2O_6^+(^4A)$	19.87(3.07);32.67(0.92);59.24(3.12);65.31(1.11);95.84(10.58);121.54(1.21);183.51(19.62);197.21(43.71);262.18(18.66);288.37(52.36);336.58(42.02);364.24(13.15);466.09(20.37);912.86(768.33);1088.31(240.81);1102.04(52.31);1128.04(145.99) ;1603.40(21.97)
Model 1 four-membered ring V_2O_6 (^1A)	77.22(6.13);147.44(6.29);180.44(2.72);201.51(17.6);232.11(5.70); 253.67(2.88);301.60(11.78);337.25(3.44);364.64(31.28);388.48(7.22);563.06(129.14);622.03(36.75);693.46(64.28);844.23(184.67);941.11(151.43); 984.32(163.12);1085.63(377.28);1094.74(119.38);
Model 1 four-membered ring V_2O_6 (^3A)	77.12(5.27);106.43(4.32);42.46(1.16);171.79(21.28);221.62(10.80); 222.79(1.49);309.40(0.42);339.56(8.39);363.40(21.51);439.07(0.98); 489.75(6.27);566.43(26.32);701.82(556.86);719.84(163.85);763.01(10.45); 1088.37(496.99);1114.30(70.78);1205.19(64.04)
Model 2 four-membered ring V_2O_6 (^1A_g)	89.58(2.03);144.50(0.00);169.69(22.72);174.42(0.00);214.36(0.00); 220.18(3.22);241.99(0.00);261.06(0.00);333.34(7.21);391.28(0.00); 430.89(2.07);490.94(0.00);617.72(43.08);711.89(0.00);751.65(0.00); 764.89(28.47);889.02(0.64);960.65(0.00)
Model 2 four-membered ring V_2O_6 (^3A)	89.56(2.04);144.46(1.09);169.69(22.71);174.41(0.89);214.3781(2.17); 220.0909(3.25);241.99(0.46)261.08(0.33);333.37(0.15);391.21(0.74); 430.63(2.06);490.68(0.33);617.47(43.04);711.61(0.47); 751.75(0.51); 764.97(28.51);889.06(0.64);960.6790(0.01)
open V_2O_6 (^1A)	29.09(7.96);40.08(12.07);51.53(0.21);110.59(4.75);132.04(24.97); 177.91(35.83);252.28(2.18);279.09(43.36);314.42(37.23);331.52(4.63); 374.62(13.87);479.31(3.91);673.04(47.43);910.83(1122.05);1066.56(214.61);1071.90(265.26);1105.78(252.42);1223.76(210.09)
open V_2O_6 (^3A)	26.90(11.58);41.72(3.26);42.86(2.22);98.21(2.25);116.77(25.39);135.07(7.40);149.31(14.43);210.35(45.17);291.47(31.58);297.25(27.54);338.47(7.00);451.97(18.02);583.38(126.89);918.25(1139.30);1069.45(136.71);1074.78(295.46);1097.43(236.24);1143.17(8.13)

Vibrational Frequency for $V_3O_y^+$ and V_3O_y (y=6-8)

	Frequency (cm^{-1})
open structure $V_3O_6^+$ (^1A)	10.58(0.78);24.26(14.61);62.90(11.68);70.34(0.81);91.54(9.43);107.86(110.41);164.32(74.48);191.49(224.46);206.55(29.63);256.84(132.23);266.67(60.65);307.96(92.84);375.68(200.70);419.49(507.62);482.96(550.44);745.73(1031.11);859.21(138.84);987.08(89.53);1005.93(88.91);1039.58(315.88);1264.30(3257.61)
open structure $V_3O_6^+$ (^3A)	11.71(0.77);44.61(146.83);99.48(68.85);103.33(24.62);144.48(294.93);176.27(140.57);208.26(15.12);225.83(553.76);243.83(273.71);262.83(188.55);286.45(719.16);353.04(221.98);397.64(764.94);470.01(373.06);505.94(488.96);544.14(139.43);638.74(1486.14);972.25(808.05);1042.13(175.27);1509.88(2471.15);1585.71(1105.97)
six-membered ring $V_3O_6^+$ ($^1A_1$)	9.78(1.09);30.63(13.37);72.40(2.23);78.54(1.47);91.28(10.01);112.63(59.94);148.29(78.44);181.94(126.26);214.19(18.03);236.45(82.22);242.37(40.56);297.96(84.92);356.84(192.60);429.46(437.32);459.63(450.37);645.73(831.19);759.21(88.97);887.83(99.57);995.39(185.01);1085.82(1215.87);1298.50(259.61)
six-membered ring $V_3O_6^+$ ($^3A''$)	13.74(0.47);39.75(146.83);98.85(49.42);108.63(14.69);150.22(99.38);179.35(240.72);218.64(35.29);229.99(458.74);247.53(171.78);275.32(157.50);289.45(527.36);343.14(329.18);387.49(664.94);450.91(473.26);520.49(386.95);575.10(194.23);684.98(1385.14);982.52(851.34);1107.15(79.72);1419.84(1947.38);1558.59(1064.87)
open structure V_3O_6 (^2A)	3.09(4.67);15.87(2.76);21.50(0.42);43.67(7.91);61.57(20.51);70.07(12.82);122.93(44.09);141.33(26.62);167.96(14.61);211.07(24.88);234.59(22.39);275.53(3.12);340.91(14.20);420.86(31.99);510.33(24.23);706.74(55.68);723.12(82.98);956.38(255.59);981.47(170.72);982.22(277.15);1011.74(165.71)
open structure V_3O_6 (^4A)	13.27(1.86);40.99(3.95);53.79(0.24);157.48(0.79);162.36(0.26);168.00(0.14);175.04(0.36);183.47(0.55);189.07(0.05);240.82(1.91);253.22(3.69);287.31(58.97);497.86(4.51);559.74(0.08);561.04(0.16);620.09(10.46);621.94(2.21);627.68(0.87);998.77(1.50);1001.80(29.34);1019.80(75.53)
six-membered ring V_3O_6 ($^2A'$)	8.99(2.17);14.53(1.86);24.47(0.95);50.73(10.82);58.34(20.51);68.53(18.62);123.13(48.32);148.83(28.35);186.74(16.37);221.39(28.49);243.36(25.84);275.98(18.39);353.81(13.40);480.69(52.19);580.33(34.28);696.74(6.93);728.92(102.86);964.83(235.58);975.70(1100.32);985.92(251.77);1027.85(178.91)
six-membered ring V_3O_6 ($^4A'$)	15.32(0.65);36.34(4.31);50.88(0.44);142.93(0.97);164.93(1.64);171.20(0.31);179.14(1.34);185.79(0.52);190.17(0.35);237.83(2.34);259.52(19.63);274.24(38.70);397.86(4.18);536.32(0.24);572.53(15.62);604.88(13.60);623.04(42.20);667.84(0.27);938.57(515.80);1011.80(830.37);1058.80(375.53)
open structure $V_3O_7^+$ (^1A)	0.53(3.51);22.66(4.57);29.94(5.48);30.80(16.50);54.24(63.47);82.57(5.21);87.54(20.60);132.39(35.67);176.11(59.24);188.04(94.66);211.86(

	9.97);284.63(57.66);327.74(26.79);331.70(47.90);420.18(38.98);517.48(7.04);568.87(26.81);618.77(64.85);939.12(1452.1);959,99(80.81);1137.(391.54);1264.14(15.29);1545.26(20.99)
open structure $V_3O_7^+$ (^3A)	0.80(2.53);17.19(1.48);40.90(4.52);53.30(9.69);74.19(8.38);79.89(5.90);123.22(6.15);168.67(2.38);178.08(11.56);226.42(30.41);241.22(26.87);279.17(26.03);295.07(16.51);338.85(32.93);386.79(1.72);453.77(10.94);535.55(12.88);601.35(2.57);708.01(16.92);831.23(270.91);921.97(141.07);990.27(81.10);1005.31(133.31);1028.99(142.27)
six-membered ring $V_3O_7^+$ ($^1A'$)	0.98(0.78);24.26(14.61);62.90(11.68);70.34(0.81);91.54(9.43);103.33(24.62);144.48(294.93);176.27(140.57);208.26(15.12);225.83(553.76);243.83(273.71);262.83(188.55);286.45(719.16);353.04(221.98);.387.49(64.94);450.91(473.26);520.49(386.95);575.10(194.23);684.98(385.14); 998.77(1.50);1001.80(29.34);1019.80(75.53);1051.22(61.90)
six-membered ring $V_3O_7^+$ ($^3A'$)	1.34(1.31);21.48(4.66);33.69(3.25);86.35(2.35);90.39(1.91);138.05(18.55);171.79(21.28);221.62(10.80);222.79(1.49);309.40(0.42);339.56(8.39);363.40(21.51);439.07(0.98);583.38(126.89);637.43(60.94);745.73(1031.11);859.21(138.84);907.08(89.53);918.25(1139.30);963.83(235.58);1069.45(136.71);1074.78(295.46);1097.43(236.24);1143.17(8.13)
open structure V_3O_7 (^2A)	3.74(0.47);26.09(3.30);43.01(0.97);58.89(3.75);85.52(1.74);98.85(49.42);111.54(9.35);157.30(7.15);207.30(56.28);239.05(4.82);277.59(33.75);304.83(30.38);391.21(0.74);430.63(2.06);490.68(0.33);539.75(146.83);617.47(43.04);711.61(0.47);751.75(0.51);764.97(28.51);889.06(0.64);960.68(471.15); 1009.88(51.68);1185.71(5.97)
open structure V_3O_7 (^4A)	4.36(0.81);28.12(7.08);40.39(1.31);54.39(1.49);80.75(3.67);98.65(5.12);149.56(35.62);180.16(40.57);234.30(7.90);276.94(51.09);281.68(9.32);292.32(72.23);299.43(45.71);309.01(57.33);331.35(2.26);436.51.(3.45);548.07(0.92);639.43(14.30);745.73(331.11);918.25(1139.30);969.45(136.71);1074.78(295.46);1097.43(236.24);1143.17(8.13)
six-membered ring V_3O_7 ($^2A'$)	0.99(1.17);24.47(0.95);50.73(10.82);68.53(18.62);93.58(6.20);123.13(48.32);148.83(28.35);186.74(16.37);221.39(28.49);243.36(25.84);275.98(18.39);298.34(20.51);353.81(13.40);413.92(4.76);480.69(52.19);580.33(34.28);696.74(6.93);814.53(1.86);923.96(1365.64);940.66(1090.32);968.83(29.53);1081.90(18.49);1104.50(432.63);1137.78(59.23)
six-membered ring V_3O_7 ($^4A'$)	2.36(0.81);28.12(7.08);40.39(1.31);54.39(1.49);80.75(3.67);98.65(5.12);139.43(14.30);149.56(35.62);180.16(40.57);234.30(7.90);276.94(51.09);281.68(9.32);292.32(72.23);299.43(45.71);309.01(57.33);386.24(17.85);395.92(29.48);458.84(17.32);500.28(30.39);636.51.(3.45);848.07(30.92);923.96(1365.64);1004.66(1090.32);1068.83(29.55)
open structure $V_3O_8^+$ (^1A)	15.47(4.59);36.20(3.58);67.88(1.28);112.20(1.34);128.53(0.99);149.55(3.94);150.01(0.08);187.07(13.35);202.73(0.03);233.88(57.12);241.92(2.37);245.76(0.77);319.28(0.20);355.22(24.75);368.23(45.76);416.62(4.67);514.29(0.80);580.09(65.73);607.58(0.93);620.65(215.81);806.67(130.27);877.33(170.83);922.70(209.97);1034.42(205.11);1110.81(200.33);1146.05(139.77);1162.67(19.77)
open structure	9.70(8.11);29.27(0.56);34.85(0.33);53.55(0.81);61.04(14.90);63.94(4.

$V_3O_8^+$ (^3A)	95);90.16(2.46);127.51(3.73);136.96(1.07);174.34(31.69);213.56(17.01);268.85(50.55);275.58(55.70)348.88(32.13);426.03(14.46);450.82(15.78);492.91(17.39);498.03(15.46);665.00(25.39);822.40(153.30);953.94(532.98);1023.37(283.77);1092.68(228.39);1109.50(20.94);1115.22(34.88);1126.70(120.34);1154.76(65.20)
six-membered ring $V_3O_8^+$ ($^1A'$)	19.52(6.26);31.42(9.30);38.44(5.81);84.55(6.92);90.81(0.17);119.20(9.37);129.77(0.12);169.15(21.32);184.59(17.64);213.12(1.06);218.71(3.84);246.54(4.85);294.45(28.82);301.47(102.26);383.89(6.01);465.39(15.48);588.74(28.69);905.90(190.26);936.34(552.49);1025.62(161.46);1028.60(257.83);1097.85(107.30);1126.62(125.08);1160.87(17.87);1194.69(0.01);1411.63(0.64);1511.93(0.46)
six-membered ring $V_3O_8^+$ ($^3A'$)	15.13(0.64);69.15(1.54);126.60(3.09);148.35(0.12);162.41(4.05);170.08(10.92);185.40(0.97);219.56(13.52);225.98(8.60);250.11(20.37);271.85(0.73);289.67(15.89);339.24(11.73);350.91(10.72);362.89(7.80);481.43(9.65);489.64(0.03);511.75(30.62);557.81(26.13);608.54(100.83)726.81(50.27);884.98(385.14);998.77(1.50);1001.80(29.34);1119.80(75.53);1251.22(61.90) ;1432.48(0.83)
open structure V_3O_8 (^2A)	10.50(2.46);26.65(2.28);51.09(16.34);73.91(1.65);119.14(1.25);137.30(3.41);147.02(17.56);200.61(16.14);210.89(2.74);234.73(0.44);291.74(5.68);328.02(0.87);356.72(47.30);455.01(36.36);458.27(2.88);476.04(30.55);519.76(1.28);659.53(384.46);705.68(351.74);779.41(155.21);846.53(151.15);1120.52(15.16);1125.34(382.64);1139.67(10/26);1206.01(101.54);1232.78(2.38);1412.34(3.71)
open structure V_3O_8 (^4A)	7.59(2.17);24.47(0.95);50.73(10.82);68.53(18.62);123.13(48.32);148.83(28.35);186.74(16.37);221.39(28.49);243.36(25.84);275.98(18.39);314.53(1.86);353.81(13.40);480.69(52.19);516.33(4.82);580.33(34.28);696.74(6.93);728.92(102.86);858.34(20.51);964.83(235.58);975.70(1100.32);985.92(251.77);1027.85(178.91);1084.42(205.11);1210.81(200.33);1298.05(139.77);1462.67(19.77)
six-membered ring V_3O_8 ($^2A'$)	13.36(1.81);28.12(7.08);40.39(1.31);54.39(1.49);80.75(3.67);98.65(5.12);149.56(35.62);180.16(40.57);234.30(7.90);276.94(51.09);281.68(9.32);292.32(72.23);299.43(45.71);309.01(57.33);331.35(2.26);436.51.(3.45);548.07(0.92);639.43(14.30);745.73(331.11);918.25(1139.30);969.45(136.71);1074.78(295.46);1097.43(236.24);1143.17(8.13);1225.86(593.10);1390.72(140.30); 1454.25(81.69)
six-membered ring V_3O_8 ($^4A'$)	17.19(1.48);40.90(4.52);53.30(9.69);74.19(8.38);79.89(5.90);123.22(6.15);168.67(2.38);178.08(11.56);226.42(30.41);241.22(26.87);279.17(26.03);295.07(16.51);338.85(32.93);386.79(1.72);453.77(10.94);535.55(12.88);601.35(2.57);708.01(16.92);831.23(270.91);921.97(141.07);990.27(81.10);1005.31(133.31);1028.99(142.27);1134.90(58.29);1290.46(100.05);1365.86(593.10);1420.72(30.40)

Vibrational Frequency for $V_4O_y^+$ and V_4O_y (y=6-8)

	Frequency (cm^{-1})
open structure $V_4O_8^+$ (^2A)	6.34(1.31);21.48(4.66);23.69(3.25);26.35(2.35);30.39(1.91);38.05(35.29);59.34(0.17);71.57(0.16);101.42(2.55);123.31(29.69);142.10(26.35);177.26(46.17);216.18(5.90);267.49(42.05);270.07(10.11);285.51(81.11);286.58(47.61);298.65(57.33);379.64(28.71);385.84(30.64);455.90(11.21);498.32(29.83);896.29(1924.55);910.19(1343.55);948.78(123.59);1081.91(13.44);1084.50(487.73);1097.78(69.24);1098.04(91.63);1101.25(116.80)
open structure $V_4O_8^+$ (^4A)	14.36(0.81);28.12(7.08);31.35(2.26);36.51.(3.45);40.39(1.31);48.07(30.92);54.39(1.49);80.75(3.67);98.65(5.12);139.43(14.30);149.56(35.62);180.16(40.57);234.30(7.90);276.94(51.09);281.68(9.32);292.32(72.23);299.43(45.71);309.01(57.33);386.24(17.85);395.92(29.48);458.84(17.32);500.28(30.39);923.96(1365.64);940.66(1090.32);968.83(29.53);1181.90(18.49);1204.50(432.63);1297.78(59.23);1315.04(87.23);1354.25(181.96)
Cage-like structure $V_4O_8^+$ ($^2A'$)	36.16(0.43);80.73(0.39);137.74(2.06);154.27(0.11);160.15(3.04);169.44(4.60);182.31(0.53);218.71(12.02);222.07(0.75);230.88(16.63);239.03(0.00);246.79(16.61);277.71(3.70);287.03(4.70);343.04(5.44);348.41(6.72);355.48(12.28);487.15(18.77);488.33(0.00);507.57(1.08);510.30(27.26);611.65(90.38);630.70(98.67);644.36(277.97);719.93(33.36);721.08(46.42);722.83(175.73);843.23(158.82);1131.99(319.30);1144.31(150.40);
Cage-like structure $V_4O_8^+$ ($^4A'$)	28.13(0.64);69.15(1.54);126.60(3.09);148.35(0.12);162.41(4.05);170.08(10.92);185.40(0.97);219.56(13.52);225.98(8.60);232.48(0.83);250.11(20.37);271.85(0.73);289.67(15.89);339.24(11.73);350.91(10.72);362.89(7.80);481.43(9.65);489.64(0.03);511.75(30.62);557.81(26.13);608.54(100.83);627.70(87.68);720.40(46.31);726.81(50.27);739.35(270.39);752.66(31.59);834.90(58.29);900.46(100.05);1125.86(593.10);1190.72(140.30)
open structure V_4O_8 (^2A)	8.95(0.98);24.38(2.64);26.47(4.52);27.91(2.30);32.50(3.46);39.16(25.23);57.63(0.56);69.58(0.83);108.24(8.45);131.23(39.34);159.05(26.50);188.96(71.69);227.45(6.43);264.81(12.75);280.19(8.09);287.48(51.33);290.73(27.10);309.34(109.54);365.42(78.12);395.50(25.31);463.21(90.11);500.53(13.98);876.59(1493.37);905.37(940.38);936.56(100.95);1058.68(43.77);1073.39(379.57);1084.94(48.30);1093.38(31.62);11110.39(47.32)
open structure V_4O_8 (^4A)	16.43(0.18);22.18(8.07);35.31(3.62);37.50.(2.54);43.90(4.82);47.08(29.30);59.34(4.92);75.80(6.37);89.56(12.50);123.94(13.49);145.96(56.32);176.16(57.42);243.30(0.90);267.48(19.05);289.50(4.02);296.29(52.23);308.43(41.57);339.06(53.13);385.73(25.46);399.42(49.84);469.84(32.17);530.94(210.93);823.69(165.45);930.96(1295.23);986.88(53.29);1090.81(49.81);1264.53(463.34);1279.78(23.59);1351.24(23.87);1396.52(196.81)
Cage-like	60.85(9.27);136.09(16.17);173.11(1.26);184.87(0.68);187.72(0.74);19

structure V_4O_8 ($^1A'$)	0.26(1.23);203.24(0.05);222.42(0.33);234.52(16.53);238.51(0.00);243.63(3.25);266.34(0.02);295.78(15.33);303.25(8.67);322.54(11.14);327.94(8.81);463.01(2.87);515.46(15.01);518.78(0.00);562.06(4.91);583.31(61.40);632.75(4.50);648.46(71.90);690.39(118.84);696.01(69.97);712.49(118.76);763.33(257.33);785.73(87.55);1093.32(474.45);1104.85(171.57)
Cage-like structure V_4O_8 ($^3A'$)	49.59(8.01);122.14(10.73);171.38(3.62);194.96(1.18);197.65(0.94);199.93(0.39);213.56(0.94);230.23(0.48);245.29(7.84);249.51(0.20);253.70(2.26);285.42(0.12);298.32(14.02);311.52(7.64);319.49(15.98);357.94(18.95);465.69(4.89);520.62(15.01);528.84(0.03);557.04(4.90);580.51(41.80);630.54(18.30);638.46(45.44);671.93(109.83);700.54(59.83);721.93(176.54);747.38(287.36);991.96(54.31);1098.20(575.22);1139.46(160.54)
Cage-like structure $V_4O_9^+$ ($^2A'$)	26.16(0.43);80.73(2.39);137.74(2.06);154.27(0.11);160.15(3.04);169.44(4.60);182.31(0.53);218.71(12.02);222.07(0.75);230.88(16.63);239.03(0.00);246.79(16.61);277.71(3.70);287.03(4.70);343.04(5.44);348.41(6.72);355.48(12.28);487.15(18.77);488.33(0.00);507.57(1.08);510.30(27.26);611.65(90.38);630.70(98.67);644.36(277.97);719.93(33.36);721.08(46.42);722.83(175.73);843.23(158.82);1131.99(319.30);1184.31(150.40); 1291.96(454.31);1318.20(74.12);1439.46(54.50)
Cage-like structure $V_4O_9^+$ ($^4A'$)	19.34(1.31);21.48(4.66);23.69(3.25);26.35(2.35);30.39(1.91);38.05(35.29);59.34(0.17);71.57(0.16);101.42(2.55);123.31(29.69);142.10(26.35);177.26(46.17);216.18(5.90);267.49(42.05);270.07(10.11);285.51(81.11);286.58(47.61);298.65(57.33);379.64(28.71);385.84(30.64);455.90(11.21);498.32(29.83);896.29(1924.55);910.19(1343.55);948.78(123.59);1031.91(13.44);1084.50(487.73);1097.78(69.24);1198.04(91.63);1131.25(616.80);1218.79(23.59);1351.24(23.87);1496.52(81.96)
Cage-like structure V_4O_9 ($^1A_1$)	50.58(3.27);136.09(16.17);173.11(1.26);184.87(0.68);187.72(0.74);190.26(1.23);203.24(0.05);222.42(0.33);234.52(16.53);238.51(0.00);243.63(3.25);266.34(0.02);295.78(15.33);303.25(8.67);322.54(11.14);327.94(8.81);463.01(2.87);515.46(15.01);518.78(0.00);562.06(4.91);583.31(61.40);632.75(4.50);648.46(71.90);690.39(118.84);696.01(69.97);712.49(118.76);763.33(257.33);785.73(87.55);951.96(54.31);1008.20(575.22); 1093.32(474.45); 1189.46(160.54);1304.85(41.57)
Cage-like structure V_4O_9 ($^3A_2$)	47.40(8.01);122.14(10.73);171.38(3.62);194.96(1.18);197.65(0.94);199.93(0.39);213.56(0.94);230.23(0.48);245.29(7.84);249.51(0.20);253.70(2.26);285.42(0.12);298.32(14.02);311.52(7.64);319.49(15.98);357.94(18.95);465.69(4.89);520.62(15.01);528.84(0.03);557.04(4.90);580.51(41.80);630.54(18.30);638.46(45.44);671.93(109.83);700.54(59.83);721.93(176.54);747.38(287.36);891.96(54.31);963.52(196.81);1002.80(575.22);1079.46(160.54);1146.53(463.34);1189.78(23.59);
Cage-like structure $V_4O_{10}^+$ ($^2A_1$)	23.52(6.26);31.42(9.30);38.44(5.81);84.55(6.92);90.81(0.17);119.20(9.37);129.77(0.12);169.15(21.32);184.59(17.64);213.12(1.06);218.71(3.84);246.54(4.85);294.45(28.82);301.47(102.26);383.89(6.01);436.39(15.48);465.69(4.89);520.62(15.01);528.84(0.03);588.74(28.69);690.39(118.84);696.01(69.97);712.49(118.76);763.33(257.33);785.73(87.5

	5);905.90(190.26);936.34(552.49);1025.62(161.46);1028.60(257.83);1097.85(107.30);1126.62(125.08);1160.87(17.87);1194.69(0.01);1266.78(23.59);1409.63(0.64);1483.74(0.46)
Cage-like structure $V_4O_{10}^+$ ($^4A'$)	15.13(0.64);23.69(3.25);26.35(2.35);30.39(1.91);69.15(1.54);126.60(3.09);148.35(0.12);162.41(4.05);170.08(10.92);185.40(0.97);219.56(13.52);225.98(8.60);250.11(20.37);271.85(0.73);289.67(15.89);339.24(11.73);350.91(10.72);362.89(7.80);455.90(11.21);468.32(29.83);481.43(9.65);494.64(0.03);511.75(30.62);557.81(26.13);608.54(100.83);621.48(4.66);726.81(50.27);884.98(385.14);896.29(1924.55);910.19(1343.55);948.78(123.59);998.77(1.50);1001.80(29.34);1119.80(75.53);1251.22(61.90) ;1432.48(0.83)
Cage-like structure V_4O_{10} ($^1T_2$)	10.50(2.46);26.65(2.28);51.09(16.34);73.91(1.65);119.14(1.25);137.30(3.41);147.02(17.56);200.61(16.14);210.89(2.74);234.73(0.44);291.74(5.68);328.02(0.87);356.72(47.30);455.01(36.36);458.27(2.88);476.04(30.55);519.76(1.28);528.84(0.03);588.74(28.69);659.53(384.46);705.68(351.74);779.41(155.21);785.73(87.55);846.53(151.15);872.69(165.45);905.90(190.26);930.96(1295.23);986.88(53.29);1090.81(49.81);1120.52(15.16);1125.34(382.64);1139.67(10.26);1206.01(101.54);1232.78(2.38);1412.34(3.71)
Cage-like structure V_4O_{10}($^3A_2$)	7.59(2.17);21.48(4.66);23.69(3.25);24.47(0.95);50.73(10.82);68.53(18.62);123.13(48.32);148.83(28.35);186.74(16.37);221.39(28.49);243.36(25.84);275.98(18.39);314.53(1.86);353.81(13.40);480.69(52.19);516.33(4.82);580.33(34.28);630.54(18.30);638.46(45.44);671.93(109.83);676.35(2.35);696.74(6.93);728.92(102.86);858.34(20.51);964.83(235.58);975.70(1100.32);985.92(251.77);1027.85(178.91);1038.60(257.83);1097.85(107.30);1126.62(125.08);1184.42(205.11);1210.81(200.33);1298.05(139.77);1462.67(19.77)

Appendix B

1. $V_2O_4^+$ ($^2A'$)

O1	0.047691,	0.084369,	1.217090	
V1	-0.069665,	-1.350972,	0.000000	
O2	0.047691,	0.084369,	-1.217090	
V2	0.047691,	1.297746,	0.000000	
O3	1.390168,	2.081142,	0.000000	
O4	-1.422373,	-2.096853,	0.000000	Total energy=-2188.9314642

2. $V_2O_4^+$ ($^2A'$)

O1	0.351607,	0.082505,	1.215623	
V1	0.172814,	-1.359121,	0.000000	
O2	0.351607,	0.082505,	-1.215623	
V2	0.351607,	1.295979,	0.000000	
O3	-1.002061,	2.061929,	0.000000	
O4	-1.208864,	-2.045405,	0.000000	Total energy= -2188.924284

3. V_2O_4 (^2A)

O1	-2.961173,	0.018120,	0.783707	
V1	-1.958495,	-0.007829,	-0.398003	
O2	-0.307546,	-0.013344,	0.038836	
V2	1.556114,	0.003152,	0.328655	
O3	2.201868,	1.278749,	-0.320575	
O4	2.223698,	-1.270078,	-0.302592	Total energy= -2188.888360

a. $V_2O_4 \bullet CH_2F_2^+$ (^2A)

O1	0.755618,	0.127965,	1.212519	
V1	2.272189,	-0.050962,	0.131907	
O2	1.045349,	0.446890,	-1.191667	
V2	-0.305050,	0.480057,	-0.109494	
O3	-0.904110,	1.915046,	0.008329	
O4	2.855685,	-1.483189,	0.013337	
C1	-3.291435,	-0.939727,	-0.332249	
F1	-1.783460,	-0.806131,	-0.476605	
F2	-3.597864,	-0.283930,	0.765922	
H1	-3.669484,	-0.459369,	-1.230757	
H2	-3.414534,	-2.014611,	-0.235243	Total energy= -2428.072708

b. $V_2O_4 \cdot CH_2F_2^+$ (^2A)

O1	0.766671,	0.384072,	1.221738	
V1	1.951684,	-0.392722,	-0.000017	
O2	0.766649,	0.384131,	-1.221713	
V2	-0.309853,	0.975028,	0.000036	
O3	-0.370950,	2.530756,	0.000074	
O4	2.006824,	-1.943178,	-0.000056	
C1	-2.970599,	-1.043159,	-0.000016	
F1	-2.172422,	0.235738,	0.000037	
F2	-2.076156,	-2.015009,	-0.000117	
H1	-3.527475,	-0.983378,	-0.930926	
H2	-3.527401,	-0.983502,	0.930945	Total energy= -2428.071665

c. $V_2O_4 \cdot CH_2F_2^+$ (^2A)

O1	0.881691,	0.187128,	1.227593	
V1	2.054335,	-0.001310,	0.000001	
O2	0.881695,	0.187130,	-1.227594	
V2	-0.545660,	0.546551,	-0.000002	
O3	-0.964496,	2.037366,	-0.000001	
O4	2.661822,	-1.440728,	0.000004	
C1	-2.902334,	-1.056076,	0.000000	
F1	-2.121006,	-0.628826,	1.084550	
F2	-2.120994,	-0.628841,	-1.084548	
H1	-3.841994,	-0.511704,	-0.000010	
H2	-2.951229,	-2.140544,	0.000007	Total energy= -2428.063479

d. $V_2O_4 \cdot CH_2F_2^+$ (^2A)

O1	-0.988347,	-0.167619,	-1.256270	
V1	-2.233421,	-0.496893,	0.111469	
O2	-0.710649,	-0.203501,	1.170020	
V2	0.297752,	0.228914,	-0.168429	
O3	0.591675,	1.762166,	-0.180241	
O4	-3.384308,	0.528718,	0.259263	
C1	3.528277,	-0.379488,	-0.297700	
F1	2.041069,	-0.697611,	-0.418617	
F2	3.695625,	0.033346,	0.937929	
H1	3.674874,	0.409905,	-1.030504	
H2	3.978621,	-1.349192,	-0.489197	Total energy=-2428.065903

e. $V_2O_4 \cdot CH_2F_2^+$ (^2A)

O1	0.646716,	-0.029122,	-1.220666	
V1	1.842940,	-0.805486,	0.001290	
O2	0.650010,	-0.023215,	1.222290	
V2	-0.281737,	0.775127,	-0.000011	
O3	-0.003089,	2.307401,	-0.004216	
O4	3.291775,	-0.257758,	-0.002554	
C1	-3.344597,	-0.561546,	0.000979	
F1	-2.268751,	0.482510,	0.002613	
F2	-2.706316,	-1.722400,	-0.002377	
H1	-3.873092,	-0.378220,	0.932259	
H2	-3.874678,	-0.373693,	-0.928496	Total energy= -2428.064301

f. $V_2O_4 \cdot CH_2F_2^+$ (^2A)

O1	-0.850167,	-0.237975,	-1.228753	
V1	-1.991779,	-0.559503,	0.000076	
O2	-0.850080,	-0.237771,	1.228813	
V2	0.497870,	0.379051,	-0.000053	
O3	0.626779,	1.920099,	-0.000205	
O4	-3.149339,	0.489827,	-0.000052	
C1	3.184819,	-0.538234,	0.000048	
F1	2.308582,	-0.378897,	-1.084791	
F2	2.308637,	-0.378521,	1.084867	
H1	3.904932,	0.274834,	-0.000111	
H2	3.573529,	-1.551704,	0.000210	Total energy= -2428.056102

g. $V_2O_4 \cdot CH_2F_2^+$ (^2A)

O1	0.744618,	-0.174053,	-1.205704	
V1	2.160032,	-0.542215,	-0.006960	
O2	0.762734,	-0.167621,	1.212766	
V2	-0.360724,	0.277460,	0.011357	
O3	-1.736154,	-0.718636,	0.024218	
O4	3.312127,	0.483398,	-0.017527	
C1	-3.148428,	-0.963833,	0.007350	
F1	-0.699373,	1.943025,	0.007429	
F2	-3.790394,	0.225738,	-0.040245	
H1	-3.360220,	-1.543149,	-0.892555	
H2	-3.391988,	-1.488065,	0.932638	Total energy=-2428.108319

h. $V_2O_4 \cdot CH_2F_2^+$ (^2A)

O1	0.422874,	-0.616323,	-0.980126	
V1	1.834960,	-0.645237,	0.192781	
O2	0.552032,	0.374210,	1.213249	
V2	-0.573009,	0.476259,	-0.018095	
O3	-1.823585,	-1.295200,	-0.190399	
O4	3.089427,	0.152397,	-0.227648	
C1	-3.046599,	-1.358374,	-0.152816	
F1	-0.318076,	1.912262,	-0.895865	
F2	-2.068850,	0.967579,	0.745912	
H1	-3.522679,	-2.340700,	-0.239895	
H2	-3.666250,	-0.461801,	-0.032022	Total energy= -2428.100762

i. $V_2O_4 \cdot CH_2F_2^+$ (^2A)

O1	0.311604,	-1.058295,	-0.932230	
V1	-1.347513,	-0.593910,	-0.266719	
O2	-0.177207,	0.702023,	0.784782	
V2	1.403597,	-0.040657,	-0.041658	
O3	2.021758,	1.030472,	-0.978063	
O4	-2.116170,	-1.616268,	0.596195	
C1	-0.894839,	1.881420,	0.620192	
F1	2.569424,	-0.777213,	0.972981	
F1	-1.956226,	1.443138,	-0.309475	
H1	-1.407688,	2.179904,	1.530890	
H2	-0.351867,	2.669849,	0.103612	Total energy= -2428.112395

j. $V_2O_4 \cdot CH_2F_2^+$ (^2A)

O1	0.388669,	-0.080279,	0.321363	
V1	2.259408,	0.060722,	0.163177	
O2	-2.318145,	1.212946,	0.019251	
V2	-1.259078,	-0.440177,	0.148572	
O3	-1.769493,	-1.148040,	1.431033	
O4	2.885297,	-1.044264,	-0.728174	
C1	-3.334360,	1.721819,	-0.448685	
F1	-1.658310,	-1.344737,	-1.256452	
F2	2.888766,	1.673266,	-0.023778	
H1	-4.020242,	1.145048,	-1.079888	
H2	-3.545910,	2.771844,	-0.223957	Total energy= -2428.130093

A. $V_2O_4 \cdot CH_3CF_2^+$ (^2A)

C1	-3.435895,	1.760813,	-0.040471	
C2	-2.988165,	0.354447,	0.004084	
F1	-1.322731,	0.468477,	-0.007972	
F2	-3.170710,	-0.315809,	1.099241	
F3	-3.181908,	-0.387222,	-1.041966	
H1	-4.530852,	1.742099,	-0.033343	
H2	-3.092462,	2.236071,	-0.957267	
H3	-3.081782,	2.296275,	0.838254	
O1	1.468410,	-0.280472,	-1.223580	
V1	2.778943,	0.230048,	0.002403	
O2	1.462367,	-0.281477,	1.221378	
V2	0.282049,	-0.626951,	-0.004179	
O3	-0.115070,	-2.136184,	-0.005704	
O4	3.174890,	1.732351,	0.003880	Total energy=-2566.704512

B. $V_2O_4 \cdot CH_3CF_2^+$ (^2A)

C1	-3.839031,	-1.386118,	-0.006961	
C2	-3.109049,	-0.103199,	0.000958	
F1	-1.493643,	-0.568191,	-0.000355	
F2	-3.140152,	0.631435,	-1.065818	
F3	-3.141798,	0.619122,	1.076059	
H1	-4.906159,	-1.139091,	-0.006240	
H2	-3.604913,	-1.958273,	0.888613	
H3	-3.603730,	-1.947896,	-0.908775	
O1	1.390494,	-0.197749,	1.222948	
V1	2.758571,	-0.567304,	0.001130	
O2	1.391243,	-0.201802,	-1.222781	
V2	0.253819,	0.277781,	-0.001053	
O3	0.048064,	1.825579,	-0.003621	
O4	3.982531,	0.386334,	-0.000088	Total energy=-2566.630625

C. $V_2O_4 \cdot CH_3CF_2^+$ (^2A)

O1	-1.402043,	0.179473,	-1.228572	
V1	-2.531970,	-0.182420,	0.000022	
O2	-1.402118,	0.179831,	1.228552	
V2	-0.043398,	0.748300,	-0.000083	
O3	0.146455,	2.286076,	-0.000132	
O4	-2.922484,	-1.695266,	0.000249	
C1	2.523154,	-0.540270,	-0.000010	
F1	1.686335,	-0.143952,	-1.077245	
F2	1.685391,	-0.144784,	1.076879	
F3	2.546373,	-1.845819,	-0.000597	
C2	3.834123,	0.151806,	0.000957	
H1	4.384740,	-0.150536,	0.892804	
H2	3.695130,	1.231952,	-0.002460	
H3	4.388572,	-0.155675,	-0.886711	Total energy= -2566.692355

D. $V_2O_4 \cdot CH_3CF_2^+$ (^2A)

O1	-1.356244,	-0.208712,	-1.229188	
V1	-2.462656,	-0.632041,	0.000083	
O2	-1.356291,	-0.208366,	1.229261	
V2	-0.059879,	0.513206,	-0.000054	
O3	-0.050917,	2.060477,	-0.000176	
O4	-3.712938,	0.305689,	-0.000064	
C1	2.674066,	-0.344328,	-0.000021	
F1	1.775647,	-0.120755,	-1.077512	
F2	1.775325,	-0.121048,	1.077338	
F3	2.951431,	-1.621159,	-0.000142	
C2	3.823365,	0.591329,	0.000365	
H1	4.423816,	0.402047,	0.891244	
H2	3.473552,	1.622809,	-0.001034	
H3	4.425840,	0.400300,	-0.888774	Total energy= -2566.685800

E. $V_2O_4 \bullet CH_3CF_2^+$ (^2A)

C1	3.582836,	-1.437288,	-0.355890	
C2	4.113203,	-0.261233,	-0.003342	
F1	-0.218362,	2.013918,	0.005771	
F2	4.387579,	0.090151,	1.226342	
F3	4.376611,	0.712568,	-0.836090	
H1	3.501331,	-1.678083,	-1.406664	
H2	3.509683,	-2.219346,	0.386917	
H3	1.904546,	-0.820197,	-0.159530	
O1	-1.566776,	-0.191566,	1.204177	
V1	-2.980492,	-0.595423,	0.023847	
O2	-1.637041,	-0.132396,	-1.218272	
V2	-0.501481,	0.329696,	-0.027231	
O3	0.907172,	-0.576766,	-0.087776	
O4	-4.193216,	0.359568,	0.082909	Total energy=-2566.700562

TSag

O1	-0.809824,	0.098539,	1.215506	
V1	-2.317977,	-0.185270,	0.154800	
O2	-1.015642,	-0.547001,	-1.132724	
V2	0.310141,	-0.145067,	-0.087659	
O3	1.299575,	-1.375496,	0.162446	
O4	-3.231630,	1.044020,	-0.103325	
C1	3.552148,	-0.084248,	-0.372378	
F1	1.443126,	1.167204,	-0.554331	
F1	3.891246,	0.496868,	0.680819	
H1	3.417378,	-1.163137,	-0.313864	
H1	3.500784,	0.529215,	-1.269722	Total energy= -2428.036448

TSgh

O1	0.565150,	-0.384303,	-1.138635	
V1	1.903645,	-0.561649,	0.142186	
O2	0.462398,	0.100992,	1.211137	
V2	-0.597899,	0.325969,	-0.075061	
O3	-1.705634,	-1.231406,	-0.504606	
O4	3.092761,	0.408724,	-0.006942	
C1	-2.871401,	-1.059307,	-0.036956	
F1	-0.571280,	1.943051,	-0.605896	
F2	-2.239902,	0.588856,	0.824412	
H1	-3.187164,	-1.624242,	0.843673	
H2	-3.633349,	-0.538497,	-0.620072	Total energy= -2428.074985

TSbi

O1	1.375804,	1.053677,	0.607304	
V1	1.810926,	-0.492231,	-0.286995	
O2	0.033266,	-0.410854,	-0.860151	
V2	-0.305174,	1.062820,	0.109331	
O3	-0.659643,	2.295191,	-0.776086	
O4	2.130861,	-1.759474,	0.564843	
C1	-2.052343,	-1.771578,	0.140504	
F1	-1.618877,	0.468155,	1.175515	
F2	-3.047837,	-1.356052,	-0.488753	
H1	-1.259240,	-2.223124,	-0.451063	
H2	-2.100857,	-1.708212,	1.226172	Total energy= -2428.029081

TSij

O1	-0.033987,	-1.220246,	0.431824	
V1	1.523966,	-0.493757,	-0.106771	
O2	-0.307999,	1.044791,	-0.786694	
V2	-1.427271,	-0.199743,	0.065194	
O3	-1.938857,	0.457852,	1.371657	
O4	2.847564,	-1.268396,	0.055598	
C1	0.344560,	2.117555,	-0.290552	
F1	-2.694110,	-0.855041,	-0.880679	
F2	1.643574,	1.494244,	0.279505	
H1	0.721949,	2.790521,	-1.056552	
H2	-0.092245,	2.589808,	0.587615	Total energy= -2428.100789

TS_{AE}

C1	3.716575,	0.775020,	-0.000182	
C2	3.040835,	-0.533248,	0.000003	
F1	1.333949,	-0.106631,	-0.000018	
F2	3.053181,	-1.248924,	-1.067610	
F3	3.053227,	-1.248645,	1.067805	
H1	4.793101,	0.564013,	-0.000155	
H2	3.467445,	1.333277,	0.900068	
H3	3.467439,	1.333025,	-0.900586	
O1	-1.489626,	0.314431,	-1.223263	
V1	-2.729218,	-0.349057,	-0.000005	
O2	-1.489617,	0.314388,	1.223270	
V2	-0.349626,	0.789809,	0.000008	
O3	-0.120248,	2.335897,	0.000034	
O4	-2.953289,	-1.887274,	-0.000032	Total energy=-2566.703423

$V_2O_3F_2^+$

V1	1.580864,	-0.293460,	0.000175	
O1	0.083046,	-0.145593,	1.198342	
V2	-1.083807,	0.045626,	-0.000122	
O2	0.083278,	-0.145777,	-1.198323	
O3	2.860995,	0.566742,	0.000358	
F1	-2.215405,	-1.215030,	-0.000104	
F2	-1.745803,	1.603609,	-0.000366	Total energy=-2313.516088

$V_2O_4HF^+$

V1	-1.584599,	-0.395429,	-0.000158	
O1	-0.134147,	-0.199992,	-1.207007	
V2	1.029872,	0.068228,	0.000204	
O2	-0.134431,	-0.200438,	1.207025	
O3	-2.584294,	0.776962,	0.000013	
O4	2.230863,	-1.134610,	0.000463	
F1	1.618311,	1.663184,	-0.000009	
H1	3.169990,	-1.378407,	-0.004950	Total energy= -2289.509859

	Frequency (cm^{-1})
1. $V_2O_4^+$ ($^2A'$)	114.78(23.35);196.11(15.27);210.79(2.54);331.64(0.92);351.80(36.54);393.62(28.09);443.77(244.37);652.18(3.32);790.18(156.71);861.66 (145.09);1128.53(320.26) ;1148.57(63.51)
2.$V_2O_4^+$ ($^2A'$)	106.34(1.07);202.55(46.69);220.01(1.62);316.98(0.01);352.88(5.37);373.21(39.55);427.53(2.66);655.82(263.98);778.93(172.99);868.29(182.25);1121.70(203.49);1153.34(142.75)
3.$V_2O_4^+$ (^2A)	42.33(18.27);71.12(29.22);97.79(33.59);171.68(8.21);267.45(36.88);302.79(85.18);359.52(5.71);451.46(9.14);942.13(827.53);1088.05(244.83);1106.93(90.22);1129.20(116.19);
a.V_2O_4•$CH_2F_2^+$ (^2A)	17.44(2.06);43.53(2.86);44.25(13.30);86.80(7.94);123.46(3.10); 165.84(12.38);200.57(14.87);217.33(5.26);304.66(4.69);328.41(0.87);356.35(59.20);449.57(21.97);454.96(3.05);476.71(62.41); 656.77(774.09);683.07(105.88);782.11(154.71);848.1428(147.71); 1114.50(11.37);1121.39(358.10);1138.87(46.31);1221.41(162.09); 1235.01(2.76);1408.49(7.34);1519.46(2.19);3117.26(2.03); 3234.26(0.53)
b.V_2O_4•$CH_2F_2^+$ (^2A)	15.45(2.46);26.66(2.28);51.16(16.34);73.91(1.65);137.29(3.41);147.02(17.56);200.60(16.14);210.89(5.68);328.02(0.87);356.72(47.30);455.02(36.39);458.27(2.88);476.04(30.52);659.53(384.38); 705.69(351.77);779.42(155.21);846.54(151.14);1120.53(15.16); 1125.34(382.64);1139.68(10.27);1206.00(161.55);1232.78(2.38); 1412.34(3.71); 1518.76(1.27);3119.13(1.27);3234.72(0.44);
c.V_2O_4•$CH_2F_2^+$ (^2A)	51.94(6.53);62.10(0.11);92.48(4.94);120.64(7.48);153.96(1.69); 169.09(24.01);182.81(5.62);215.15(8.48);224.45(4.85);334.38(0.47);370.82(61.40);381.51(35.53);434.77(4.04);581.39(54.10);619.85(197.24);814.43(120.33);874.60(145.18);923.60(207.06);1035.59(193.05);1116.03(302.07);1141.19(82.58);1163.69(18.50);1202.82(0.01); 1416.81(0.57);1514.95(0.17);3128.66(1.01);3241.99(2.46);
d.V_2O_4•$CH_2F_2^+$ (^2A)	23.66(4.05);34.82(0.84);48.38(11.22);92.67(2.01);109.67(6.04);144.55(10.23);222.05(39.26);234.16(2.85);306.56(21.92);313.08(0.12); 359.98(19.13);438.44(28.45);443.26(1.73);475.93(78.00);650.48(906.03);679.69(11.20);773.46(167.86);851.19(174.32);1113.36(38.60);1114.57(202.26);1144.82(158.91);1225.98(160.06);1236.62(3.49);1407.24(7.56);1518.59(3.06);3115.79(2.25);3233.62(0.57)
e.V_2O_4•$CH_2F_2^+$ (^2A)	24.64(6.53);28.18(0.83));51.25(8.07);76.13(2.63);122.52(20.31); 129.80(0.90);200.82(27.62);232.86(0.94);285.60(25.80);443.69(1.92);483.05(25.42);662.60(454.61);721.43(402.11);769.87(170.35); 850.06(172.01);1119.88(212.06);1125.66(15.41);1145.86(163.94); 1195.56(160.86);1232.68(2.15);1415.14(4.89);1518.11(1.31); 3119.96(1.24);3234.98(0.52)
f.V_2O_4•$CH_2F_2^+$ (^2A)	55.47(4.59);66.20(3.58);67.88(1.28);112.20(1.34);149.55(3.94); 150.01(0.08);187.07(13.35);233.89(57.12);245.76(0.77);319.28(0.20);355.22(24.75);368.23(45.76);416.62(4.67);580.09(65.73);620.65(215.81);806.67(130.27);877.33(170.83);922.70(209.97);1034.42(20

	5.11);1110.81(200.33);1146.05(139.77);1162.67(19.77);1202.73(0.03);1416.55(0.58);1514.29(0.20);3128.53(0.99); 3241.92(2.37);
g.V_2O_4•$CH_2F_2^+$ (^{2}A)	4.64(1.77);44.69(0.68);80.89(6.39);87.99(2.66);159.72(2.51);176.22(12.75);194.95(19.72);234.17(7.24);292.10(0.33);338.12(28.38);367.25(10.95);437.33(2.09);510.53(24.46);644.15(297.11);682.0(58.52);799.41(159.97);828.69(101.82);891.88(390.50);1007.46(906.38);1110.06(14.23);1132.59(142.91);1151.14(141.31);1252.40(0.00);1431.54(14.14);1500.45(10.04);3067.04(9.51);3147.07(1.32);
h.V_2O_4•$CH_2F_2^+$ (^{2}A)	45.88(4.37);76.91(8.07);82.75(5.60);141.90(13.97);172.36(6.70);209.65(12.48);228.84(24.99);242.02(17.01);280.28(19.65);310.19(13.99);331.75(4.85);364.74(8.66);376.40(27.09);427.56(2.85);464.28(10.70);650.34(229.49);718.43(196.66);765.40(208.63);801.11(160.48);892.87(292.44);1144.42(202.77);1228.19(8.38);1250.27(7.51);1497.62(52.67);1714.04(156.34);3019.77(0.84);3138.59(0.31)
i.V_2O_4•$CH_2F_2^+$ (^{2}A)	70.03(3.08);98.83(0.74);133.57(3.77);149.60(7.60);161.84(7.06);180.30(12.15);234.15(2.98);258.81(9.06);298.22(10.32);325.04(4.14);354.90(11.36);380.14(7.65);513.88(62.48);615.21(103.04);660.58(132.45);752.22(110.51);797.02(143.78);846.24(478.36);1108.63(233.62);1132.49(10.67);1143.40(320.97);1154.75(70.41);1199.38(10.81);1392.55(3.81);1517.65(1.33);3109.56(0.62);3211.34(2.87);
j.V_2O_4•$CH_2F_2^+$ (^{2}A)	21.71(10.20);33.22(7.50);42.24(2.81);66.16(12.90);76.49(18.18);115.01(9.93);140.64(30.33);181.82(9.51);188.90(19.39);233.38(8.62);268.68(12.99);279.94(12.07);313.78(29.37);332.90(10.67);391.07(75.18);473.92(39.20);763.13(229.40);799.86(104.38);941.17(964.16);1133.59(201.39);1141.06(130.74);1237.13(7.47);1245.66(10.27);1518.15(68.95);1720.96(307.36);3027.93(2.05);3155.73(1.17)
A.V_2O_4•$CH_3CF_2^+$ (^{2}A)	11.73(0.85);30.93(2.60);31.87(2.60);70.83(15.69);130.12(0.07);152.80(1.18);199.78(47.42);201.17(13.65);215.10(0.16);225.81(41.35);273.32(534.52);326.22(1.11);338.28(4.25);358.93(8.07);371.70(48.08);447.47(1.48);459.03(2.43);472.93(322.39);573.98(36.51);604.99(47.35);672.25(265.82);775.26(148.92);837.22(200.95);872.76(3.15);1020.25(18.41);1055.43(109.61);1119.28(390.78);1135.42(23.15);1352.93(299.58);1363.25(104.50);1433.13(143.57);1468.30(7.32);1469.27(20.53);3051.00(20.48);3135.59(4.63);3177.41(3.03);
B. V_2O_4•$CH_3CF_2^+$ (^{2}A)	11.07(0.53);32.44(0.01);39.46(2.63);81.45(3.14);115.12(7.26);123.75(35.55);196.37(31.73);217.88(0.00);233.00(7.75);237.12(2.37);258.86(604.27);312.64(0.18);337.97(4.36);361.20(9.87);368.89(20.13);446.94(2.18);448.92(0.54);474.02(311.84);573.60(54.69);603.97(52.61);674.03(285.70);765.19(162.93);837.99(236.54);873.21(1.70);1021.76(17.49);1054.40(112.67);1113.12(245.50);1141.50(149.93);1357.00(297.94);1365.08(101.78);1434.30(143.27);1469.08(8.22);1469.89(26.45);3049.81(22.71);3134.96(5.04);3177.81(3.00)
C. V_2O_4•$CH_3CF_2^+$ (^{2}A)	31.80(2.02);43.39(0.71);79.95(3.62);81.91(2.84);140.87(18.33);148.53(5.06);155.98(10.71);210.82(6.03);218.94(2.98);222.13(0.60);333.09(0.64);342.67(1.33);362.13(26.16);379.73(55.52);390.28(52.19);433.63(2.74);511.93(2.80);547.40(9.79);598.45(106.99);616.48(

	179.66);765.17(78.65);803.32(1.12);825.79(272.07);874.48(141.34);987.47(80.75);1113.74(89.62); 1114.63(300.92); 1138.03(99.18); 1183.97(319.14);1348.11(167.84);1438.09(105.42);1467.24(5.16); 1472.71(0.80);3064.78(12.44);3146.77(4.50); 3160.30(1.79);
D. V_2O_4•$CH_3CF_2^+$ (^2A)	33.91(4.90);50.24(7.43);63.83(3.61);84.65(0.51);118.80(0.55); 144.53(0.48);156.14(2.14);216.62(0.41);229.85(64.79);247.22(0.09);318.47(0.40);342.94(1.80);350.82(15.67);364.12(29.46);390.78(55.90);417.62(3.20);512.10(2.84);548.79(14.89);597.57(106.68);618.93(210.84);764.99(85.09);799.40(3.89);823.21(281.13);879.04(171.37);986.96(88.98);1108.95(225.60);1113.93(90.36);1143.09(168.31); 1183.56(314.31);1347.09(177.53);1437.99(105.82);1467.25(5.17);1472.11(0.62);3064.31(12.83);3146.82(4.71);3159.54(2.20)
E. V_2O_4•$CH_3CF_2^+$ (^2A)	8.16(0.15);17.72(0.01);20.39(1.01);48.40(3.88);64.93(0.51);92.94(3.37);154.47(25.08);175.29(11.53);200.75(93.17);224.81(3.82);226.34(4.58);293.89(0.64);366.19(25.00);374.51(9.94);438.77(1.09);443.00(0.05);559.26(17.27);652.08(34.25);658.55(514.50);664.48(26.58);693.10(88.73);786.08(63.62);796.85(155.07);870.77(81.17);876.92(608.20);899.35(101.14);958.21(221.66);964.74(40.04);980.92(23.17);1145.99(239.11);1355.22(260.88);1410.91(51.40);1683.43(1027.08);2626.42(1932.77);3169.45(19.05);3274.99(8.63);
TSag	-342.78(29.97);30.00(2.60);38.14(8.44);72.62(12.27);111.62(7.47); 176.23(31.38);180.93(3.70);217.75(18.88);249.85(5.75);306.07(172.47);320.37(5.50);339.35(73.83);375.40(38.65);393.79(1.63);460.4088(2.19);661.88(86.35);678.03(303.47);779.41(159.78);845.52(282.17);1031.87(465.90);1133.12(186.35);1171.81(3.32);1247.05(13.13);1409.63(220.16);1555.82(58.76);3097.36(23.11); 3270.65(29.12)
TSgh	-307.01(42.84);43.26(2.05);74.45(2.06);111.21(8.61);153.19(19.97); 179.61(6.06);213.91(19.39);250.36(13.61);270.44(8.36);324.57(27.91);363.07(8.14);408.76(10.59);449.81(62.92);470.74(21.39);536.25(6.36);604.21(163.36);669.24(344.05);763.29(164.78);800.95(161.50);879.76(299.83);1149.86(201.74);1215.53(9.29);1229.41(6.64); 1416.99(230.81);1581.70(77.19);3057.05(0.12)
TSbi	-311.63(31.09);23.66(6.76);37.34(7.07);86.89(8.44);111.17(11.01); 178.88(0.64);199.06(15.74);200.40(17.19);231.20(10.26);263.65(57.70);325.07(24.11);328.19(53.85);363.34(39.39);379.44(3.64);476.50(4.00);663.26(70.08);680.97(373.76);720.41(212.79);804.21(160.90);1115.95(351.93);1133.73(86.22);1167.62(4.32);1246.11(11.59);1412.14(209.18);1554.87(60.62);3104.15(15.51);3277.93(25.65);
TSij	-299.53(8.44);68.73(6.31);100.54(0.87);113.05(11.44);146.04(8.11); 179.00(17.16);188.81(1.07);238.27(6.82);286.05(10.45);299.36(3.97);329.93(4.05);361.46(11.41);510.73(76.08);588.01(80.36);612.57(18.69);689.26(119.34);772.72(399.48);835.35(460.50);1094.21(5.45);1142.39(298.48);1148.10(97.42);1193.99(168.73);1214.01(145.81);1370.41(0.90);1524.24(2.74);3102.01(1.02);3205.78(1.97);
TS_{AE}	-231.42(23.36);16.52(1.38);24.50(2.23);55.84(4.30);57.89(1.36); 81.49(5.32);147.92(239.77);184.52(4.86);197.23(63.96);221.32(12.

	21);272.37(156.54);315.09(0.24);351.59(127.84);389.79(2.24);417.80(2.58);443.85(1.12);464.59(1.35);584.61(10.15);605.82(26.10);677.17(365.87);742.51(85.21);771.99(160.92);842.37(385.76);927.32(11.97);972.12(701.24);998.42(424.08);1024.59(5.08);1129.44(191.52);1319.83(50.22);1335.27(89.89);1416.46(208.83);1494.12(253.09);1522.69(675.56);2141.94(100.82);3094.96(42.53); 3185.02(22.27)
$V_2O_3F_2^+(^2A)$	82.47(4.68);139.78(20.51);154.89(8.40);202.00(12.30);228.04(1.44);255.84(0.10);364.30(17.59);386.01(30.30);414.00(3.18);625.17(189.32);792.60(98.55);817.15(178.88);880.60(196.93);930.93(343.96);1149.67(213.73)
$V_2O_4HF^+(^2A)$	86.27(0.88);114.85(149.81);172.39(0.44);185.18(12.09);194.63(16.51);241.37(36.80);289.47(4.97);293.02(224.10);361.27(32.27);366.99(6.82);431.32(2.23);655.26(249.32);796.61(60.88);809.84(171.39);891.42(195.68);922.51(383.64);1152.94(170.04); 3766.18(825.55)
open structure $V_4O_8^+(^2A)$	6.34(1.31);21.48(4.66);23.69(3.25);26.35(2.35);30.39(1.91);38.05(35.29);59.34(0.17);71.57(0.16);101.4(2.55);123.31(29.69);142.10(26.35);177.26(46.17);216.18(5.90);267.49(42.05);270.07(10.11);285.51(81.11);286.58(47.61);298.65(57.33);379.64(28.71);385.84(30.64);455.90(11.21);498.32(29.83);896.29(1924.55);910.19(1343.55);948.78(123.59);1081.91(13.44);1084.50(487.73);1097.78(69.24);1098.04(91.63);1101.25(116.80)
Cage-like $V_4O_8^+(^2A')$	36.16(0.43);80.73(0.39);137.74(2.06);154.27(0.11);160.15(3.04);169.44(4.60);182.31(0.53);218.71(12.02);222.07(0.75);230.88(16.63) 239.03(0.00);246.79(16.61);277.71(3.70);287.03(4.70);343.04(5.44);348.41(6.72);355.48(12.28);487.15(18.77);488.33(0.00);507.57(1.08);510.30(27.26);611.65(90.38);630.70(98.67);644.36(277.97);719.93(33.36);721.08(46.42);722.83(175.73);843.23(158.82);1131.99(319.30);1144.31(150.40);